Investigation of oxygenated and intermediate-volatility organic compounds (OVOCs/IVOCs) with a Proton Transfer Reaction - Time Of Flight - Mass Spectrometer (PTR-TOF-MS)

Dissertation zur Erlangung des Grades

“Doktor der Naturwissenschaften”

im Promotionsfach Analytische Chemie
am Fachbereich Chemie, Pharmazie und Geowissenschaften
der Johannes Gutenberg-Universität
in Mainz

Bettina Derstroff
geboren in Zweibrücken

Mainz, den 15.07.2016

Termin der Prüfung:

26.08.2016

"Out of all those millions and millions of planets floating around there in space, this is our planet, this is our little one, so we just got to be aware of it and take care of it."

Paul McCartney

Abstract. Volatile organic compounds (VOCs) play an important role in chemical and physical processes of the atmosphere. They can influence the formation of secondary organic aerosol, change the oxidative capacity of the atmosphere or themselves be toxins, which impact air quality and human health.
For the measurement of VOCs a Proton Transfer Reaction-Time Of Flight-Mass Spectrometer (PTR-TOF-MS) is especially suitable, because it can monitor with high time and mass resolution. In this work various air chemistry applications for a PTR-TOF-MS are shown and the focus is placed on elucidating oxygenated VOCs (OVOCs) and intermediate-volatility VOCs (IVOCs).
To compare and improve the various measurement techniques an OVOC-inter-comparison between several Gas Chromatography (GC) and PTR-TOF-MS instruments was performed at the meteorological observatory in Hohenpeißenberg in 2013. This work concentrates on the results of the PTR-TOF-MS instruments. In general a very good agreement was found, only methanol and acetaldehyde showed, in part, significant discrepancies. The main reasons were the high polarity and therefore stickiness of methanol to surfaces as well as the production of acetaldehyde via the heterogeneous reaction between ozone and unsaturated compounds inside the tubing. Measures were taken to minimize these effects in the following studies.
A field campaign was conducted on the island of Cyprus in summer 2014 in order to investigate highly oxidized air advected from both Eastern and Western Europe. The most abundant VOC compounds measured there were methanol, acetone and acetic acid. Methanol and acetone did not show a diel cycle, but were mainly influenced by long distance transport. The mixing ratios of acetic acid, on the other hand, followed a distinct diel cycle during one part of the measurement campaign while its values were dominated by transport processes during the rest of the study. The analysis of these three long-lived compounds has given an insight into the role of the marine boundary layer (MBL) in transport phenomena.
A second application, in stark contrast to the clean air measured in Cyprus, was the analysis of exhaust gases directly emitted from a diesel and a gasoline vehicle. So far only the results of PTR-quadrupole-MS instruments, which have a lower mass resolution, have been found in the literature. It is shown that the PTR-TOF-MS represents a promising technique to monitor car emissions fast and efficiently, particularly as the higher transmission efficiencies at high masses reveal a poorly documented semivolatile fraction of VOCs. This complex mixture was dominated by alkanes, OVOCs and aromatic compounds. Clear differences in the chemical composition between gasoline and diesel vehicles were determined, e.g. diesel exhaust showed a higher amount of IVOCs.

Zusammenfassung. Flüchtige organische Verbindungen (VOCs) spielen eine wichtige Rolle in den chemischen und physikalischen Prozessen der Atmosphäre. Sie können die Bildung sekundärer organischer Aerosole beeinflussen, die Oxidationskapazität der Atmosphäre verändern oder sie stellen Giftstoffe dar, die die Luftqualität und die menschliche Gesundheit beeinträchtigen.
Für die Messung von VOCs ist ein Proton-Transfer-Reaction-Time-Of-Flight-Mass-Spectrometer (PTR-TOF-MS) besonders geeignet, weil es in Echtzeit mit hoher Massen- und Zeitauflösung misst. In dieser Arbeit werden verschiedene Anwendungen für ein PTR-TOF-MS beschrieben und das Augenmerk wird auf oxidierte VOCs (OVOCs) und intermediate-volatility organic compounds (IVOCs) gelegt.
Um verschiedene Messtechniken zu vergleichen und zu verbessern, wurde 2013 eine OVOC-Vergleichskampagne zwischen mehreren Gas Chromatographie- (GC) und PTR-TOF-MS-Instrumenten im Meteorologischen Observatorium in Hohenpeißenberg durchgeführt. Diese Arbeit konzentriert sich auf die Ergebnisse der PTR-TOF-MS-Instrumente. Im Allgemeinen wurde eine gute Übereinstimmung zwischen den Geräten festgestellt, nur Methanol und Acetaldehyd zeigten teilweise signifikante Unterschiede. Die Hauptgründe hierfür waren die hohe Polarität von Methanol, sowie die Produktion von Acetaldehyd über die heterogene Reaktion zwischen Ozon und ungesättigten Substanzen innerhalb der Leitungen.
Eine Feldmesskampagne wurde im Sommer 2014 auf Zypern durchgeführt, um oxidierte Luftmassen zu untersuchen, die sowohl aus Ost- als auch aus Westeuropa heranströmten. Die interessantesten Stoffe, die dort gemessen wurden, waren Methanol, Aceton und Essigsäure. Methanol und Aceton zeigten keine ausgeprägten Tagesgänge, sondern wurden hauptsächlich durch Transport über weite Entfernungen beeinflusst. Dagegen folgten die Mischungsverhältnisse von Essigsäure in einem Teil der Kampagne einem deutlichen Tagesgang, während die Werte im restlichen Teil der Messkampagne von Transportprozessen beeinflusst wurden. Die Analyse dieser drei langlebigen Stoffe ergab Einblick in die Rolle der marinen Grenzschicht (MBL) bei Transportphänomenen.
Eine weitere Anwendung, ganz im Kontrast zur sauberen Luft auf Zypern, war die Analyse von Abgasen, die unmittelbar von einem Benzin- und einem Dieselfahrzeug emittiert wurden. Bisher konnten nur die Ergebnisse von Messungen mit einem PTR-Quadrupol-MS, das eine wesentlich schlechtere Massenauflösung aufweist, in der Literatur gefunden werden. Das PTR-TOF-MS stellt daher eine vielversprechende Methode für die schnelle und effiziente Überwachung von Autoabgasen dar, vor allem weil die höhere Transmissionseffizienz für hohe Massen die Messung des bisher nur wenig untersuchten halbflüchtigen Anteils an VOCs ermöglicht. Die komplexe Mischung der Emissionen von Benzin- und Dieselmotoren wurde dominiert von Alkanen, OVOCs und aromatischen Verbindungen. Unterschiede zwischen dem Benzin- und dem Dieselfahrzeug wurden bestimmt, beispielsweise zeigten Dieselabgase wesentlich höhere Mengen an IVOCs.

Note to Chapter 4

Chapter 4 in this thesis represents a paper in preparation. After submission of the thesis it has been revised and published. It is available for download at:

https://www.atmos-chem-phys.net/17/9547/2017/

Reference:
Derstroff, B., Hüser, I., Bourtsoukidis, E., Crowley, J. N., Fischer, H., Gromov, S., Harder, H., Janssen, R. H. H., Kesselmeier, J., Lelieveld, J., Mallik, C., Martinez, M., Novelli, A., Parchatka, U., Phillips, G. J., Sander, R., Sauvage, C., Schuladen, J., Stönner, C., Tomsche, L., and Williams, J.: Volatile organic compounds (VOCs) in photochemically aged air from the eastern and western Mediterranean, Atmos. Chem. Phys., 17, 9547-9566, doi:10.5194/acp-17-9547-2017, URL https://www.atmos-chem-phys.net/17/9547/2017/, 2017.

Contents

1. Introduction

1.1. The Atmosphere

The atmosphere is the envelope of gas around the surface of the Earth and an indispensable requisite for life. From the variations in temperature with height, the atmosphere can be divided into layers (see Figure 1.1). The total mass of the atmosphere amounts to 5.2×10^{18} kg and 99.9 % of it can be found below 50 km (Jacob, 1999). A quasi-exponential decrease of the pressure and the density is observed for increasing altitude. This work is focused within the lower most layer, which is called troposhere. It extends from the surface up to 8-18 km depending on season and latitude and is subdivided into the planetary boundary layer (PBL) and the free troposphere. The PBL develops due to interactions with the earth surface and comprises the first 1 or 2 km of the atmosphere. Stull (1988) defines the boundary layer as "that part of the troposphere that is directly influenced by the presence of the earth's surface, and responds to surface forcings with a timescale of about an hour or less." (Stull, 1988). The temperature within the troposphere decreases by approximately 6 °C/km (Holloway and Wayne, 2010). Since the highest temperature can be found at the surface, vertical mixing by means of convection takes place. But temperature inversions, which hinder vertical mixing, can occur as well. This shows that the conditions within the PBL are highly variable. At the so called tropopause, which lies between 10 and 20 km, the temperature reaches a local minimum of -50 to -80 °C. In the next layer, the stratosphere, the temperature rises again. The reason is the ozone layer, which lies between 15 and 35 km (Warneck, 2000). It contains 90 % (ca. 10 ppmv) of the atmospheric ozone, which absorbs UV-B radiation and transfers heat to the surrounding air. Ozone itself is produced by the photolysis of O_2 and the layer is formed in this height, because at lower altitudes the radiation is too weak while at higher altitudes the oxygen concentration decreases. Very little water is present in the stratosphere, because it condenses with increasing altitude in the troposphere and finally freezes out in the temperature minimum of the tropopause. The temperature profile in the stratosphere represents the stable situation, where warm air lies over cold, thus little convective mixing takes place. Vertical transport does occur due to eddy diffusion and planetary scale waves. On average a single molecule emitted at the surface is transported through the 10 km troposphere in a few days or even less. However, it takes several years to pass the stratosphere. In roughly 50 km, where the temperature starts to decrease again, the boundary of the stratosphere, the so called stratopause, is located. The temperature decline in the next layer, the mesosphere, can be traced back to radiative cooling mainly by CO_2 molecules, which release the heat into space. A minimum temperature of - 88 °C is reached (Warneck, 2000). Above the mesopause the temperature rises rapidly in the so called thermosphere, because strong UV radiation is absorbed by N_2 and O_2 molecules as well as atoms. The last layer is named exosphere and represents the transition into space.
Chemical reactions depend on temperature and pressure and therefore can vary consider-

ably in rate within the atmosphere. Meteorology and physical processes, such as condensation and evaporation, influence chemical reactions, because they occur not only in the gas phase, but also on the surface of solid particles or in the aqueous phase of droplets.
The atmosphere is composed of 78 % nitrogen, 21 % oxygen, 0.9 % argon and 0.035 % of CO_2. These gases do not react with each other under ambient conditions and the reactions in the troposphere and lower stratosphere are mainly driven by trace gases in the range of parts per million (ppmv) to parts per trillion (pptv) and below. Among atmospheric chemists it is common to use mixing ratios instead of concentrations as units, because these are independent of the pressure. These units will be used throughout the thesis.
Important trace compounds for atmospheric chemistry are sulfur containing organic species like DMS, inorganic species like COS, SO_2, H_2S or nitrogen containing compounds, e.g. NO_2, NO, N_2O. Furthermore, organic hydrocarbons, which occur in a high variety in the troposphere, play an important role.
Not only CO_2, but also other gases, such as CH_4 or N_2O, act as greenhouse gases (GHGs). The most important GHG is water vapor. The greenhouse effect arises from the fact that the atmosphere is transparent for shorter wavelength, but absorbs IR radiation. The radiation with shorter wavelength is transformed into those with longer wavelength on the Earth's surface. This heat radiation is in turn absorbed by IR active compounds in the atmosphere and transferred to air molecules. Only a small part is released into space. Figure 1.2 shows the global annual mean energy budget based on Kiehl et al. (1997). It can be seen that a high amount, 324 W/m^2, is radiated back from the atmosphere. Without the greenhouse effect the temperature on Earth would be only -19 °C (Finlayson-Pitts and Pitts, 2000).
In this work the focus is placed on volatile organic compounds (VOCs), which are ubiquitous in the troposphere and can have various sources. The World Health Organization (WHO) defined a VOC as any organic compound which has a saturation vapor pressure greater than 102 kPA at 25 °C (Warneck, 2000). The group of VOCs includes nonmethane hydrocarbons (NMHCs) and oxygenated volatile organic compounds (OVOCs). Substances consisting only of hydrogen and carbon atoms, such as alkanes, alkenes and aromatic compounds, count among NMHCs while oxygen containing species, such as alcohols, aldehydes, ketones, esters and organic acids, belong to the group of OVOCs. The sources of VOCs are diverse and can comprise terrestrial vegetation (e.g. isoprene, monoterpenes; Kesselmeier and Staudt, 1999), the ocean (e.g. dimethylsulfide (DMS); Cline and Bates, 1983; Mesarchaki et al., 2014), biomass burning (e.g. acetonitrile; Holzinger et al., 1999; Karl et al., 2007) or anthropogenic processes, such as fuel combustion or industrial procedures (e.g. benzene, toluene; Piccot et al., 1992). Heavier molecules with a carbon chain length of C_{10} to C_{20} belong to the intermediate-volatily organic compounds (IVOCs). In the following section the OVOCs and IVOCs are addressed in more detail.

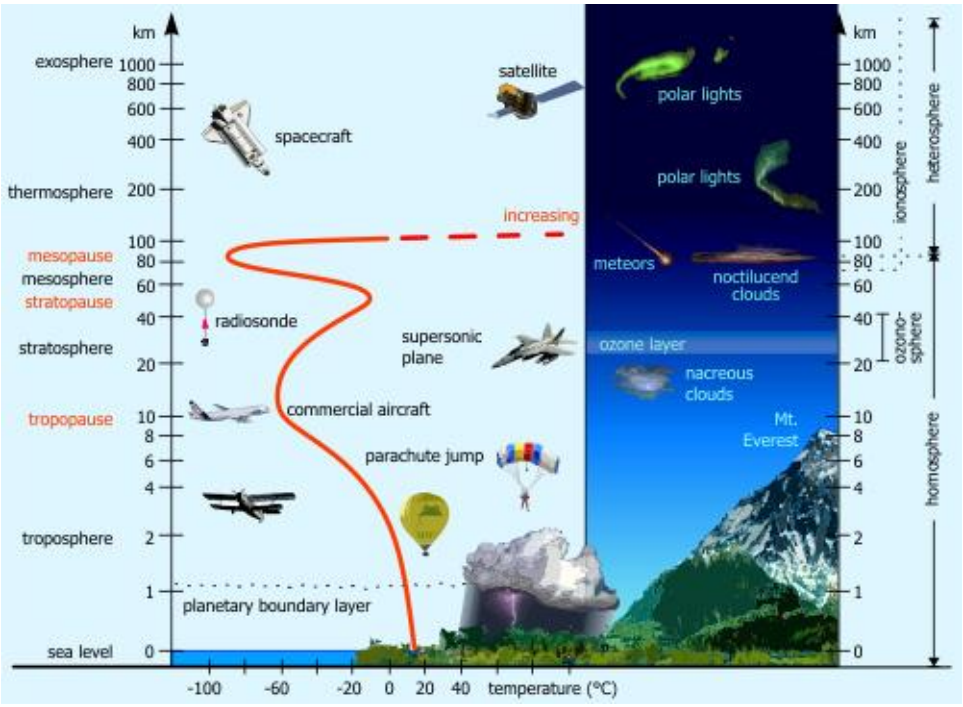

Figure 1.1.: Structure of the atmosphere. Source: *http://www.theozonehole.com/atmosphere.htm*; accessed on 24th of May 2016.

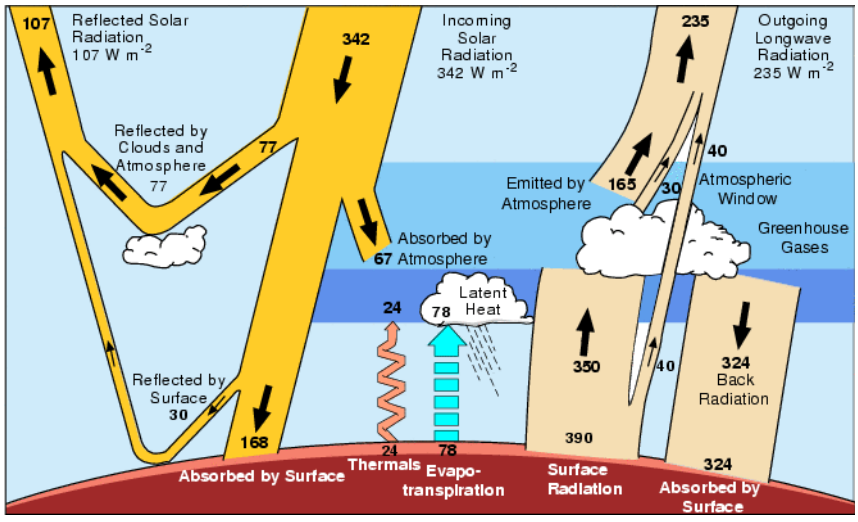

Figure 1.2.: Annual global mean energy budget of the Earth in W/m^2. Source: *http:www.windows2universe.org/earth/climate/greenhouse_effect_gases.html*; accessed on 24th of May 2016, originally from Kiehl and Trenberth, 1997.

1.2. Oxygenated volatile organic compounds (OVOCs)

OVOCs were measured in terrestrial and marine, rural and urban sites in the Northern and Southern Hemisphere (e.g. Goldan et al., 1995; Singh et al., 1994, 1995, 2000, 2004; Kesselmeier, 2001; Williams et al., 2004; de Gouw et al., 2005; Galbally et al., 2007; Legreid et al., 2007; Read et al., 2012; Louie et al., 2013; Borbon et al., 2013) and play an important role in the chemical processes of the atmosphere. They can influence the ozone budget, represent precursors for farther secondary pollutants, e.g. peroxyacetyl nitrate (PAN), produce HOx in the upper troposphere and significantly impact total OH reactivity (e.g. Singh et al., 1995; Millet et al., 2008; Read et al., 2012). Their sources are manifold and cover anthropogenic and biogenic emissions, biomass burning and emissions from the ocean. OVOCs can either be emitted directly or produced secondarily through photochemistry. From measurements in the Pacific troposphere Singh et al. (2004) reported that the sum of the OVOCs were nearly two times larger than the sum of the C_2-C_8 hydrocarbons and that the OH reactivity is ca. 5 times higher than that of the NMHCs. Due to their relatively long atmospheric lifetimes of several days, OVOCs can be used to investigate for long distance transport, although it needs to be differentiated between them being primarily emitted and then transported or being produced during transport. In the following sections compounds pertinent to the succeeding chapters will be detailed.

1.2.1. Methanol

Methanol is one of the most abundant OVOCs in the atmosphere. Its main source is biogenic. Methanol is a by-product of the pectin demethylation during leaf growth and is emitted through the stomata (MacDonald and Fall, 1993; Fall and Benson, 1996). But plants as well as methylotrophic bacteria also consume methanol so that the net emission must be regarded as the sum of consumption and production (Fall and Benson, 1996). Other known sources are emission from the decay of dead plants (MacDonald and Fall, 1993; Fall and Benson, 1996; Warneke et al., 1999), biomass burning (McKenzie et al., 1994; Holzinger et al., 1999; Andreae and Merlet, 2001; Yokelson et al., 1999, 2003; Christian et al., 2003; Karl et al., 2007), secondary production by the oxidation of hydrocarbons, especially methane, and other precursors (Madronich and Calvert, 1990; Tyndall et al., 2001; Holzinger et al., 2005) as well as direct anthropogenic emissions (e.g. Singh et al., 1995; Holzinger et al., 2001; de Gouw et al., 2005; Wei et al., 2008). In contrast to Holzinger et al. (2005), de Gouw et al. (2005) as well as Dufour et al. (2006) did not find an evidence for the secondary production of methanol from anthropogenic precursors. Its major tropospheric sink is oxidation by OH radicals (Galbally and Kirstine, 2002; Jacob et al., 2005; Millet et al., 2008). Methanol has a total atmospheric lifetime of ~ 5 days (Millet et al., 2008) and a lifetime of roughly 13 days with respect to OH if a diel mean OH concentration of 10^6 molec/cm^3 (Spivakovsky et al., 2000; Lawrence et al., 2001) is assumed. The rate coefficient k for the reaction with OH amounts to 9×10^{-13} cm^3 molec^{-1} s^{-1} and originates IUPAC[1]. It shows average mixing ratios between 0.5 and 10 ppbv in the Northern Hemisphere and between 0.2 and 2 ppbv in the Southern Hemisphere (Warneck and Williams,

[1] http://iupac.pole-ether.fr/index.html; accessed on 12$^{\text{th}}$ of July 2016

2012). Heikes et al.(2002) stated the following typical mixing ratios for methanol: remote ocean 0.9 ppbv, continental background 2 ppbv, grasslands 6 ppbv, coniferous and deciduous forests 10 ppbv, urban sites < 20 ppbv and free troposphere 0.6 ppbv. It plays a significant role in the production of formaldehyde (Millet et al., 2006) and a minor one regarding the HOx and ozone budget (Millet et al., 2008). Tie et al. (2003) calculated that the methanol influence on ozone and HOx is strongest in the tropical upper troposphere and that it increases ozone there by 1-2 %, HO_2 by 3-5 %, but decreases OH by 1-3 %. Several global budgets were modeled and can be found in Table 1.1.

Table 1.1.: Global atmospheric methanol budgets calculated by Galbally et al. 2002, Heikes et al. 2002, Jacob et al. 2005 and Millet et al. 2008

	Galbally 2002	Heikes 2002	Jacob 2005	Millet 2008
Sources				
Primary anthropogenic emission	4	8	4	5
Primary biogenic emission	100	280	128	80
Atmospheric production	19	30	38	37
Plant decay	13	20	23	23
Biomass burning	13	12	13	12
Ocean	small	?	0	85
Sum	149	345	206	242

Sinks				
Ocean uptake	small	85	10	101
Oxidation by OH	109	100	129	88
Dry deposition land	24	70	55	40
Wet deposition	11 (land)	5 (land)	12	13
In-cloud oxidation	5	10	< 1	< 1
Sum	149	270	206	242

Galbally et al. (2002) state that the overall methanol sink by OH radicals of 109 Tg/yr subdivides into 69 Tg/yr in the free atmosphere and 40 Tg/yr in the continental boundary layer. Heikes et al. (2002) report a dry deposition over the ocean of 80 Tg/yr and a wet deposition over the ocean of 5 Tg/yr, which was summed up in Table 1.1. According to Heikes et al. (2002) the ocean source can lie between 0 and 80 Tg/yr and is stated with a question mark due to this large uncertainty. Millet et al. (2008) give a high ocean source of 85 Tg/yr, but a still higher ocean sink of 101 Tg/yr, which would result in a net sink of 16 Tg/yr. Jacob et al. (2005), on the other hand, directly stated a total net sink of 10 Tg/yr, which is in quite good agreement with Millet et al (2008). It becomes clear

that biogenic emissions represent the most important source for methanol, but the source estimates vary strongly. Heikes et al. (2002) report a particularly high value of 280 Tg/yr, but it should be noted that high uncertainties are given in this reference: Primary biogenic emissions range from 50 - 280 Tg/yr, the total sources from 90 - 490 Tg/yr and the total sinks from 160 - 570 Tg/yr. The most significant sink is oxidation by OH radicals, although Heikes et al. (2002) also estimate quite high values for dry deposition over land and over ocean (70 Tg/yr and 80 Tg/yr, respectively). Galbally et al. (2002) determined the influence of the ocean to be small. Millet et al. (2008), on the other hand, suggest that the ocean is a large source and a slightly larger sink for methanol resulting in an small net sink. Downwind of continents the methanol mixing ratios are high so that the ocean represents a sink while in regions with low mixing ratios of methanol and high temperatures the ocean can be a source (Millet et al., 2008). Measurements performed by Williams et al. (2004) and Yang et al. (2013) yielded negative fluxes of -33.7 mol/m^2/day and -14 mol/m^2/day, respectively. Heikes et al. (2002) as well as Jacob et al. (2005) give an atmospheric inventory for methanol of 4 Tg. An inter-comparison of methanol measuring instruments is described in chapter 3 and detailed information about the measurement of methanol during the CYPHEX campaign 2014 on the island of Cyprus can be found in chapter 4.

1.2.2. Acetone

Acetone is the most abundant carbonyl species in the atmosphere after formaldehyde. It has a mean tropospheric lifetime of 14 days (Fischer et al., 2012). If only the reaction with OH radicals is regarded the lifetime amounts to 64 days (using a rate coefficient of 1.8×10^{-13} cm^3 molec^{-1} s^{-1} from IUPAC[2] and assuming an OH concentration of 10^6 molec/cm^3 (Spivakovsky et al., 2000; Lawrence et al., 2001). It shows mixing ratios of 0.5-0.8 ppbv over the ocean and 1-2 ppbv over the continent (Warneck and Williams, 2012). Acetone acts as a precursor for PAN and represents a source of HOx in the upper troposphere (Singh et al., 1994, 1995; Wennberg et al., 1998). It therefore has an impact on the oxidation capacity of the atmosphere and on the ozone budget (Singh et al., 1995, 2001). Its sources are direct emission from plants (Goldan et al., 1995; Kesselmeier and Staudt, 1999; Schade and Goldstein, 2006) and from decaying plant material (Warneke et al., 1999), biomass burning (Holzinger et al., 1999; Yokelson et al., 1999, 2009; Andreae and Merlet, 2001; Christian et al., 2003; Karl et al., 2007; Akagi et al., 2011), anthropogenic emissions (Sigsby et al., 1987; Singh et al., 1994; de Gouw et al., 2005) and secondary production from photo-oxidation of hydrocarbons such as propane (e.g. Singh et al., 1994; Goldstein and Schade, 2000; de Gouw et al., 2005; Holzinger et al., 2005; Pozzer et al., 2010; Schade and Goldstein, 2006). Photolysis and oxidation by OH radicals are the major sinks (Jacob et al., 2002; Khan et al., 2015). The global burden amounts to 3.8 Tg (Jacob et al., 2002). Table 1.2 shows calculated global acetone budgets from several references.
In Fischer et al. (2012) the source by plant decay is included in the biogenic emissions. Singh et al. (2004) stated that the ocean is a small net sink for acetone, but no further sinks are discussed. Singh et al. (1994) report a total sink strength of 40-60 Tg/yr, but this is not in balance with the net source of 95 Tg/yr given by Singh et al. (2004). It becomes

[2]http://iupac.pole-ether.fr/index.html; accessed on 12$^{\text{th}}$ of July 2016

Table 1.2.: Global atmospheric acetone budgets modeled by Jacob et al. 2002, Singh et al. 2004 and Fischer et al. 2012

	Jacob 2002	Singh 2004	Fischer 2012
Sources			
Primary anthropogenic emission	1.1	2	0.73
Primary biogenic emission	33	50	32
Atmospheric production	28	28	31
Plant decay	2	6	/
Biomass burning	4.5	9	2.8
Ocean	27	0	80
Sum	95	95	146
Sinks			
Ocean uptake	14	/	82
Oxidation by OH	27	/	33
Photolysis	46	/	19
Dry deposition land	9	/	12
Sum	96	/	146

clear that terrestrial emissions and secondary production represent the most important sources. In Jacob et al. (2002) photolysis is the major sink while Fischer et al. (2012) attach more importance to the reaction with OH than to photolysis. The reason for these differences is: It was found that the quantum yield of acetone photolysis was temperature dependent and was less than the previously assumed value of 1 (Blitz et al., 2004). This effectively lengthened the lifetime of acetone. The role of the ocean is the most uncertain issue: While Jacob et al. (2002) state a rather small marine influence and describe the ocean as a net source of 13 Tg/yr, Fischer et al. (2012) consider that the ocean is of high importance and a net sink of 2 Tg/yr. Marandino et al. (2005) measurements performed in the North Pacific showed that the ocean was a large net sink. Other field measurements have shown that acetone can be taken up by the ocean, but under high biological activity it can also be released (Zhou and Mopper, 1997; Williams et al., 2004; Sinha et al., 2007; Taddei et al., 2009).

1.2.3. Acetic acid

Among all the organic acids, formic acid (CH_2O_2) and acetic acid ($C_2H_4O_2$) are the most abundant in the troposphere (Grosjean, 1989; Jardine et al., 2011). The sources for acetic acid are anthropogenic emissions (Kawamura et al., 1985; Puxbaum et al., 1988; Talbot

et al., 1988; Grosjean, 1989; Shaw et al., 2007), biomass burning (Talbot et al., 1988; Hartmann et al., 1989; Yokelson et al., 1999, 2003), emissions from soil (Sanhueza and Andreae, 1991; Paulot et al., 2011) and vegetation (Andreae et al., 1988; Talbot et al., 1988; Kesselmeier and Staudt, 1999; Kesselmeier, 2001) as well as secondary production (Andreae et al., 1988; Grosjean, 1989; Grosjean et al., 1994; Tyndall et al., 2001; de Gouw et al., 2005; Dillon and Crowley, 2008). Secondary production comprises ozonolysis of alkenes (Calvert and Stockwell, 1983; Grosjean, 1992; Grosjean et al., 1994; Grazyna E. Orzechowska and Paulson, 2005) and reactions of acetyl peroxy radicals with HO_2 or other peroxy radicals (Madronich and Calvert, 1990; Tyndall et al., 2001; Dillon and Crowley, 2008; Paulot et al., 2011; Groß et al., 2014). In remote areas acetic together with formic acid are responsible for the acidity of precipitation (Keene and Galloway, 1988). Keene et al.(1984) report that organic acids contribute to 18-35 % to volume weighted free acidity in central Virginia, but their impact on acidification in the long term perspective is of no importance, because they are easily consumed by microorganism. Yu et al. (2000) report that acetic acid does not form aerosols due to its high volatility. But the acid can be adsorbed on the surface of aerosols (Andreae et al., 1988) and thereby alter the hygroscopicity because of its high polarity (Yu, 2000). This process facilitates the growth of the aerosols and enhances the possibility of a particle to become a cloud condensation nuclei (CCN). These CCN in turn influence precipitation and the earth's radiation budget (e.g. Charlson et al., 1987). Flux measurements of formic and acetic acid were performed in the tropics by Sanhueza et al. (1991) and it was found that the acids were consumed in forest soil while they were emitted from savanna soil. When savanna soil is watered, the formic acid emission flux decreases dramatically while the acetic acid flux increases. This has been explained by the high solubility of formic acid, which stays in the wet soil, and the biological production of acetic acid (Sanhueza and Andreae, 1991). The major sinks are wet and dry deposition (Andreae et al., 1988; Paulot et al., 2011), because the chemical depletion in the atmosphere is rather slow (Grosjean, 1989). The overall atmospheric lifetime amounts to 2.3 days (Paulot et al., 2011) while the lifetime with respect to OH is 16 days ([OH] = 10^6 molec/cm^3, k= 6.9×10^{-13} cm^3 molec^{-1} s^{-1} from IUPAC[3]). Paulot et al. report the global budget for acetic acid shown in Table 1.3: It becomes clear that secondary production from biogenic precursors represents the major source of acetic acid. According to Warneck (2000) the imbalanced budget requires a further source, which is most probable the oxidation of hydrocarbons. But the comparison to Paulot et al. (2011) rather suggests an overestimation of the deposition rates. The behavior of acetic acid during marine boundary layer transport is investigated in chapter 4.

[3]http://iupac.pole-ether.fr/index.html; accessed on 12th of July 2016

Table 1.3.: Global atmospheric budget of acetic acid calculated by Warneck (2000) and Paulot et al. (2011)

	Warneck 2000	Paulot 2011
Sources		
Photochemical production		
Biogenic	44.1	57.3
Anthropogenic and biomass burning	/	1.3
Direct emissions		
Anthropogenic	0.006	0.4
Biofuel burning	/	6.9
Biomass burning	12.6	11.2
Cattle	/	2.4
Soil	1.4	3.4
Terrestrial vegetation	4.2	2.6
Sum	62.3	85.5

Sinks		
Photochemical reactions	/	24.8
Dry deposition	102.1 (land) 37.8 (ocean)	31.3
Wet deposition	24 (land) 18 (ocean)	27.1
Dust	/	2.4
Sum	181.9	85.6

1.3. Intermediate-volatility organic compounds (IVOCs)

Compounds with an effective saturation concentration between 10^3 and $10^6\,\mu g/m^3$ are classified as intermediate-volatility organic carbons. These values correlate with a carbon number between C_{10} to C_{20} (Tkacik et al., 2012). IVOCs can have biogenic or anthropogenic sources, for example emissions from gas and diesel vehicles (Tkacik et al., 2012). The most important proxy for biogenic IVOCs are sesquiterpenes (C_{15} terpenoids), which are emitted from vegetation, but their emissions vary greatly between different plant species (Arey et al., 1995; König et al., 1995; Helmig et al., 1999; Kesselmeier and Staudt, 1999). IVOCs play an important role in the production of secondary organic aerosol (SOA). Tkacik et al. (2012) studied the SOA yields of various IVOCs and found that branched alkanes reached a lower yield than the unbranched C-equivalent. Furthermore, the SOA yield of cyclic alkanes is similar to linear alkanes which are 3 or 4 C atoms larger (Tkacik et al., 2012). In the Rocky Mountain Biogenic Aerosol Study 2011, Chan et al. (2016) measured various IVOCs: Alkanes were in the range of 0.03-0.1 pptv, PAHs showed values between 0.03 and 0.17 pptv and sesquiterpenes together with other terpenoids lay in the range of 0.03-0.36 pptv (Chan et al., 2016). It becomes clear that the mixing ratios of IVOCs are

several magnitudes lower than the ones that would be expected for VOCs or OVOCs due to their high uptake rates and reaction rates with OH and ozone.

1.3.1. Polycyclic aromatic hydrocarbons (PAHs)

Many PAHs are regarded as carcinogenic (Nisbet and LaGoy, 1992; Boffetta et al., 1997; Boström et al., 2002) and an overview of the most important PAHs is shown in Figure 1.3. Molecules with 2- 4 rings are gaseous while those with 5 or more rings are mainly affiliated with particles (Vione et al., 2004). Therefore, PAHs can also be found in urban dust (e.g. Takada et al., 1990; Nielsen et al., 1999) as well as in water and soil samples (e.g. Wild and Jones, 1995; Fernandes et al., 1997; Yunker et al., 2002). PAHs are mainly produced by incomplete combustion processes (e.g. Ramdahl et al., 1983; Benner Jr. et al., 1989; Venkataraman and Friedlander, 1994; Khalili et al., 1995; Schauer et al., 1999; Boström et al., 2002; Yang et al., 2005), they are thermally stable and have a low vapor pressure (Pozzoli et al., 2004). Boström et al. (2002) report that modern diesel vehicles emit 5 times more PAHs than modern gasoline cars. Older cars with obsolescent catalytic converters produce 5- 10 times more PAHs than modern ones (Boström et al., 2002). But the major source is residential and commercial biomass burning, which accounts for 60.5 % of the total sources. Motor vehicles contribute to 12.8 %, open field biomass burning (e.g. deforestation or wildfire) to 13.6 % (Shen et al., 2013). The lifetime of the PAHs is less than 1 day and their main sinks are the reactions with OH, ozone, NO_2 and NO_3 to form more polar and therefore more water soluble compounds (Boström et al., 2002; Vione et al., 2004). Another important sink for PAHs, which are associated to particulate matter, is deposition. Heterogeneous and multiphase reactions on aerosols occur much slower than in the gas phase (Vione et al., 2004). Due to the thus longer lifetime, long distance transport is possible (Vione et al., 2004). Also their toxicological effect can be different when adsorbed on particles. Bofetta et al. (1997) state that heavy exposure to PAHs increases the risk of lung, skin and bladder cancer. The exposure arises from different industries and occupations, e.g. coke production, tar distillation, roofing, road paving and also work that involves the exposure to diesel engine exhaust (Boffetta et al., 1997). To estimate the impact on health of single PAHs the "toxic equivalent factor" (TEF) was developed. Benzo[a]pyrene was ascribed to a TEF value of 1 as a reference. Anthracene for example has a relative value of 0.01 while naphthalene, fluorene and phenanthrene show a value of 0.001 (Nisbet and LaGoy, 1992). Shen et al. (2013) investigated 16 PAHs from 69 sources in the time frame from 1960 until 2030. In 1995 the highest annual global emission of 592 Gg was reached. A decrease to 499 Gg in 2008 was recorded. The main sources vary for different countries: For example the main source in Brazil is deforestation/wildfire while in India it is indoor firewood burning. Simulations for the time period 2009-2030 result in a decline of PAH emissions of 46 - 71 % for developed countries and 48 - 64 % for developing countries (Shen et al., 2013). Measurement of PAHs and other IVOCs can be found in chapter 5.

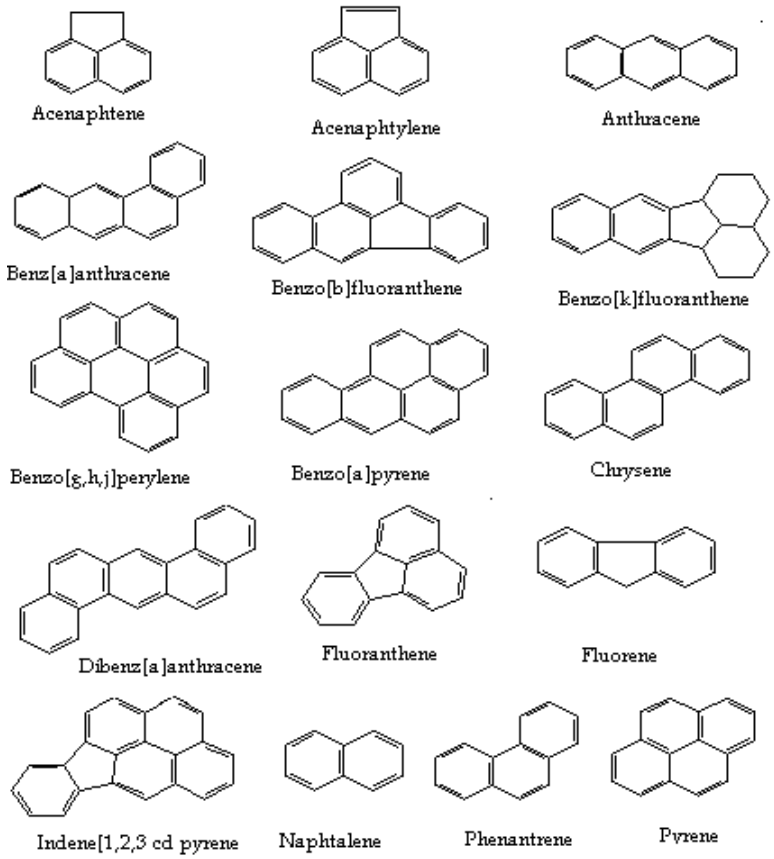

Figure 1.3.: Molecular structures of important PAHs. Source: (Mugica et al., 2010).

1.3.2. Summary

In this thesis the measurement of OVOCs and IVOCs was targeted.
The results of the inter-comparison campaign described in section 3 show that the PTR-TOF-MS records OVOCs with high reliability. Ideas for improvement originating from the inter-comparison were applied for the CYPHEX campaign, which is addressed in chapter 4. In the CYPHEX data the behavior of the OVOCs methanol, acetone and acetic acid in particular in the marine boundary layer (MBL) was investigated.
Although IVOCs play an important role in particle formation and have a strong impact on human health, they are poorly understood. Therefore, as a last project for this thesis, IVOCs were measured from car exhaust, which is described in chapter 5.

2. General information about the Proton Transfer Reaction - Time of Flight - Mass Spectrometer (PTR-TOF-MS)

2.1. Method

The measurement technique of a PTR-TOF-MS comprises three stages: the production of the primary ions in the ion source, proton transfer reactions in the drift tube and detection by mass spectrometry (see figure 2.1). During the ionization step oxonium ions (mass to charge ratio (m/z) 19 amu, H_3O^+) are produced from water vapor, which is ionized in a hollow cathode discharge. The proton transfer from a oxonium ion to a sample molecule occurs in the adjacent drift tube, which is maintained at 2.2 mbar and 60 °C. The protonation process is soft (i.e. much lower than it is typical for electron ionization, 70 eV) so that almost no fragmentation takes place and the detected ion is in most cases the molecular mass of the sample plus one proton. After the drift tube the protonated molecular ions are accelerated by an electric field to the same kinetic energy, focused via a lens system and led into the extraction region. There a pulse of ions is sent vertically to the flow direction into the flight tube. In this part the sample ions are separated according to their mass-to-charge-ratio, which determines their velocity. Since all ions begin with the same kinetic energy, the smaller masses will travel faster through the flight tube. A multi-channel plate serves as detector. The PTR-TOF-MS instrument can simultaneously measure compounds with a proton affinity higher than water, e.g. aldehydes, ketones, aromatic compounds, alcohols, organosulphur compounds, carboxylic acids and ester compounds. This is a distinct advantage over the quadrupole version of this instrument, which must sequentially analyze the ions produced at unit amu resolution. The PTR-TOF-MS is characterized by its high time resolution, mass resolution and exquisite sensitivity. Online measurements can be performed at parts per trillion levels. Determination of the limit of detection will be further explained in section 2.2.6. While a PTR-quadrupole-MS can distinguish only integer masses, (1 amu, e.g. one peak on m/z 69), the PTR-TOF-MS is able to separate isobaric masses. The instrument can differentiate for example between furan with a mass of 69.0335 amu and isoprene, which has a mass of 69.0699 amu. The higher mass resolution permits a much higher degree of specificity and confidence in molecular identification. For this thesis a PTR-TOF 8000 by Ionicon Analytik (Innsbruck, Austria) was used. More information about the original design can be found in Graus et al. (2010), Lindinger et al. (1998) and de Gouw et al. (2007) and an example of field application is given in Veres et al. (2013).

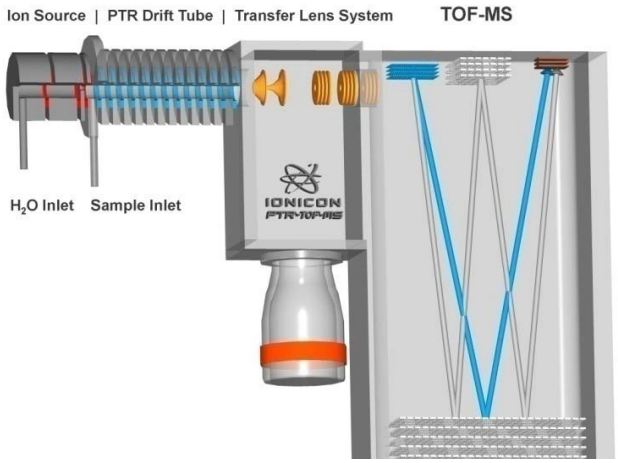

Figure 2.1.: Sketch of the PTR-TOF-MS (source: IONICON)

2.2. Technical details

2.2.1. Inlet system

The inlet system of the PTR-TOF-MS (see Figure 2.2) consists of a 1/8" (0.318 cm) PEEK tubing, which is flexible, insulated and permanently heated to 60 °C (1). All the following parts are situated inside an insulated body, where the temperature is also continuously maintained at 60 °C. Under standard conditions, the minimum required flow into the PTR-TOF-MS amounts to ca. 30 standard mL/min, but in the section prior to the first PEEK T-piece (2) the flow can be increased up to 1 L/min by means of a mass flow controller (3) to minimize wall losses. The three way valves (4 a and b) are regulated by an electronic control module "V25", which is described in the dissertation of A. M. Johnson (2011). The valves guarantee the automatic switching between sample air and background measurement. The air is either directly led into the ion source or bypassed through the catalytic converter (5), in which the volatile organic compounds present are oxidized at high temperature in the presence of platinum to CO_2 and H_2O. To perform mass scale calibration 1,3,5-trichlorobenzene is permanently added to the sample air by a permeation source (6). The pressure controller (7) ensures that the pressure inside the PTR-TOF-MS remains constant. All lines are built of 1/16" (0.159 cm) Teflon or PEEK tubing. Only the parts directly in front of and after the second T-piece (8) have a smaller inner diameter of 0.18 mm and 0.25 mm, respectively. These line restrictions create a drop in pressure so that 2.2 mbar can be maintained in the drift tube (not shown). The ion (9) source is aging over time and has to be cleaned from carbon coating every 3 to 6 months.

2.2.2. Tuning

In general, the PTR-TOF-MS consists of three main parts: the ion source, the drift tube and the MS-part, where the analytes are separated. Each of these parts is controlled

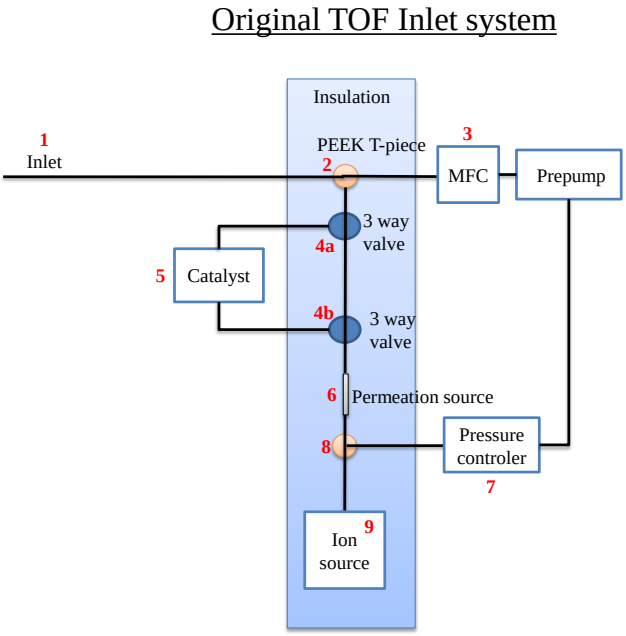

Figure 2.2.: Inlet system of the PTR-TOF-MS

by different software: The PTR-Manager (for ion source and drift tube) and the TPS controller (TOF). During all measurements documented in this thesis, except for the car exhaust experiment, the drift pressure was maintained at 2.20 mbar and the drift voltage 600 V (E/N 137 Td) in the PTR Manager. All other voltages in both programs were adjusted at regular intervals to optimize the sensitivity of the instrument. The aim of the tuning process was to increase the signal of the primary ions on m/z 19, which are measured via their oxygen isotope on m/z 21 due to saturation of m/z 19. The values of m/z 21 should show at least 3500 cps. Furthermore, oxygen and the water clusters should be kept below 10 % of the primary ion signal and a resolution of at least 3500 - 4000 for m/z 21 should be gained. A third software, the TOF DAQ recorder/viewer, was used to display and record the spectra and traces of selected compounds. It should be kept in mind that the ^{18}O isotopes of the oxonium ion (m/z 21 instead of m/z 19), of the water cluster (m/z 39 instead of m/z 37) and of oxygen (m/z 34 instead of m/z 32) are regarded, because the actual signals are saturated and cannot be analyzed. In the following the important settings and their influence are explained:

1. PTR Manager

   - SV (source valve): A valve that controls the vent going out of the ion source and into the pump, which leads to the exhaust. The value should be set between 38 and 45 %. Oxygen decreases and the water cluster increases with decreasing SV.
   - H_2O flow: An increase of the water flow into the ion source leads to higher

signals for m/z 21 and m/z 39 and lower oxygen, as long as it does not exceed 8 to 9 standard mL/min. Normally it has a set point of around 5 standard mL/min.

- Us and Us_O: These are the voltages at the end of the ion source, which determine the transfer time of the ions from the source into the drift tube. If they are small the transfer time is long and more collisions can take place. For the production of H_3O^+ they should be rather small to guarantee a high number of collision and therefore a high production rate of primary ions (Us between 80 and 120 V; Us_O between 60 and 100 V). If O_2^+ is used as primary ion the voltages should be high so that the extraction into the drift tube is fast, because O_2^+ ions are produced very quickly.
- Ihc: This is the current inside the ion source. It normally lies between 3 - 5 mA and increases the m/z 21 signal with higher values. The older and thus more coated the ion source is, the higher the current needs to be set. Its limit is 10 mA. But already before the limit is reached, the ion source should be cleaned, in general every 3 to 6 month.
- U_{drift} and Udx represent the voltages at the drift tube and were set to 600 V and 35 V, respectively, in most of the measurements described here. Only during the measurement of car exhaust the voltages were reduced. Lower voltages promote clustering, but lessen fragmentation in the drift tube.

2. TPS controler
   Here only the important settings are explained, for more details please refer to the Ionicon manual.

   - Multi channel plate (MCP): The MCP serves as detector. An increase of its voltage leads to a higher primary ion signal. However, a too high voltage will shorten the lifetime of the detector. The best way to find the optimum value is to increase the voltage starting from circa 2000 V (new MCP) in 50 V steps and compare each time the signal strength of a high mass, e.g. 1,3,5-trichlorobenzene on m/z 181.9373. The reason is that the amplification of the MCP is proportional to the velocity of the ions. Since higher masses have a lower velocity, they are discriminated and the MCP should be adjusted using a high mass. If the signal changes less than 10 %, the plateau of best transmission has been reached and the instrument can be operated in this mode until the detector degrades and the voltage needs to be reset.
   - Reflector backplane and reflector grid: The reflector is situated in the lower part of the flight tube and serves the purpose of sending the ions back towards the detector. Thereby a V-shaped flight path is created. It is very sensitive and should be changed in small steps only.
   - Hardmirror: This mirror is used to change from the so called V-mode into the W-mode. This means that the flight path of the ions will be doubled so that it follows a W shape instead of a V-shape. Its values stay zero in the V-mode. For

all experiments shown in this work the V-mode was used, because the detection limit is lower than in the W-mode. The advantage of the W-mode, on the other hand, is a higher mass resolution.

- Drift: This is the acceleration voltage in the time-of-flight part and normally stays at 3000 V.
- Post. Acc.: It is the last grid before the ions reach the detector and it can have values between 3000 and 5000 V.
- Skimmer: This is the first lens after the drift tube and should be changed in 10 V steps or less.
- Lens system (Lens 1, 2, Ion Extractor, Primary Beam): The lenses focus the ion beam, they should be changed in 1 or 10 V steps and can be used to reduce an inadvertent shoulder on the left side of the m/z 21 peak.
- Deflector and Defl. Flange: These are the plates that focus the beam. Large changes should be performed on both values for the same amount and in the same direction.
- $U_{\text{-low}}$ and $U_{\text{+high}}$ as well as $U_{\text{-high}}$ and $U_{\text{+low}}$ control the extraction region. $U_{\text{-low}}$ and $U_{\text{+high}}$ lie roughly between 650 V and 750 V (absolute values) and send a pulse of ions into the time-of-flight part. During one pulse the values of $U_{\text{-high}}$ and $U_{\text{+low}}$, which are relatively low (ca. 25-50 V), are set in the extraction region. In that time no pulse is created and ions get lost. In later data analysis procedures corrections for this loss are applied.

In general, the tuning should be started with a parameter that has a large effect on the signal for example "Reflector Backplane" of "Reflector Grid". If the isotope of the primary ion m/z 21 is close to saturation, which can be seen when an unreal "ghost peak" next to m/z 21 occurs, then the amplification is too high and should be reduced by adjustment of a screw in the back of the instrument. The values of the amplification lie roughly between 15-25 mV. By means of the TOF DAQ viewer the range of the mass spectrum can be changed and typically extends from mass 0 to mass 350. The range is intended to cover all important signals, otherwise the heavier molecules will be detected in the beginning of the next spectrum.

2.2.3. Measurement

To determine the mixing ratio of the analyte correctly it is necessary to know the internal background of the instrument for the specific compound. Therefore, "clean air" needs to be measured to quantify the amount of the species inside the PTR-TOF-MS itself. Since the sensitivity of the instrument changes with humidity, it is imperative to measure the background at the same humidity as the ambient air. For this purpose the sample air is led through a catalytic converter containing platinum/palladium pellets, which are heated to 320 °C. Inside the catalyst all VOCs are burned to CO_2 while the humidity level stays unaltered since the H_2O produced in VOC combustion is minimal compared with ambient levels. Some compounds, such as acetaldehyde or DMS, cause problems, because under

certain conditions they are not quantitatively combusted in the catalyst and can even be produced inside the catalyst. Acetaldehyde is known to be formed via a heterogeneous oxidation of unsaturated organic substances by ozone (Northway et al., 2004; Goldan et al., 2004) while the reason for the signal at the mass of DMS is so far unknown. This can potentially lead to an underestimation of the actual mixing ratios of these compounds, as then an artificially high background would be subtracted from the signal. In the worst case the background cannot be used at all if the values emitted from the converter are even higher than in ambient air. This problem has been addressed in more detail in chapter 2. For some species it takes several minutes until the background reaches a stable level. Therefore, it is necessary to find an appropriate length and frequency of the background measurement so that the steady states are properly reached without losing too much sample time. For example during the CYPHEX campaign the background was determined every two hours for twenty minutes. This was primarily determined by acetaldehyde.
Changes in temperature during the measurement can cause the flight tube to expand or shrink to a very small degree. This can lead to significant mass shifts, because the flight path for the ionized sample molecules is slightly different. To correct for this effect compounds, whose exact mass is known and which are permanently measured, are necessary. In the H_3O^+ mode, the isotope of the H_3O^+ ion (m/z 21.022087) and the isotope of the water cluster (m/z 39.0326) were used, because they can be found in each spectrum. In the NO^+ mode the H_3O^+ ion (m/z 19.0178) as well as the $NO[O^{18}]^+$ ion (m/z 47.9966) were chosen. For an accurate mass calibration a higher mass is needed as well. Therefore, 1,3,5-trichlorobenzene (m/z 180.93731, protonated) or 1,3-diodobenzene (m/z 330.8475, protonated, for the measurement of high masses) were permanently bled into the sample stream as an internal standard by a permeation source. The mass scale calibration can be performed automatically or manually by use of the program "TOF DAQ viewer".

2.2.4. Data analysis

Since the PTR-TOF-MS produces a large amount of data (ca. 300 MB per day at an 1 min time resolution) a powerful software tool for data analysis is necessary. A mass spectrum, which reaches up to a mass-to-charge ratio of e.g. 500, consists of 400000 data bins (0.1 ns bin width, pulsing frequency of ca. 25000 Hz). To process the data, the program "PTR DATA ANALYZER" is used (Müller et al., 2013). The software tool performs several different corrections of effects, which occur due to technical limitations, and applies methods to determine the peak shape and calculate the peak area. In the following, these procedures are described briefly, for detailed information please refer to Müller et al. (2013) (Müller et al., 2013).

- After the impact of one ion the detector shows a dead time of 10 ns. Within that time frame no further ions can be detected. Poisson counting statistics is used to correct for this problem.

- The baseline is corrected for each m/z unit separately by subtracting a linear fit between the baseline before and after a peak.

- Due to temperature changes during measurement, the mass scale can shift slightly and therefore precise mass scale calibrations are imperative. To achieve this, compounds with known non-isobaric masses, to which the axis can be adjusted, are necessary.

- From the masses chosen for the mass scale calibration the reference peak shape and the expected peak widths are calculated. These features are applied to detect and fit other peaks.

- If the time resolution is very high and therefore the signal intensity reduced, stick spectra calculations represent the method of choice. In a first step the peaks are analyzed from an integrated spectrum of the whole measurement. These time integrated spectra guarantee that the signals are acceptably high so that time intervals can be correlated to specific peaks. Within these intervals stick spectra add up the ion counts for the data with high temporal resolution. Using a correction factor the stick spectra were adapted to the integrated spectrum.

- As a last amendment the mass discrimination corrections should be mentioned. During the time a pulse of ions flies through the TOF path, other ions pass the drift tube without entering the flight path and thus get lost. The loss rate is higher for lighter ions, because they have a higher velocity and, hence, scatter across a larger range. To account for this discrepancy in the transmission all signals are multiplied by the factor:

$$\sqrt{\frac{(m/z)_{max}}{m/z}} \tag{2.1}$$

  Here $(m/z)_{max}$ coincides with an ion that has the flight time of 1/(TOF pulsing frequency).

The software produces a result file in h5 format. Post processing was performed using the program "Igor Pro 6.32", where specific macros for PTR-TOF-MS data analysis were written by different members of our group. The PTR DATA ANALYZER is also able to normalize the data, but in our case normalization was executed later on in Igor depending on the primary ion (H_3O^+, NO^+ or $O_2{}^+$). For this reason, the "duty-corrected-area" of a peak was loaded from the result.h5 file. Normally oxonium ions were used and the signals were therefore normalized to H_3O^+ and the first water cluster by means of the following formula:

$$[R^+]_{ncps} = \frac{[R^+]_{cps} * p * 10^6 * 298.15}{([m21] * 500 + [m39] * 250) * T * 2} \tag{2.2}$$

Here $[R^+]_{ncps}$ is the signal of the reagent ion in normalized counts per second (ncps), $[R^+]_{cps}$ the signal of the reagent ion in counts per second (cps), p the pressure, T the temperature, [m21] the counts per second of the ^{18}O isotope of H_3O^+ and [m39] the counts per second of the ^{18}O isotope of the first water cluster of the primary ion. The factors 500 and 250 are necessary to transform the signal of the isotopes into the signal of the actual ion, which

cannot be measured directly due to saturation. ^{18}O atoms naturally occur to a percentage of 0.2 % or a possibility of 1:500. If an ion contains one oxygen atom than the signal of the isotope has to be multiplied by 500 to gain the signal of the ^{16}O equivalent. If an ion contains two oxygen atoms, than the possibility that one is an ^{18}O isotope is twice as high, so 1:250. That is why the signal of m/z 39, which contains two oxygen atoms, must be multiplied by 250. Furthermore, it is consensus that the signal is normalized to a temperature of 298.15 K and a pressure of 2 mbar. As a next step the background needs to be subtracted. Hence, a key is created, which differentiates between the background and the actual measurement. After subtraction the data is divided by the calibration factors to transform normalized counts per second into parts per billion. How the calibration factors were determined can be found in chapter 2.2.5.

2.2.5. Calibration

To accurately convert the signal of the instrument into parts per billion mixing ratios, regular calibrations to a standard of known mixing ratio are required. To this end a commercial gas standard (Apel-Riemer Environmental, Inc.) containing 14 compounds was used. Apel-Riemer prepares its gas standards gravimetrically in a high-pressure aluminium cylinder by using calibrated microbalances and microsyringes. Since the sensitivity of the PTR-TOF-MS depends on humidity, calibrations need to be performed at different humidity levels. In Figure 2.3 a schematic diagram of the setup can be found. Synthetic air was used for the dilution of the calibration gas, which contained mixing ratio levels of around 500 ppbv. To create different humidity levels the zero air flow was split into two streams, one being completely dry and the other being humidified by means of a wash bottle. The ratio of the flows was adjusted by two mass flow controllers (MFCs). The buffer bottle and the Teflon filter prevented water aerosols to enter the instrument. The humidity was quantified by calculating the ratio of the water cluster isotope and the oxonium isotope signals (m/z 39 : m/z 21). For zero air 1/4 “(0.635 cm) and for the calibration gas 1/8” (0.318 cm) Teflon tubing was used. Where both flows meet, the 1/8” line was inserted into the 1/4 “ tubing to ensure accurate mixing. An overflow, from which the instrument drew a minimum of ca. 30 standard mL/min, was established. To guarantee accurate data analysis, calibrations should be performed at two different humidities at the least. Each calibration in turn should consist of three to four different mixing ratio steps. Time permitting, even more steps are recommended. The levels should lie in the range of the measured sample air, which means typically between 0.5 and 10 ppbv for ambient air. Figure 2.4 shows a typical calibration run for acetone with four different steps as well as background measurements in the beginning and at the end. From each step a stable section was selected and averaged. Then the averaged counts per second were plotted against the expected values in ppbv. These were determined by multiplying the content of the calibration gas bottle by the dilution factor, which is the ratio of the calibration gas flow and the zero air flows. A linear fit was applied, because the instrument acted linearly for all calibrations performed in this work over more than 3 orders of magnitude from 10 pptv to 50 ppbv. The slope represents the calibration factor m given in ncps/ppbv. To convert signals measured by the PTR-TOF-MS into ppbv the values in ncps need to be divided by m. In general, it was found that the sensitivity of the instrument decreased

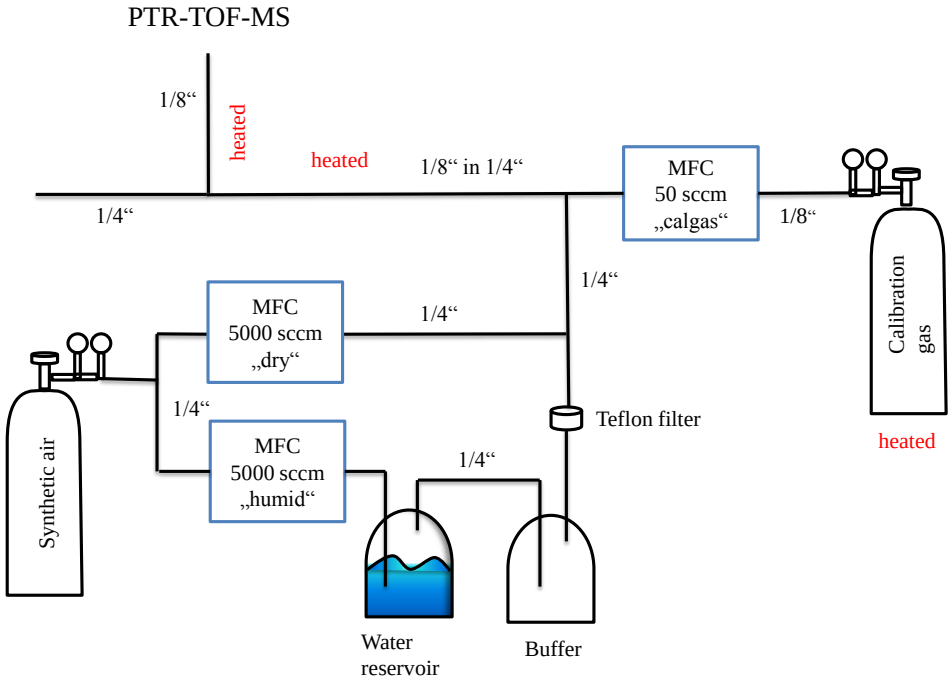

Figure 2.3.: Calibration system

exponentially with increasing humidity for most of the compounds. When the humidity was increased from 0 to 10 % the sensitivity dropped relatively strongly while during a change from 40 to 60 % almost no change occurred. It was therefore necessary to fit the determined calibration factors exponentially depending on humidity for most of the substances. For some compounds the humidity dependency was slightly different so that the fit had to be made for each compound individually. Isoprene for example showed almost no humidity dependency while benzene was strongly dependent on the humidity level, because it does not react with the water cluster. Examples of the humidity dependency measured during the campaign in Cyprus can be found in Figure 2.5. The fit for trimethylbenzene (lowest panel) was common for many other compounds while isoprene needed to be fit linearly. The reason why isoprene is almost independent of humidity changes is that it has roughly the same rate coefficients for the reaction with the primary ion as well as the water cluster (Smith et al., 2001; Warneke et al., 2001). Benzene, on the other hand, did not reach a linear domain within the humidity range displayed here. This shows its strong humidity dependency. To apply these calibration factors the humidity of each single measuring point was considered and the factor for that specific humidity was employed. A similar procedure was followed when the sensitivity changes over time. A linear fit between the calibration factors measured at different times was performed. The respective factor calculated for the specific time of measurement was then applied. For implementation, macros were written in Igor Pro to automate the procedure.

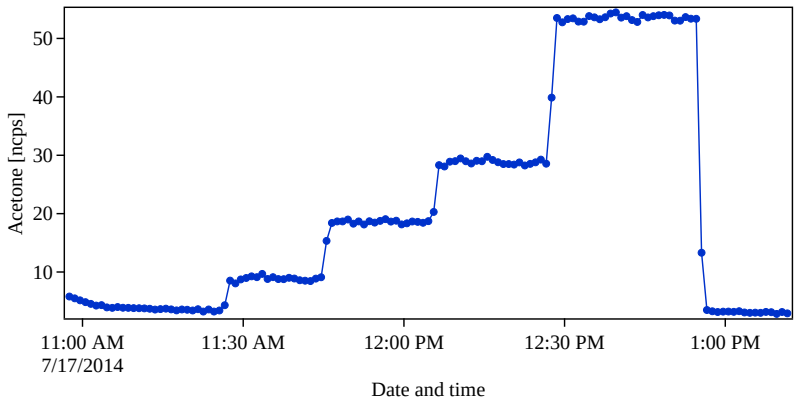

Figure 2.4.: An example calibration of acetone between 0.3 ppbv and 2.5 ppbv

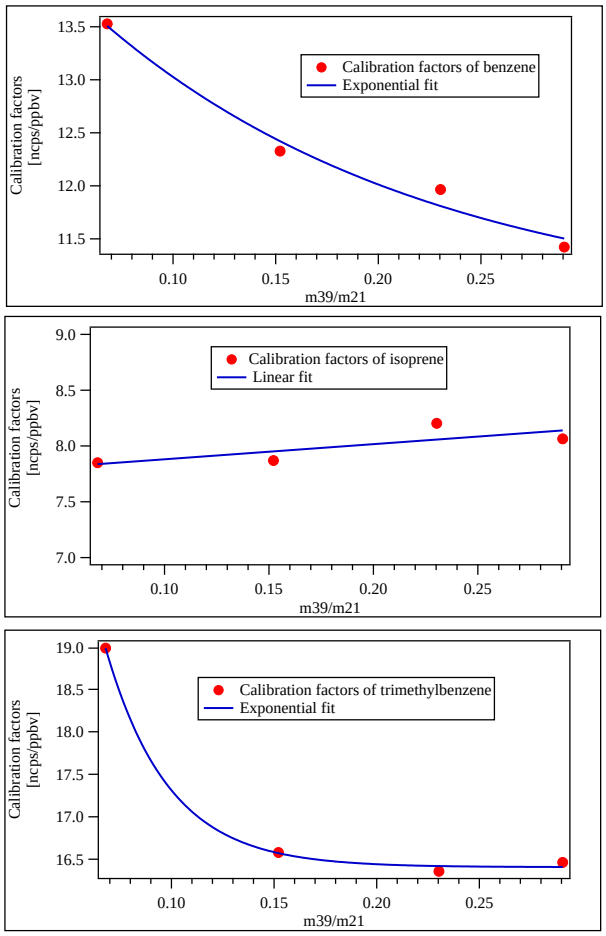

Figure 2.5.: Calibration factors in ncps/ppbv of benzene, isoprene and trimethylbenzene (from top to bottom) plotted against the ratio of the water cluster and the primary ion

2.2.6. Error calculation

Systematic and statistical errors were determined separately by means of the estimate of the largest possible error. The following formulas were applied:

$$Sys_{error}[\,\%] = \sqrt{a^2 + b^2 + t^2 + h^2 + c^2} \tag{2.3}$$

Thereby a is the error of the calibration gas bottle given by the producer (5 %), b is the error of the mass flow controler used for regulation of the flows during the calibration given by the company (1 %), t is the error occurring due to the changes of sensitivity over time, h the error due to the humidity dependency of the sensitivities and c is the calibration error. t represents the percentage variation of the calibration factors over time. It was determined by calculating the standard deviation and the average of the calibration factors from the very first and the very last calibration. Their ratio equals the percentage error. If calibrations were performed at different humidities, this ratio was calculated for the highest and the lowest humidity and the largest percentage was used. The parameter h is the ratio of the standard deviation and the average of the calibration factors measured for different humidities for one specific day. This calculation was performed for each calibration day and the largest value was applied. As explained in chapter 2.5 the slope of the linear fit between the measured and the expected values from a calibration is the calibration factor. The parameter c was calculated by dividing the standard deviation of the linear fit by the slope of the fit for each calibration. The highest percentage was employed.
The statistical error is represented by the noise of the measurement calculated by dividing the standard deviation of one calibration step (Δcal), which lies in the range of the sample measurement, by the average value of this step ($calstep$).

$$Stat_{error}[\,\%] = \Delta cal/calstep \tag{2.4}$$

Both errors were combined to give the overall error:

$$Overall_{error}[\,\%] = \sqrt{Sys^2_{error} + Stat^2_{error}} \tag{2.5}$$

Three times the standard deviation of the background (3σ) was taken to define the detection limit. The standard deviation was derived for each background measurement of one experiment separately and the highest value was used.

3. Inter-comparison campaign for oxygenated volatile organic compounds (OVOCs) at the meteorological observatory Hohenpeißenberg

3.1. Motivation

The goal of this measurement campaign was to compare the performance of 8 different online VOC instruments and 2 cartridge sampling systems when measuring oxygenated volatile organic compounds under various conditions. OVOCs play an important role in the atmosphere and can be present in high mixing ratios even in remote regions (see chapter 1, (Singh et al., 1995, 2001). Some of them photolyze to form HOx, which can increase the production of ozone in the upper troposphere (Singh et al., 1995; Wennberg et al., 1998; Müller and Brasseur, 1999). Furthermore, some OVOCs, especially acetaldehyde and acetone, can produce peroxyacetylnitrate (PAN), that presents a reservoir for NO_2 (Singh and Hanst, 1981). OVOCs were measured all around the world: in Europe (Lewis et al., 2005; Legreid et al., 2007; Yang et al., 2013), the U.S. (Riemer et al., 1998), South America (Bon et al., 2011), in China (Louie et al., 2013) as well as over the Indian Ocean (Wisthaler et al., 2002), the Pacific (Singh et al., 1995, 2001, 2004) and the Atlantic (Singh et al., 2000). However the accuracy and precision of the measurements might be questioned due to the diverse nature of the analytical methods. Therefore, inter-comparison campaigns are essential to bring insights into potential systematic measurement problems and put the values reported in publications thus far in perspective. Some OVOC inter-comparisons can be found in literature, but in very few PTR-TOF-MS instruments were used. The measurements have been mainly performed with a PTR-quadrupol-MS (PTR-MS). Apel et al. (1998) compared cartridge systems, GC-FID (Gas Chromatograph with a Flame Ionization Detector) and GC-MS (Gas Chromatograph combined with a Mass Spectrometer) instruments at a rural site in Nashville,Tennessee. Around ten years later Apel et al. (2008) conducted a large scale inter-comparison at the SAPHIR chamber in Jülich, Germany. 15 instruments took part, among them a PTR-TOF-MS, several PTR-quadrupole-MS, GC-FID and GC-MS systems. In the course of the New England Air Quality Study 2002 de Gouw et al. compared PTR-MS and GC-MS measurements from a ship cruise (de Gouw et al., 2003). They also performed airborne measurements in the Mediterranean using two differently configured PTR-MS systems, which showed good agreement (de Gouw et al., 2004). Kuster et al. (2004) compared amongst others acetone and acetaldehyde data from a PTR-MS and a GC-ITMS (Gas Chromatograph with a quadrupole Ion Trap Mass Spectrometer) during the Texas Air Quality Study 2000. In a deciduous forest Ammann et al. (2004) analyzed biogenic VOCs, some of them oxygenated, using a PTR-MS and a online GC-FID. During the Indian Ocean Experiment (INDOEX) 1999 Sprung et. al. (2001) compared PTR-MS data to AP-CIMS (Atmospheric Pressure Chemical lonization Mass Spectrometer) data. An overview over different inter-comparison campaigns, not

only comparing OVOCs, but also other VOCs, can be found in de Gouw and Warneke (2007). The inter-comparison campaign described here was the most comprehensive to date, made a valuable contribution to the so far gathered insights and led to a better understanding and an improvement of the measurement techniques.

3.2. Instrumentation

During the inter-comparison OVOC measurement results by Gas Chromatographic methods, cartridge sampling systems as well as various Proton Transfer Reaction-Time of Flight-Mass Spectrometry systems were compared. Ten different instruments from seven different groups took part in the campaign. In the following, emphasis will be placed on the PTR-TOF-MS data. The three participating groups working with a PTR-TOF-MS were: École des Mines de Dôuai, France (MD), Norwegian Institute for Air Research, Kjeller/ University of Innsbruck, Austria (NILU) and our group from the Max Planck Institute for Chemistry, Mainz (MPIC). The instruments were connected to a manifold and different gas standards at various humidities as well as ambient and spiked ambient air were measured. The positioning of the instruments relative to the inlet and the gas dilution unit can be found in the Figures 3.1 and 3.2.
The time resolution of our instrument was set to obtain one measurement every 30 s and background measurements were performed every hour for 15 minutes by means of a catalytic converter. Unfortunately our own converter was found to be contaminated when set in operation at the site so that we shared one with the NILU group (Parker Balston, Haverhill, MA). Instrumental details and operating conditions can be found in Table 3.3.

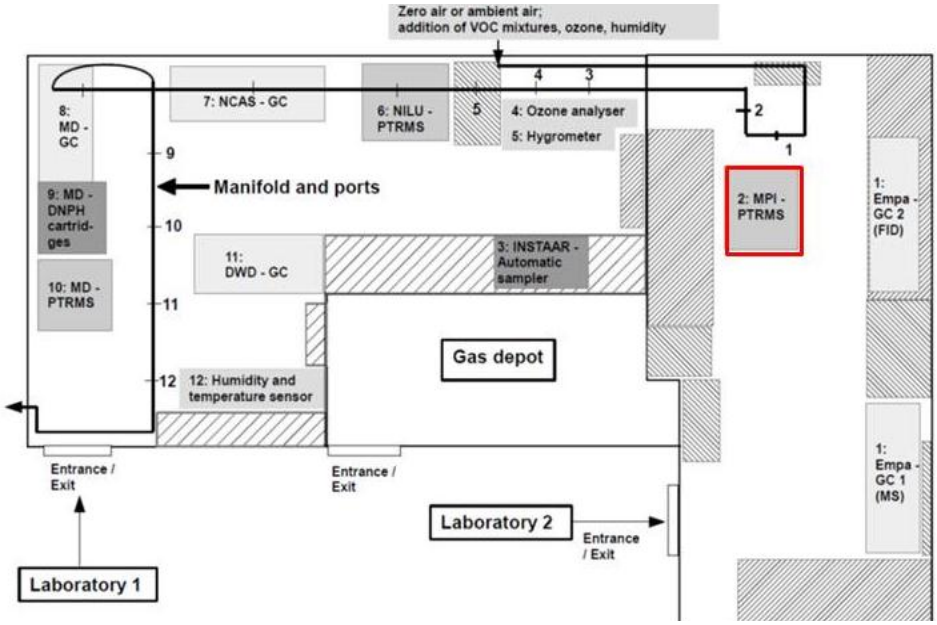

Figure 3.1.: Experimetal set-up for comparison (source: Deutscher Wetterdienst, DWD)

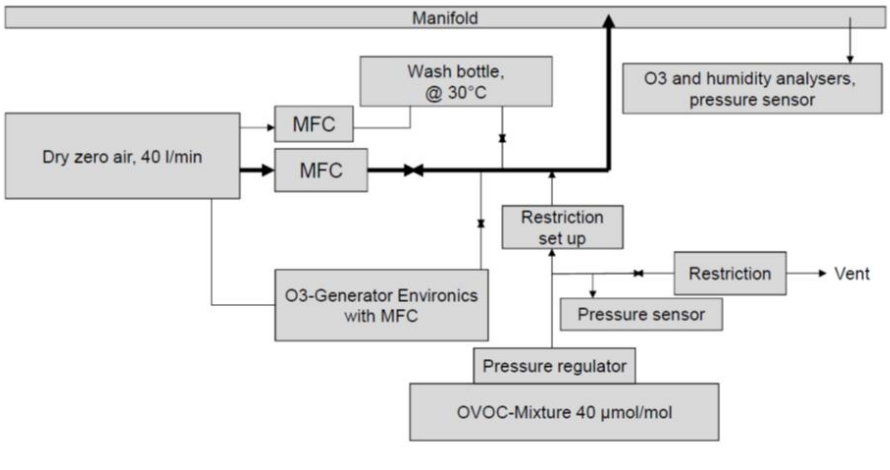

Figure 3.2.: A schematic diagram of the gas dilution system used in the comparison (source: Deutscher Wetterdienst, DWD)

	Model	Sampling line	Zero air	Standard	Resolution (m/Δm)	PTR operating conditions: Reactor Pres. (mbar)	Reactor Temp. (°C)	E/N (Td)	Flow rate (SCCM)	Primary H3O+ (cts)	m37/m19 (40-50% RH, amb. Temp.) (%)	m30/m19 (%)	m32/m19 (%)
Mines Douai	KORE Inc. 2nd generation	5-m PFA 1/4" / 50°C 1.2 SLPM 4-s residence time	Pt wool 350°C 1.5 SLPM	Restek (15-component mix), Praxair (9-component mix)	3000-5000	1.33	40	136	150	1.50E+05	≈ 24%	< 0.5	< 2
MPI	IONICON PTR-TOF 8000	1.2 m PEEK 1/16 " heated to 60°C 2m PFA 1/8" not heated 3-4 s residence time	Zero air from NILU catalyst	AiR® (14-component mix)	3500-4000	2.2	60	136-137	500	2.50E+06	about 15%	0.2	5.0
NILU	IONICON PTR-TOF 8000	1.75-m PFA 1/8" 0.5 SLPM / 40-55°C 0.7-s residence time	Pt/Pd catalyst (Parker Balston, Haverhill, MA) 320°C 2.0 SLPM	AiR® (11-component mix)	3500-4000	2.30	55	118	N/A	1.50E+06	≈ 31%	< 0.2	< 0.6

AiR® = Apel-Riemer Environmental Incorporated, USA.

Figure 3.3.: Operating conditions of the three PTR-TOF-MS systems (provided by Dr. Sébastien Dusanter from MD). (SLPM= standard liter per minute, PEEK= polyether ether ketone, PFA= perfluoroalkoxy alkane)

3.3. Experiments

The following experiments were performed using different gas standards (see Table 3.1 and 3.2:

1. At the beginning, zero air was measured under dry and humid conditions to establish the typical signals of a clean environment and to determine possible contaminations as early as possible.

2. In the second experiment the impact of humidity was investigated. OVOC Mix I (see Table 3.1) was diluted to 8 ppbv and measured at various humidities (dry, dew point = 14.5 °C (ca. 46 % at 27 °C) and dew point = -4 °C (ca. 12 % at 27 °C)). A rather high mixing ratio was chosen, because it can easily be measured by all systems. The different dew points were reached by leading a fraction of the dry zero air through a wash bottle filled with distilled water. By changing the ratio of the dry and the humidified flow using mass flow controler the humidity level was altered.

3. OVOC Mix I was used to measure different, typical ambient mixing ratios reaching from 60 pptv up to 8 ppbv to explore the range, especially at low levels.

4. Ambient and spiked ambient air was analyzed. The spiking was especially interesting, because the gas standard was measured in a different matrix than zero air. Measurements of the same mixing ratios of specific compounds can be different in zero air and in ambient air, because interferences with other molecules might occur.

5. Common Standard I, II, III (see Table 3.2) were investigated at dew point 5 °C.

6. A NMHC Mix as well as zero air were measured with and without O_3. When ozone is added, alkenes can undergo ozonolysis and are thus depleted while OVOCs are formed. Furthermore, ozone can react with wall coatings so that OVOCs are created as well.

The standards used in this study did not only contain OVOCs, but also VOCs like isoprene or benzene, which will also be shown in the next sections. The results should reveal whether the various instruments in the comparison delivered equivalent mixing ratios under the same conditions.

Table 3.1.: Compounds in "OVOC Mix 1 and 2"

Compound	OVOC Mix 1 [ppmv]	OVOC Mix 2 [ppmv]
Methanol	45	13
Acetone	40	24
MEK (methylethylketone)	46	15
MVK (methylvinylketone)	26	10
Acetaldehyde	30	16
Isoprene	41	40
Benzene	42	25
Toluene	44	15
Ethanol		10
2-Propanol (isopropanol)		8
Propanal		30
Butanal		25
Pentanal		15
Hexanal		2
Methacrolein		18
Benzaldehyde		0.4
Acetonitrile		18
Ethylacetate		25
Butylacetate		4
Eucalyptol (1,8-Cineol)		not determined
cis-3-Hexen-1-ol		not determined
cis-3-Hexenylacetate		not determined
Linalool		not determined

Table 3.2.: Contents of the standards “Common 1, 2 and 3”

Compound	“”Common1” [ppmv] NPL Standard DWD	“”Common2” [ppmv] Praxair standard	“”Common3” [ppmv] NPL Standard York
Benzene			4.85 ± 0.10
Propane			5.31 ± 0.11
Hexane	4.95 ± 0.25		4.85 ± 0.10
Methanol	4.99 ± 0.25	4.94 ± 0.10	
Furan		$2,96 \pm 0.15$	
2-Methyl furan		$2,98 \pm 0.15$	
Toluene		$2,98 \pm 0.15$	
Acetaldehyde	5.00 ± 0.25	$3,04 \pm 0.15$	4.98 ± 0.25
Tertbutylethylether (ETBE)		$2,93 \pm 0.15$	
Tertbutylmethylether (MTBE)		$3,31 \pm 0.17$	
Tertamylethylether(TAME)		$3,34 \pm 0.17$	
Methacrolein		$2,96 \pm 0.15$	
Acetonitrile	5.04 ± 0.25	$2,86 \pm 0.14$	
Butanal		$3,00 \pm 0.15$	
Acetone	4.99 ± 0.10	$2,95 \pm 0.15$	5.08 ± 0.10
Pentanal		$3,43 \pm 0.17$	
MVK		$2,98 \pm 0.15$	
Ethylacetate		$3,00 \pm 0.15$	
2-Butanone (MEK)	4.95 ± 0.25	$3,00 \pm 0.15$	
Ethanol	5.08 ± 0.10	$3,15 \pm 0.16$	
Hexanal		$3,36 \pm 0.17$	
Isopropanol		$3,08 \pm 0.15$	
2-Pentanone		$3,39 \pm 0.17$	
Heptanal		$3,39 \pm 0.17$	
4-Methyl-2-pentanone(MIBK)		$3,39 \pm 0.17$	
Isobutanol		$3,15 \pm 0.16$	
Tertbutanol		$3,39 \pm 0.17$	
Butylacetate		$3,00 \pm 0.15$	
2-Hexanone		$3,39 \pm 0.17$	
Butanol		$3,09 \pm 0.15$	
Benzaldehyde		$2,96 \pm 0.15$	
2-Heptanone		$3,39 \pm 0.17$	
3-Methyl-2-buten-1-ol		$3,39 \pm 0.17$	

3.4. Results

3.4.1. Zero air measurements

Figure 3.4 displays the measurements by the three different PTR-TOF-MS systems of zero air, which was led through the manifold at a dew point of -4 °C. During the data analysis the background of the instruments determined by the catalytic converter was subtracted from the recorded zero air data points. Negative values therefore mean that the catalyst was releasing more than the manifold. It can be seen that isoprene, the sum of methylvinylketone and methacrolein (MVK+MAC) and methylethylketone (MEK) show reasonably close values for all three groups. In contrast, some 80 -100 pptv of acetone were measured by the three instruments even in zero air. The likely reason was that the manifold had been cleaned with acetone prior to the campaign and a residual background of around 90 pptv remained. MD measured slightly negative values for benzene, which can be explained by a background measurement that was too high. Either the lines between the catalytic converter and the instrument or the converter itself released benzene so that a too high background was subtracted. Furthermore, MD recorded a toluene value that was slightly higher than the zero air background. This might be traced back to a small contamination in their instrument. The largest discrepancies were found for acetaldehyde and methanol. The disagreement between NILU and MPIC was especially striking, because the two groups were using the same catalytic converter. The only difference was that the MPIC instrument required a longer Teflon line (length: ca. 8 m, OD: 0.635 cm) to connect from the catalyst to the instrument. The high values of methanol and acetaldehyde measured by NILU can be interpreted as an internal contamination of their instrument, because if the source would have been the manifold, the other instruments would have recorded it as well. The negative values of methanol reported by the MPIC system had their origin in a subtracted background value that was too high. This could have been a contamination either of the catalyst or of the long Teflon line connecting the catalytic converter and the MPIC PTR-TOF-MS. In this case, problems with the catalyst can be ruled out, because NILU was using the same catalytic converter. Moreover the NILU methanol data agreed well with the expected value in other experiments, e.g. in the dilution series, which is described in the next chapter. Therefore, the reason for the negative methanol data of MPIC was most likely a slight contamination of the Teflon line from the catalyst to the instrument.

3.4.2. Humidity

Detailed information about the impact of humidity on PTR-TOF-MS measurements can be found in this work in chapter 2, section 2.2.5. Figure 3.5 displays measurements of 8 different VOC compounds from OVOC Mix 1, including 5 OVOCs, at various humidities from MPIC system only. During this experiment the mixing ratios were kept constant, only the humidity was altered. Reference values were calculated by the DWD using the dilution ratios and are shown in grey. We calibrated our system for humidities which were very close to the ones in the experiment. The best way to compare the humidities between measurement and calibration is to examine the ratios of the water cluster "m/z 39" to the primary ions "m/z 21": The ratio for the dry calibration amounted to 0.040 while it was

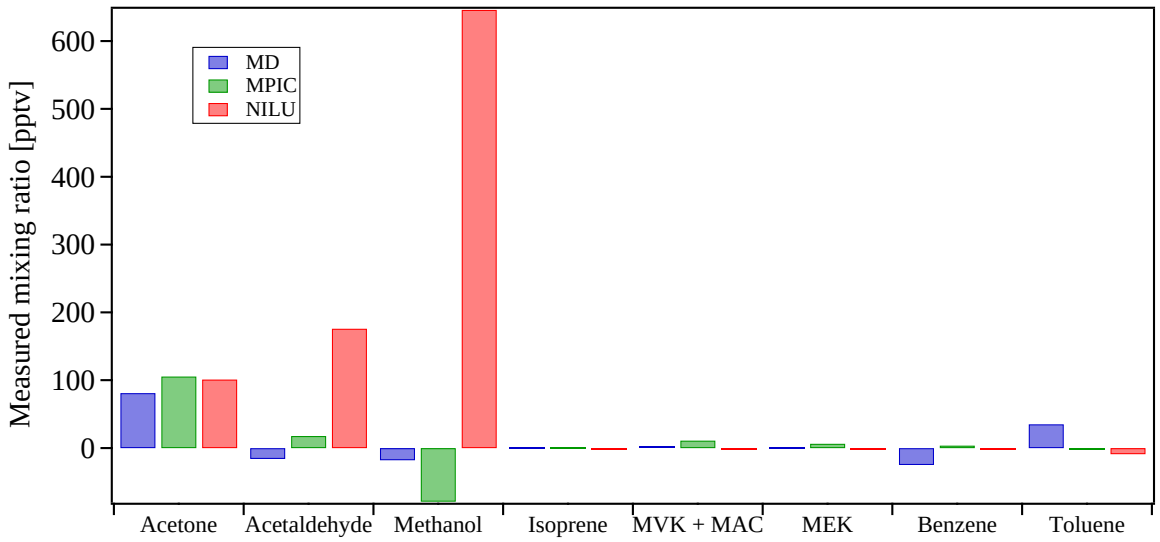

Figure 3.4.: Zero air measurement

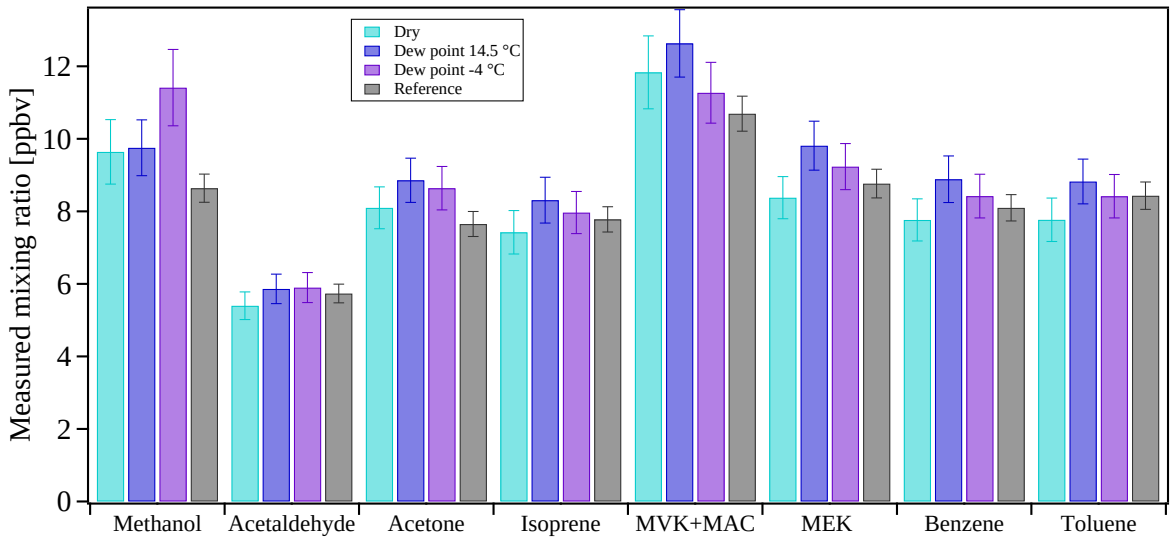

Figure 3.5.: Mixing ratios of selected VOCs when supplied at constant mixing ratio at three different humidities

0.037 during the measurement under dry conditions. For a dew point of -4 °C (roughly 12 % relative humidity at 27 °C) and of 14.5 °C (roughly 46 % relative humidity at 27 °C) the ratios were 0.068 and 0.21 during measurement, respectively. The equivalent ratios of the calibrations were 0.071 and 0.20. It can be found that the differences in the humidity levels during calibration and measurement were very small so that only a minor error could be expected from this discrepancy. As already described in chapter 2 it was determined that the sensitivity of the MPIC PTR-TOF-MS decreased when measuring under humid instead of dry conditions. Increasing from 0 % to 10 or 20 % of relative humidity led to a relatively large difference in sensitivity ($\sim$ 10 - 25 % variation in this study) while a further increase in relative humidity resulted in small variations ($\sim$ 2 - 10 % for an increase from 25 to 50 % RH in this study). Exceptions would be benzene, which doesn't react with the water cluster and thus shows a stronger humidity dependency, or isoprene, which shows almost no humidity dependency. Furthermore, the calibrations performed during this campaign resulted in no specific trend for the calibration factors of methanol and MVK. It needs to be kept in mind that the data compared here are already in ppbv, which means that changes in sensitivity due to alteration in humidity should be taken into account by applying different calibration factors. In the ideal case the results in ppbv should show no variation while the raw data in normalized counts per second (ncps) should display higher count numbers at low humidities for most of the compounds except methanol, MVK and isoprene. The expected trend was only found in the raw data, but the mixing ratios in ppbv shown in Figure 3.5 changed slightly with humidity. A pattern could be distinguished: data measured under dry conditions showed the lowest and under highest humidity (14.5 °C dew point) showed the highest values in ppbv. For the results of acetaldehyde, MEK, isoprene, benzene and toluene these differences were only minor (<20 %) and lay within the error bars. Most probably the small discrepancies in the ppbv data have their origin in slightly erroneous calibration factors. Only the results of methanol, acetone and MVK + MAC lay beyond the error range. The reason for the discrepancies could either be unsatisfactory calibrations or a slight contamination of the water used for humidification. At the beginning of the campaign zero air was measured at a rather high dew point of around 11 °C. The experiment is not shown here, because problems with the catalytic converter of the MPIC system occurred. Still a sharp increase of OVOCs, especially methanol, acetone and acetaldehyde, could be observed when the humidification system was turned on. These compounds were released from the water, but after several hours of flushing of the distilled water with zero air the levels decreased strongly. When the water bottle was refilled during the campaign, it was conditioned for 4 hours to minimize these artifacts from the water. A contamination of the water cannot completely be ruled out, but should play only a minor role.

For methanol two effects could be the reason for the deviating results. On the one hand problems during calibration and, on the other hand, a wrong value for methanol given for the content of the calibration gas bottle. To guarantee complete mixing during calibration we added ca. 1 m of 1/4″ (OD= 0.635 cm) Teflon line to our calibration system. Unfortunately this caused wall effects for sticky compounds like methanol so that the plateaus of some calibration steps were not properly reached even after measurement time of 30 min. Figure 3.6 shows the calibration of methanol and of acetone for comparison at dry conditions as well as at the dew points of ca. - 4 °C and 14.5 °C.

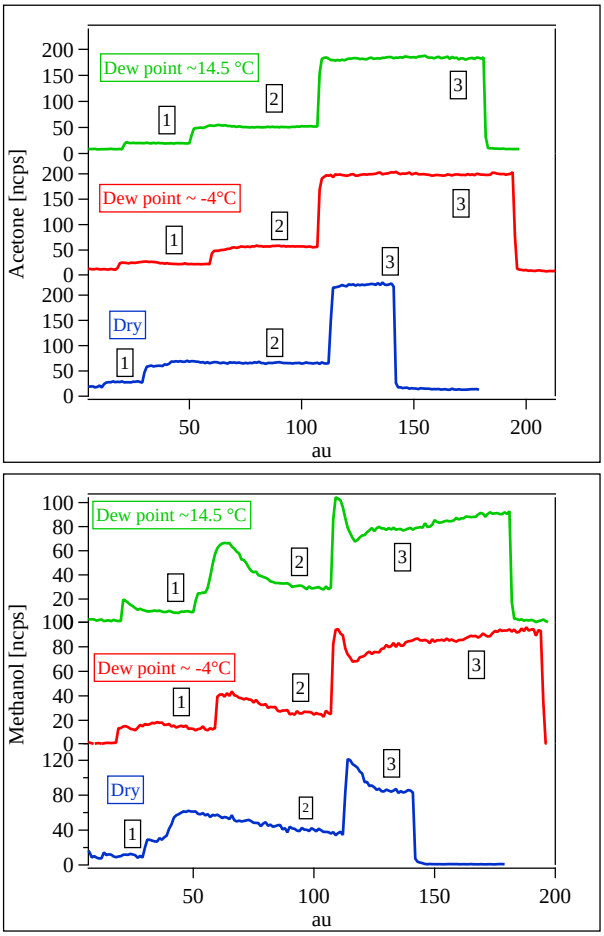

Figure 3.6.: Calibrations of acetone and methanol in normalized counts per second (ncps) at 3 different humidities. The x axis has arbitrary units, because the calibrations were performed at different days.

Due to the instabilities of the calibration steps for methanol, inaccurate calibration factors were obtained. The range of the calibration steps lay between 0.7 and 10 ppbv and thus covered the measured mixing ratios. Additionally the group from MD calibrated their system using different calibration gas bottles at the end of the campaign. The calibration factors gained from the bottle of NILU and from their own bottle varied only by 4 % while the result from the MPIC bottle was 30 % too low. This would lead to an overestimation of methanol. The other experiments during the inter-comparison showed the same trend: the MPIC instrument overestimated methanol data especially at high mixing ratios (see following sections). Since the overestimation lay in some experiments even higher than 30 % it could be concluded that a combination of both problems was the reason for the unsatisfactory results.
The minor inaccuracy of acetone might be traced back to the slight contamination of the manifold, which was determined during zero air measurement. During high humidity the emission of acetone from the manifold might have increased.

OVOC Mix 1 was used in this experiment and contained not only MVK, but also MAC. The PTR-TOF-MS cannot separate these two compounds, because they are isobaric. This means that the sum is recorded. The calibration gas bottle from MPIC contained only MVK so that the calibration factor gained for MVK was applied on the sum of the two compounds. Therefore, the reason for the discrepancy might be that MAC would have a slightly different calibration factor or would show a different humidity dependency.
Another small problem occurred in the background data. During the humidity experiment the background changed slightly between the humidities. At highest humidity the catalytic converter emitted the highest values, e.g. 0.46 ppbv during wet in contrast to 0.14 ppbv during dry conditions for methanol, humidity dependency already taken into account. But this effect played only a minor role, because the background values accounted for less than 5 % of the measured data for most of the compounds. Only for acetaldehyde the background was up to 20 % of the data, which means that a deficient background would have affected the results to a higher degree. But since the acetaldehyde data showed the least discrepancy a large effect of the background measurement can be excluded.

3.4.3. Dilution series

OVOC Mix I was diluted to generate 5 steps of around 60 pptv, 280 pptv, 1.8 ppbv, 5 ppbv and 8 ppbv. The content of the OVOC Mix I bottle as well as the exact mixing ratios of the dilution series can be found in Table 3.3. Figure 3.7 shows linear regressions of the measured data points plotted against the expected ones. For the regression a bivariate fit function, which minimizes the distance from the line to the data points not vertically but perpendicularly during the fitting process, was used. For further information please refer to York et al. (2004) (York et al., 2004). All three instruments were able to measure isoprene very accurately and precisely relative to the standard. Acetaldehyde was captured quite accurately by the MPIC system while the group from NILU and from MD both underestimated the actual values, although all groups measured with high precision. This can be seen in the r^2 values, which show the quality of the fit and lay between 0.9 and 1 for all three groups. Conversely, acetone was accurately recorded by NILU and MD while the MPIC measurement of the high dilution step exceeded the reference value by $\sim$13 %, which was slightly out of the error range of the reference value (not shown). The reason for these discrepancies may have been slightly inaccurate calibrations of the respective instrument. While NILU and MD measured methanol quite accurately the MPIC instrument performed comparatively poorly. The MPIC system slightly underestimated the low and overestimated the high mixing ratios. The underestimation can be explained by the previously discussed too high background value originating from the long Teflon supply line (see section 2.4.1). This contamination played a significant role for small mixing ratios, whereas for high values, it was only a relatively small percentage. If the negative mixing ratio for methanol measured during the zero air experiment (-79 pptv) is regarded as the value of the contamination, then it would present almost 100 % of the smallest dilution step (73 pptv), but only 1 % of the highest (8640 pptv). The overestimation was either due to problems during calibration or due to an erroneous value of methanol in the calibration gas bottle as described in the previous section.

Table 3.3.: Contents of OVOC MIX 1 and volume mixing ratios (VMR) of the dilution series. No uncertainty values were available for the contents of the bottle, because the mixtures were self-made by DWD. The uncertainties of the steps were calculated from the errors occuring during the dilution process.

Compound	(VMR) bottle [ppmv]	VMR step 1 [pptv]	VMR step 2 [pptv]	VMR step 3 [pptv]	VMR step 4 [pptv]	VMR step 5 [pptv]
Methanol	45	73 ± 33	373 ± 37	1842 ± 18	5592 ± 56	8640 ± 389
Acetaldehyde	30	52 ± 23	263 ± 26	1299 ± 13	3943 ± 39	6090 ± 276
MAC (methacrolein) + MVK (methylvinylketone)	30 (MAC) 26 (MVK)	91 ± 41	462 ± 46	2280 ± 23	6921 ± 69	10693 ± 481
Acetone	40	65 ± 29	330 ± 33	1632 ± 16	4954 ± 50	7654 ± 344
MEK (methylethylketone)	46	74 ± 33	378 ± 38	1869 ± 19	5673 ± 57	8765 ± 394
Benzene	42	69 ± 31	350 ± 35	1727 ± 17	5241 ± 52	8098 ± 364
Toluene	44	72 ± 32	364 ± 36	1798 ± 18	5457 ± 55	8432 ± 379
Isoprene	41	66 ± 30	336 ± 34	1659 ± 17	5035 ± 50	7780 ± 350

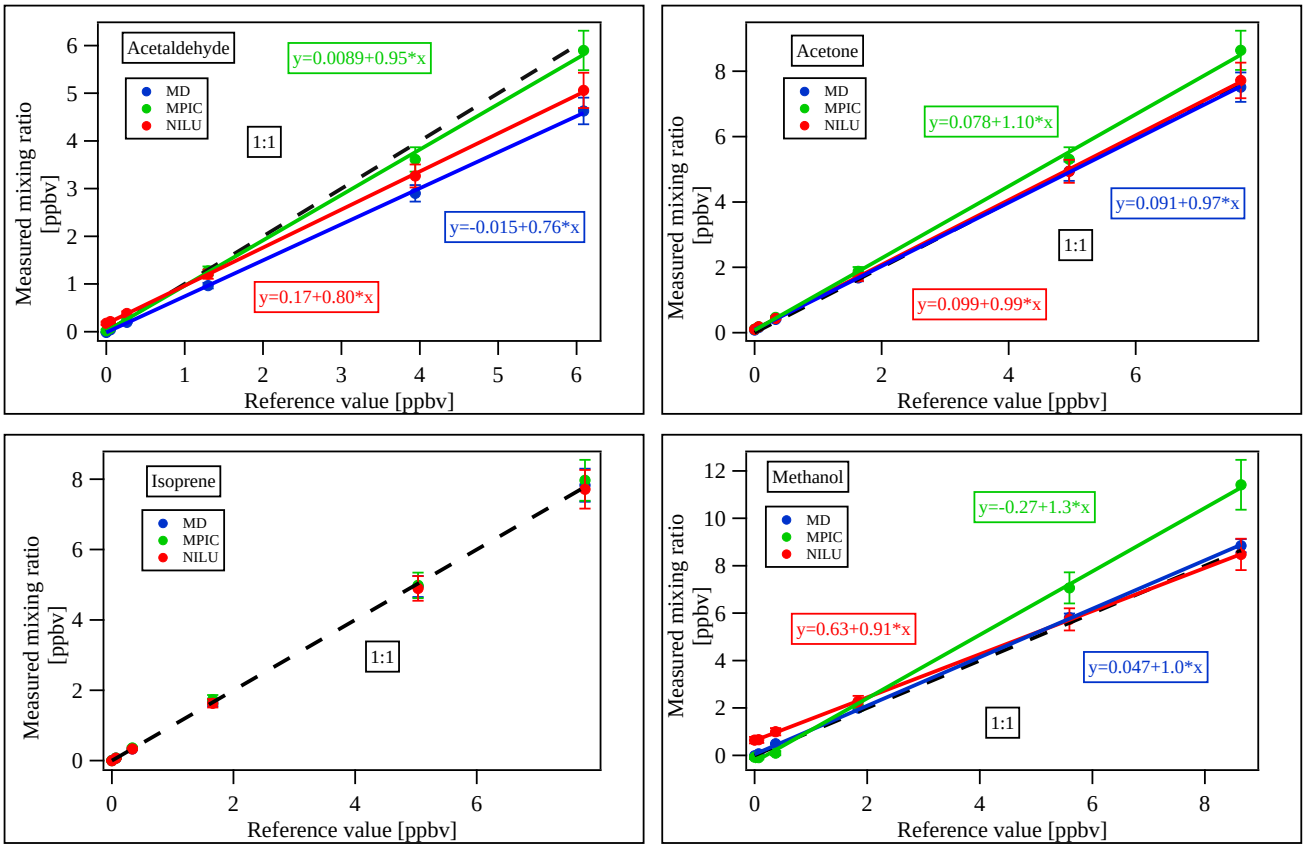

Figure 3.7.: Results of a dilution series for acetaldehyde, acetone, isoprene and methanol. Measured mixing ratios were plotted against the reference values and linear regression was performed using a bivariate fit algorithm.

3.4.4. Ambient air measurement

As part of this comparison ambient air was led through the common manifold and analyzed by all systems. Figure 3.8 displays measurements of acetaldehyde, methanol and acetone over the time period of two days. In Figure 3.9 correlations between MD and MPIC as well as NILU and MPIC are displayed. All plots show that the three groups measured acetone very consistently in ambient air despite the fact that a certain fraction of the mass of acetone is likely to be propanal. These two molecules are isomers and cannot be separated by a PTR-TOF-MS, both being measured at m/z 59.0491. The agreement for acetone was high although the MPIC system showed a slight overestimation during the dilution series at high mixing ratios of ca. 8 ppbv. But this overassessment was almost of no consequence in the range of lower mixing ratios so that this problem cannot be found in the relatively low ambient levels of acetone (650 pptv - 2 ppbv). On the other hand, the acetaldehyde data followed consistently the same pattern but were offset. MD underestimated the acetaldehyde values relative to NILU and MPIC, which is consistent with the dilution series experiment (Fig. 3.7). The slope of the linear regression between the acetaldehyde data of MD and MPIC was 1, but the y axis intercept showed a negative value representing

this offset (−0.18 ppbv). Although the NILU instrument underestimated the acetaldehyde value during the dilution series (Fig. 3.7), it slightly overestimated the ambient levels. This interpretation is only valid if the measurements of MPIC are regarded as correct as they were during the dilution experiment. In later experiments acetaldehyde caused some problems for the MPIC instrument as well. A factor that needs to be kept in mind during ambient measurements is the matrix of the air. When pure substances are diluted with zero air, no potentially disturbing other compounds are present while ambient air could always contain interfering substances. Methanol was the most problematic compound, especially for the MPIC instrument. As already shown in the dilution series MPIC underestimated small and overestimated high methanol mixing ratios. This leads to slopes being smaller than 1 and high intercept values. The background measurement could not be the explanation for the discrepancy, because the values were low and consistent. As already found in the previous chapters the main reasons were either unstable steps during calibration and/or the flawed content of the calibration gas bottle.

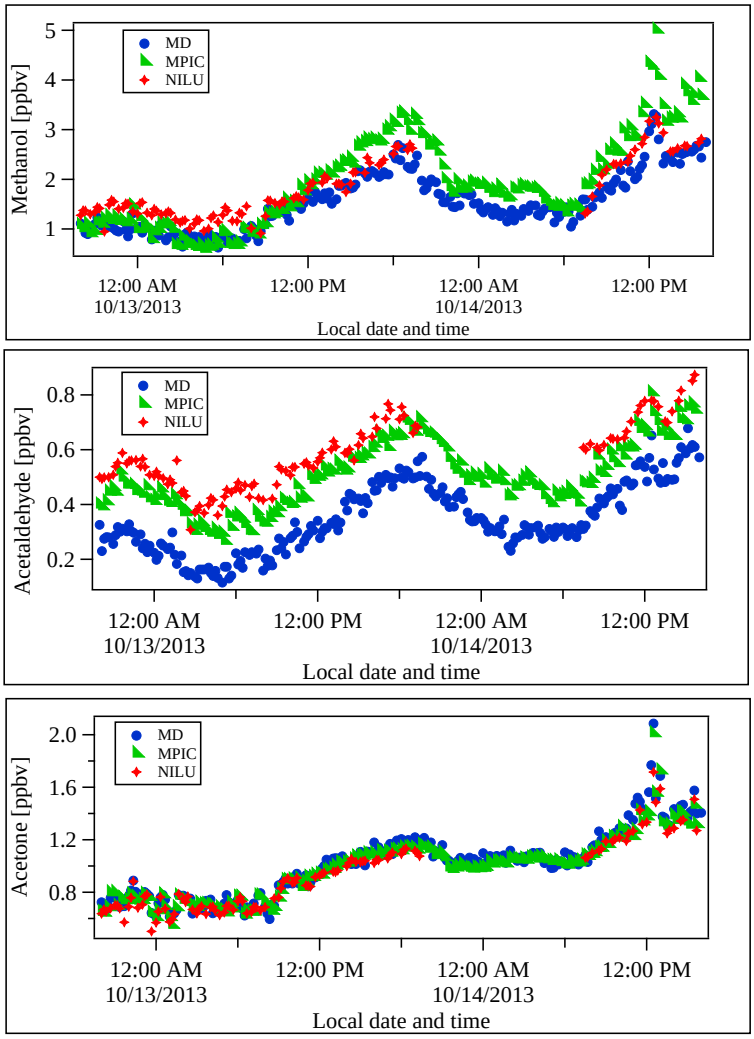

Figure 3.8.: Ambient air measurements of methanol, acetaldehyde and acetone

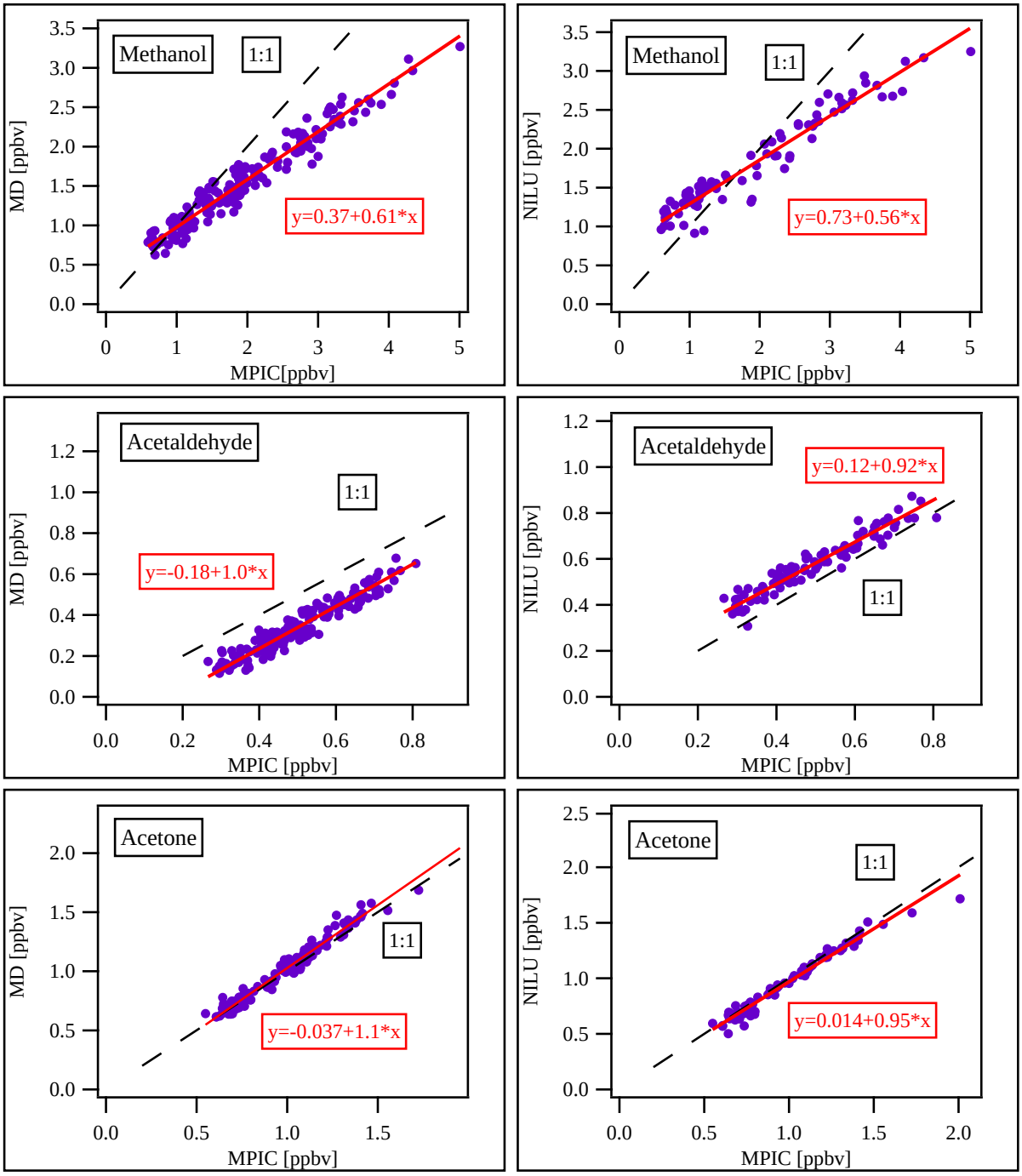

Figure 3.9.: Correlations between the results of MD and MPIC (left) as well as NILU and MPIC (right)

3.4.5. Spiked ambient air measurement

Ambient air was spiked for 12 h with OVOC Mix 1 and for 6 h with OVOC Mix 2, which were both diluted to create around 10 ppbv. The compounds which are included in OVOC Mix 1 and 2 can be found in Table 3.1. In Figure 3.10 the mixing ratios of methanol and

isoprene reported from all three groups can be found. Figure 3.11 displays the mixing ratio of acetaldehyde and the sum of acetone and propanal measured by the three PTR-TOF-MS instruments and by GC systems from MD (acetaldehyde only), DWD (German Meteorological Service, Hohenpeißenberg Observatory) and EMPA (Swiss Federal Laboratories for Materials Science and Technology, Dübendorf). The levels of standard gas added to the ambient air are plotted as well. It needs to be kept in mind that these reference values represent only a rough orientation, because the actual mixing ratio of the specific compound in ambient air was unknown. MD, MPIC and NILU all agreed well on isoprene when measuring the first mixture. During OVOC Mix 2 all three groups agreed within their individual error estimation, but lay around 70 % above the added standard value. The most probable reason was that the second mix contained methylbutenol, which fragments inside the instruments via the loss of water to form an ion with the same mass as isoprene (Amelynck et al., 2005). Methanol was overestimated by MPIC by 50-60 % in comparison to the other groups, which was consistent with previous measurements where high values of methanol were constantly overestimated by the MPIC instrument either due to deficient calibrations or a deficient specification of the methanol content in the calibration gas bottle (see section 3.4.2).
Acetone values reported by NILU differed by around 5 % from the MD and MPIC results during the first standard addition, but the discrepancy was so small that it lay within the error bar. Interestingly, MPIC measured a decrease while MD and NILU reported an increase for acetone during the measurement of OVOC Mix 2. One explanation could be that the standard added contained propanal, which is isobaric to acetone. If the measured data are compared to the sum of the added mixing ratios of acetone and propanal, then all three groups were underestimating the level, but to a different degree. The GC systems, on the other hand, report data lying 7-10 % (0.6-0.8 ppbv) over the added standard value, which is quite reasonable, because the ambient values (acetone ca. 1 ppbv on average during the measurement of ambient air) still needed to be added to the reference value. The GC data might be more accurate than the PTR data in this case, because the GC systems are able to measure acetone and propanal separately while the PTR-TOF-MS systems just measure the sum and were only calibrated for acetone without taking propanal into account. This would suggest that the three instruments had shown different sensitivities for propanal, not only in comparison to each other, but also if compared to the acetone value. Making some small assumptions an easy calculation can provide a rough calibration factor for propanal for the MPIC instrument. The reference value consisted of 3.5 ppbv propanal and 5.1 ppbv acetone. MPIC reported an average value of 7.1 ppbv for the sum of the two compounds. Now it is assumed that the MPIC instrument would have measured acetone correctly. This would mean that from the reported 7.1 ppbv 5.1 ppbv were acetone. The remaining number of 2.0 ppbv is erroneous and can be transferred back into ncps by multiplying with the calibration factor of acetone (18.4 ncps/ppbv). This leads to 36.8 ncps, which should be equivalent to the actual 3.5 ppbv of propanal. By dividing the count number by the expected value for propanal a calibration factor of 10.5 ncps/ppbv would be yielded.

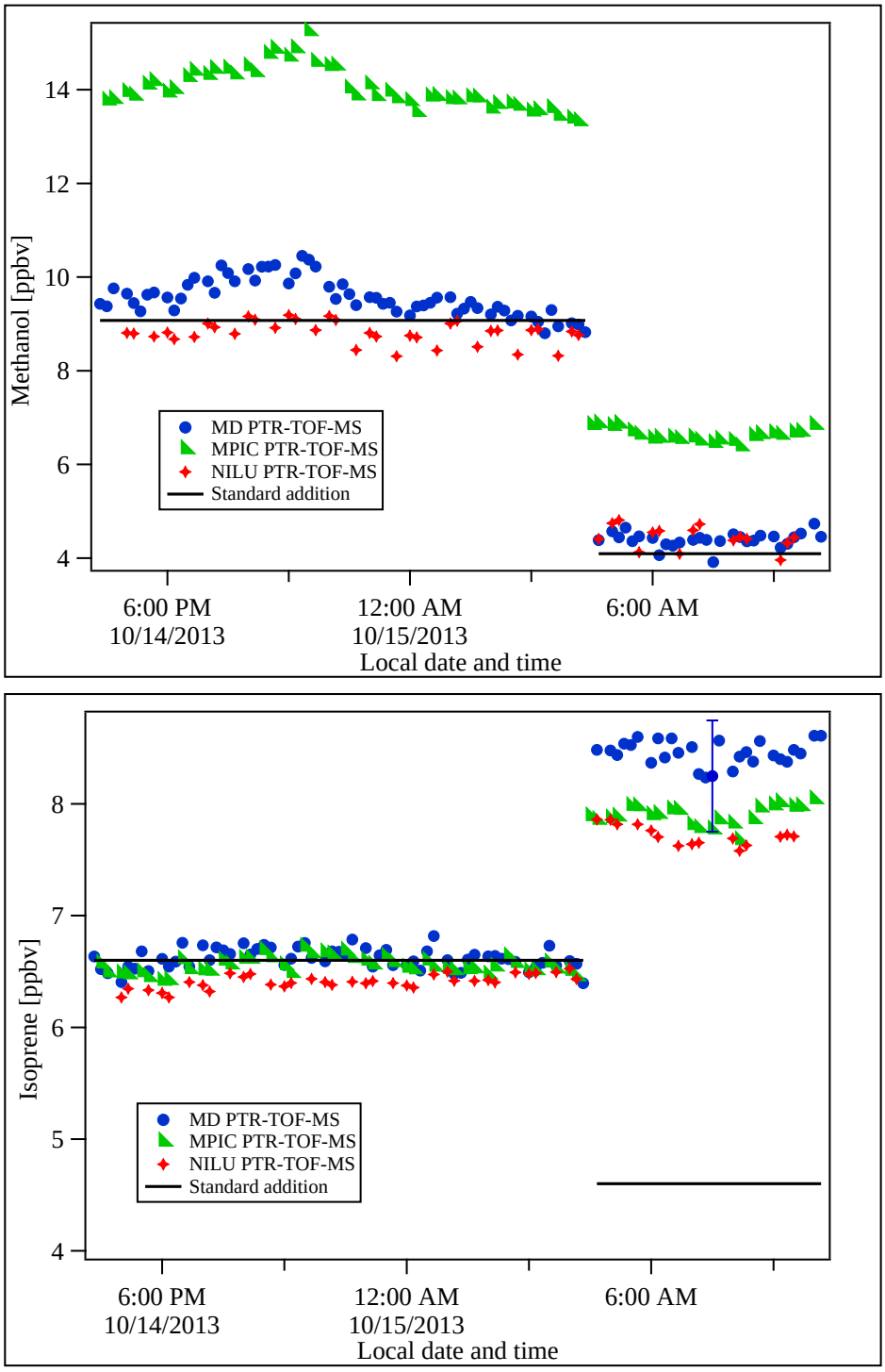

Figure 3.10.: Time traces of methanol, and isoprene and acetaldehyde for spiked ambient air from all three groups. A single example error bar is included so as not to mask the traces.

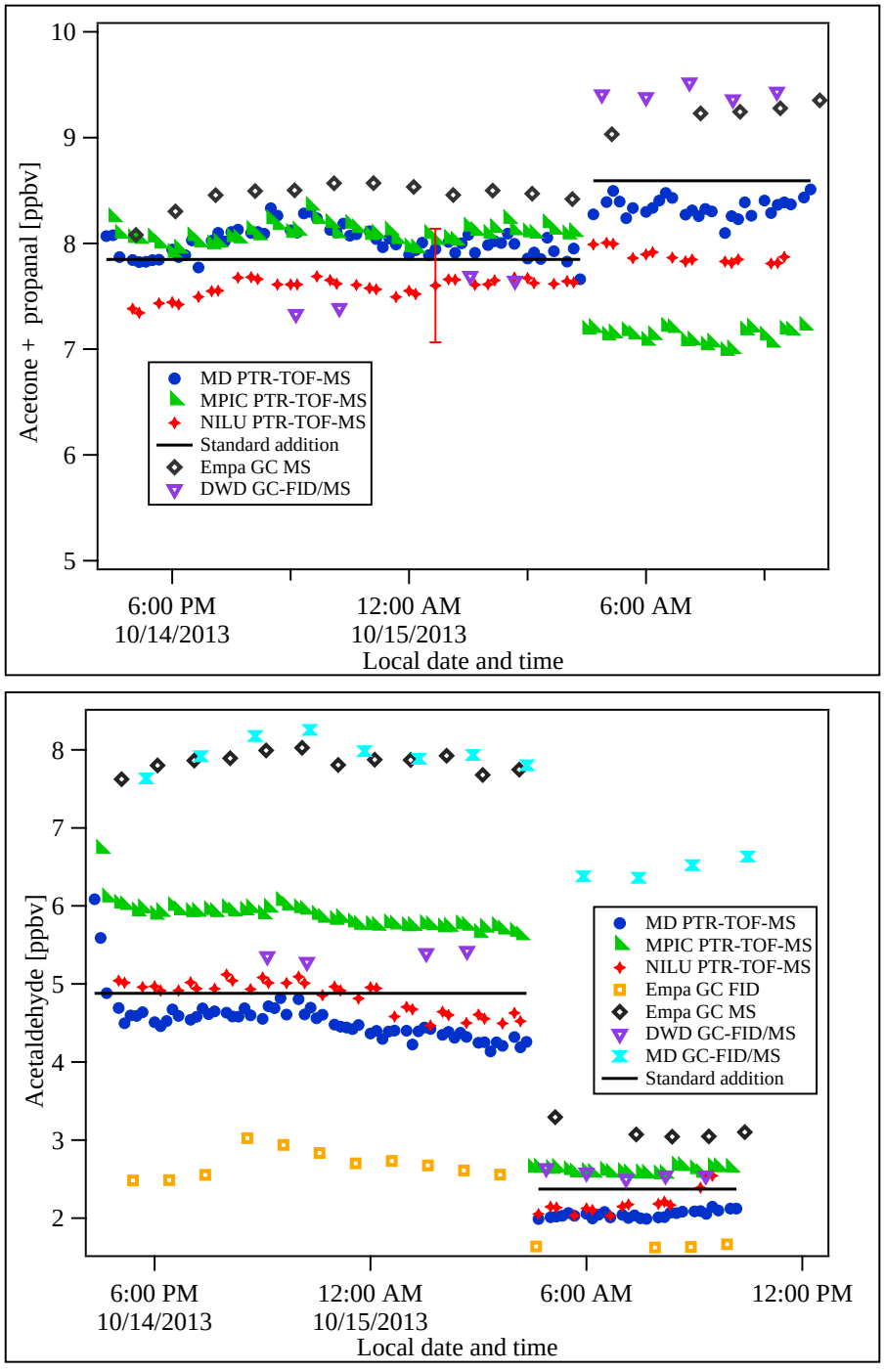

Figure 3.11.: Time traces of acetone plus propanal and acetaldehyde for spiked ambient air measured by the three PTR-TOF-MS systems from MD, NILU and MPIC and by three GC systems, one from DWD (German Meteorological Service, Hohenpeißenberg Observatory), one from EMPA (Swiss Federal Laboratories for Materials Science and Technology, Dübendorf) and one from MD (acetaldehyde only). A single example error bar is included so as not to mask the traces.

MPIC reported 20 to 30 % more acetaldehyde than MD or NILU. The dilution series showed that the MPIC instrument measured acetaldehyde accurately while the other two groups reported slightly too low values. In this experiment the data of NILU and MD lay partly below the added standard level, which represents a proof of their underestimation and was consistent with the dilution series. Interestingly the MPIC data were 20 % higher than the reference value during measurement of the first mixture but only 10 % higher than the reference value of the second mixture. A possible artifact from OVOC Mix 1 being measured on the mass of acetaldehyde and thus increasing the signal can be excluded, because none of the species comprised in OVOC Mix 1 fragments to the mass of acetaldehyde (m/z 45.0335). In addition the humidity cannot play a role, because the calibration factor applied was determined at the same water cluster to primary ion ratio as in the measurement. Furthermore, the effect of the ambient air level and its changes should be taken into account. If the ambient values would have been quite high, then the discrepancy between the MPIC data and the actual value (reference + ambient level) would decrease while the difference between the NILU or MD results and the reference would increase. This scenario would agree with the results from the dilution series where MPIC captured acetaldehyde well while NILU and MD were underestimating the values. Unfortunately the GC data showed even higher discrepancies (possibly because of other issues) and therefore cannot confirm this idea. Still, if the ambient air measurement of the previous experiment would be used, then the reference value would have to be increased by roughly 500 pptv. This would lead to an overestimation by MPIC of only 10 % for OVOC Mix 1 and even an underestimation by MPIC of 10 % for OVOC Mix 2. The MPIC data for acetaldehyde had a total uncertainty of ca. 7 %. This shows that MPIC measured acetaldehyde quite accurately in this experiment.

3.4.6. Common standards

In Table 3.2 the contents of three gas standards are given ("Common 1", "Common 2" and "Common 3"). These were diluted with zero air to ca. 1 ppbv, 0.6 ppbv and 1 ppbv, respectively, and measured for several hours each at a dew point of 5 °C. The exact values can be found as reference bars in Figure 3.12. The upper panel of Figure 3.12 shows the results of the mixing ratio determinations of Common 1 by each system.
Acetonitrile was determined very accurately by NILU and MPIC, the values corresponding well to the standard levels within the error estimates. MD did not report acetonitrile data. MPIC captured acetone very well, the reported values by NILU lay within the error bars of the reference while MD overestimated the acetone level by 16 %. Methanol was underestimated by NILU by 35 % and overestimated by MPIC by 27 %. The MPIC PTR-TOF-MS measurements were consistent with the overestimation of methanol in the previous experiments (see section 3.4.2). Acetaldehyde was well captured by NILU and MD, but underestimated by MPIC by 25 % despite the accurate measurement of acetaldehyde by MPIC during the dilution series and the spiked ambient air measurement. In general, a too high background level can be a reason for an underestimation. But the background of acetaldehyde in this experiment was low and stable and hence cannot be the reason for the discrepancy. The calibration factor applied was determined at the same water cluster to primary ion ratio as the measurement (ratio = 0.1) and the fit of the calibration points

was linear in the range between 0.8 and 10 ppbv. In contrast to the underestimate MPIC reported too high values of acetaldehyde (25 %) during the measurement of Common 2, which was performed right after Common 1 and can be found in the middle part of Figure 3.12.

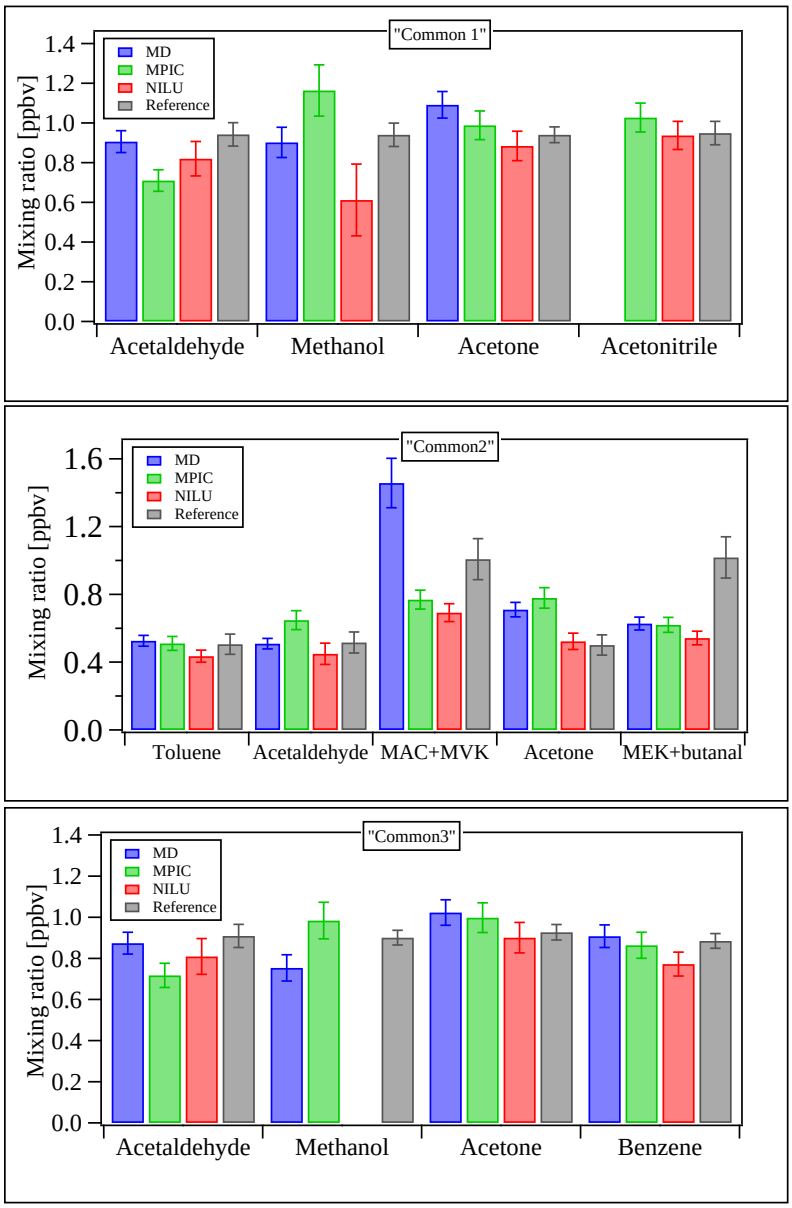

Figure 3.12.: Measurement of common standard 1 (upper panel), common standard 2 (middle part) and common standard 3 C (lower panel) at a dew point of 5 °C

Interestingly, the acetaldehyde level measured by MPIC was almost the same in both experiments although it should vary by around 400 pptv. It could be interpreted that the MPIC instrument responded too late on the changes in both cases. But since the experiments were performed for several hours this idea cannot be the explanation. Another

reason for the overestimated values measured by MPIC in Common 2 could be the high E/N value we used in the drift tube. While NILU applied only 118 Td the group of MPIC as well as MD used a value of around 136 Td. The higher energy in the drift tube promoted fragmentation. Common 2 contained ester compounds (ethyl and butyl acetate, see Table 3.2), which fragment to form CH_3CO^+ at mass of 43 (Buhr et al., 2002). The ^{18}O isotope of this fragment lies on mass m/z 45.0221 and a resolution of 4000 would be needed to separate this fragment from the acetaldehyde ion. Unfortunately, the resolution of the MPIC instrument was only around 3700 during that experiment. This means that no separation was possible. MD, on the other hand, reported a resolution between 3000 and 5000 (see Table 3.3). Hence MD might have been able to resolve the two peaks while the acetaldehyde signal of the MPIC instrument could have been increased due to the isotope of the CH_3CO^+ fragment.
During the measurement of Common 2 problems with the water bath occurred and the temperature dropped, leading to a lowering of the humidity. This caused a decreasing primary ion and water cluster signal and their ratio declined slowly from 0.1 to 0.08. In general, the sensitivity of a PTR-TOF-MS increases with decreasing humidity. Since no humidity interpolation was applied on this data set, only the calibration factor referring to a ratio of 0.1 was used. This means that a too low sensitivity,that led to an overestimation, was assumed . But this overassessment was only small and cannot explain for example the acetone level of MPIC, which lay 55 % above the reference value. As an example the calibration factor for acetone changed by only 7 % when the primary ion to water cluster ratio was altered from 0.07 (around 15 % relative humidity) to 0.2 (around 50 % relative humidity). Another explanation could be that Common 2 included tertbutylmethylether (MTBE) and tertbutylethylether (ETBE, see Table 3.2), which might influence the acetone signal due to fragmentation. As mentioned above, fragmentation is favored at higher energies in the drift tube. Consequently NILU captured acetone well while MD and MPIC reported an overestimated value. But Rogers et al. (2006) report that MTBE forms fragments measured on the protonated mass m/z 57 within a PTR-MS (Rogers et al., 2006). Since this fragment refers most probably to the sum formula $C_4H_9^+$, the ion as well as its isotopes would not impact the acetone signal on mass m/z 59. A further reason for the higher acetone values could be a contamination. The manifold showed a general contamination of ca. 90 pptv for acetone, but this could not have been the problem, because the other groups would have seen it as well. Therefore, the contamination might have been within the line leading from the manifold to the MPIC PTR-TOF-MS. The background measured only revealed contaminations within the instrument, but did not cover that piece of line. During the experiment Common 3 the MPIC PTR-TOF-MS still overestimated acetone, but the value was already within the error range. Thus, it could be concluded that the contamination had already been fading away.
The reason for the MVK+MAC inconsistency in Common 2 may lie in the inability of the PTR-TOF-MS to separate the two isomers. The calibration gas used from MPIC for calibration only contained MVK, but not MAC. The discrepancy could arise, because MAC might have a different calibration factor. In the same way as for propanal in the previous section a calibration factor for MAC can be estimated. The reference value for MVK was 5.1 ppbv, for MAC 5.0 ppbv. The MPIC PTR-TOF-MS measured 7.7 ppbv in total. Now it is assumed that the MPIC instrument recorded MVK correctly, which means that 5.1 ppbv

can be subtracted from 7.7 ppbv. The remaining 2.6 ppbv need to be transferred into the correct value for MAC. Therefore, the value in ppbv needs to be converted back into ncps by multiplying with the wrongfully applied calibration factor of MVK (11.3 ncps/ppbv). A count number of 29.4 is gained and needs to be divided by the correct mixing ratio of 5.0 ppbv for MAC. As a result a calibration factor of around 6 ncps/ppbv is determined. The same problem as for MVK and MAC arose from the two isomers MEK and butanal. All three groups underestimated the summed up reference value for the two compounds substantially: MD and MPIC by almost 40 %, NILU by almost 50 %. By performing the same calculation as for MVK and MAC using the MPIC data a calibration factor of around 4 ncps/ppbv for butanal was achieved. This value is ca. 4.5 times smaller than the calibration factor of MEK, which means that the instrument is much less sensitive for butanal than for MEK. Toluene was corresponding well to the standard levels within the error bars for all three groups.
The measurement of acetaldehyde during Common 3 showed the same pattern as during Common 1: NILU and MD agreed within the error bars while MPIC underestimated the actual value slightly. Unfortunately, as already shown for Common 1 no reason could be found for this behavior. Methanol measurement of MPIC was again too high for the reasons given in the previous sections, but still lay within the error range. All groups agreed for acetone within the error bars while benzene was well captured from MD and MPIC, but underestimated by NILU. The reason for the underestimation could be a too high background measurement, but since NILU and MPIC were sharing a catalytic converter, this can be excluded. No further information about other possible reasons was provided by NILU. A suggestion could be an unsatisfactory determination of the calibration factor.

3.4.7. Ozone experiment

During the ozone experiment a standard containing 53 NMHCs was diluted to ca. 600 pptv and first measured without and then with addition of 100 ppbv of ozone. The goal was to determine OVOCs which are produced due to reactions of NMHCs with ozone. The results from MPIC and MD are shown in Figure 3.13. From NILU no data were available. Not only OVOCs (acetaldehyde, sum of acetone and propanal, MEK), but also NMHCs (benzene, toluene and isoprene) were plotted. When no ozone was added, the values for acetaldehyde and MEK measured by MPIC were below the detection limit while MD recorded 30 and 21 pptv, respectively. During ozone addition both groups agreed nicely on the MEK value, but MPIC measured 82 % more acetaldehyde than MD. No reference value exists for the OVOC data, because they were formed in situ. Thus, a comparison is difficult. Still one reason for the difference in acetaldehyde might be the line connecting the respective instruments to the manifold. If the line from MPIC was already used before, then the surface may have been coated with compounds, that react with ozone to form acetaldehyde. If the line from MD, on the other hand, was new or comparatively less coated, then this difference could have caused the divergence in acetaldehyde. Without ozone, both groups recorded around 120 pptv of acetone, which can be traced back to the contamination of the manifold. When ozone was added, MPIC recorded 28 % more acetone. As already mentioned the reason might be that propanal, which is isobaric to acetone, was formed as well. The discrepancy could occur due to different calibration

factors for acetone and propanal. Toluene was captured accurately by both groups while MPIC measured 30-40 % more benzene and 15 % more isoprene. A comparison is difficult, because no exact reference values were available. The results of this experiment show that during measurements with rather high ozone levels OVOC artifacts, especially for acetaldehyde, must be considered. Unfortunately no precise data can be given, because the amount of artifacts depends on the mixing ratio of ozone and the precursors as well as on the coating of the lines.

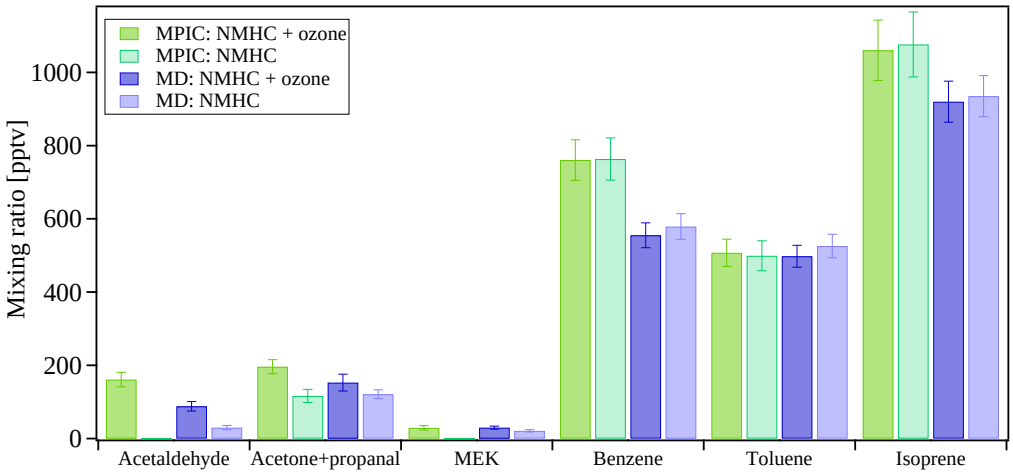

Figure 3.13.: Measurement of OVOCs and NMHCs by MD and MPIC with and without the addition of ozone

3.5. Improvement measures undertaken

The experiments have shown that the measurements of acetaldehyde and methanol represent the biggest challenge. For the MPIC system the most likely explanation is the deficient characterization of the calibration factors and their humidity dependency. To guarantee a stable, reproducible calibration several alterations were made to the MPIC calibration system post campaign: The lines were made as short as possible to minimize wall losses. The connection from the mass flow controler (MFC) of the calibration gas up to the inlet of the instrument should not exceed 0.5 m. A sketch can be found in Figure 2.2 in chapter 2. Furthermore, the calibration bottle as well as the lines from the point where the calibration gas meets the humidified zero air were insulated and heated to ∼50 °C. Moreover before the calibration was started, the pressure controller was flushed several times by building up and releasing the pressure. Unfortunately, no clear improvement was achieved. The only change that had a slight effect was the shortening of the lines in the calibration system. During the calibrations made at the inter-comparison campaign the steps were measured between 20 to 45 min and still did not stabilize. Further tests revealed that the first calibration step takes at least one hour for stabilization. The reason was that the lines needed to be conditioned and therefore the shortening of the lines represented an

improvement. The following steps needed in general between 30 to 45 min. In the light of these results we consider it essential for accurate measurements to perform full calibrations at the beginning and at the end of a campaign so that no measurement time is lost. It is recommended that calibrations are performed at three different humidities or more so that interpolation is possible. Each of these calibrations should contain at least 3 steps. As already mentioned the first step should last around 1 h, the remaining between 30-45 min. Furthermore, it is suggested that the zero air applied for mixing and not the catalytic converter is used to measure the background during calibration. If the zero air, which is led through the whole calibration system, is used, then a possible contamination, especially of the water for humidification, can be detected and subtracted. For the following campaigns a mostly exponential interpolation was performed between the calibration factors at different humidities. This allows the calculation of calibration factors at each specific humidity value occurring during a campaign and guarantees an accurate conversion from counts into mixing ratios. During the inter-comparison campaign we shared the catalytic converter with the NILU group. Their catalyst was permanently flushed so that a contamination and spikes when switching between sample an background measurement were avoided. Since the converter performed well, disregarding the long connecting line, we established an inlet system for our instrument in which the catalytic converter is permanently flushed as well. Before the modification, the converter was only opened for background measurement and remained closed during the sample air measurement. A sketch of the modified system can be found in Figure 3.14. The lines were kept as short as possible and a compressor was added, which permanently pumped air into the catalytic converter. The needle valve and the ca. 10 m long Teflon line with an outer diameter of 0.318 cm were needed to regulate the pressure so that the flow controller reached the required flow of 30-100 standard mL/min. The flow through the catalyst could not be increased any further, because the PTR-TOF-MS inlet system draws only ca. 30 standard mL/min. A small overflow can be balanced by the pressure controller inside the TOF, but should not be too high. On the other hand, the flow through the inlet outside the instrument can be set to max 1 L/min to reduce wall losses. The electronic three way valves were controlled by a V25, a control unit specially designed for these purposes (see also section 2). During the sample measurement the flow through the catalytic converter was set to "vent" and the air through the inlet was led directly into the ion source. For the determination of the internal background the valves were switched so that the air went first through the converter and then into the ion source. The switching was automated, controlled by the V25, and occurred in freely selectable intervals. For the field measurements described in chapter 4 all improvements illustrated here were applied. Figure 3.15 displays one measurement with flushing the catalytic converter (upper panel) and one without (lower panel). Ambient air is colored in red while background values are shown in purple. In the upper panel the acetaldehyde level in ambient air was higher, but the background was a little lower than in the second graph (7 normalized counts per second (ncps) instead of 8 ncps). Yet the numbers need to be regarded with caution, because the two measurements were performed with different settings and therefore a varied sensitivity. It can be seen that a high spike occurred during the switch from ambient to catalyzed air, when the converter was not flushed. This effect disappeared, when the improved system was used. Another problem was that the background for acetaldehyde needed a long time until it reached its steady state. In the

upper panel of Figure 3.15 the background was measured for 20 min, but it still had not properly achieved a stable level. In the lower plot the background was only recorded for 5 min. Here it seems stable, but it is hard to tell due to the short time period. The challenge is to find a good compromise between reaching a stable background value and not losing to much sample time.

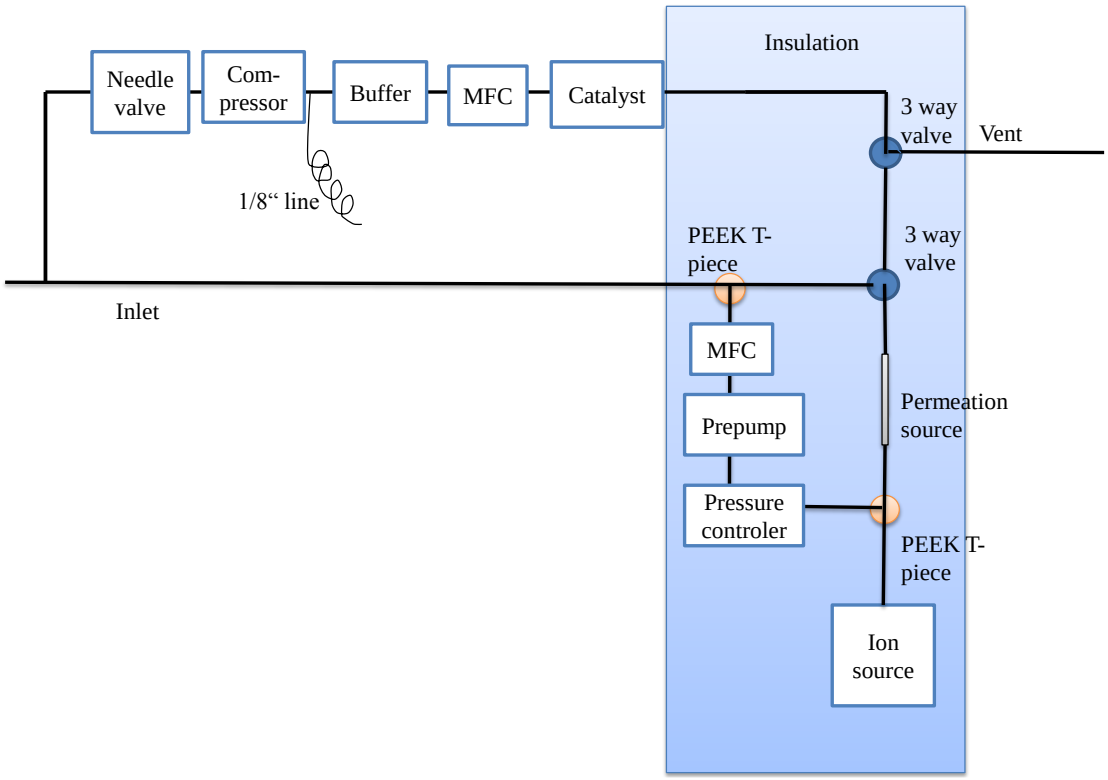

Figure 3.14.: Modified inlet system

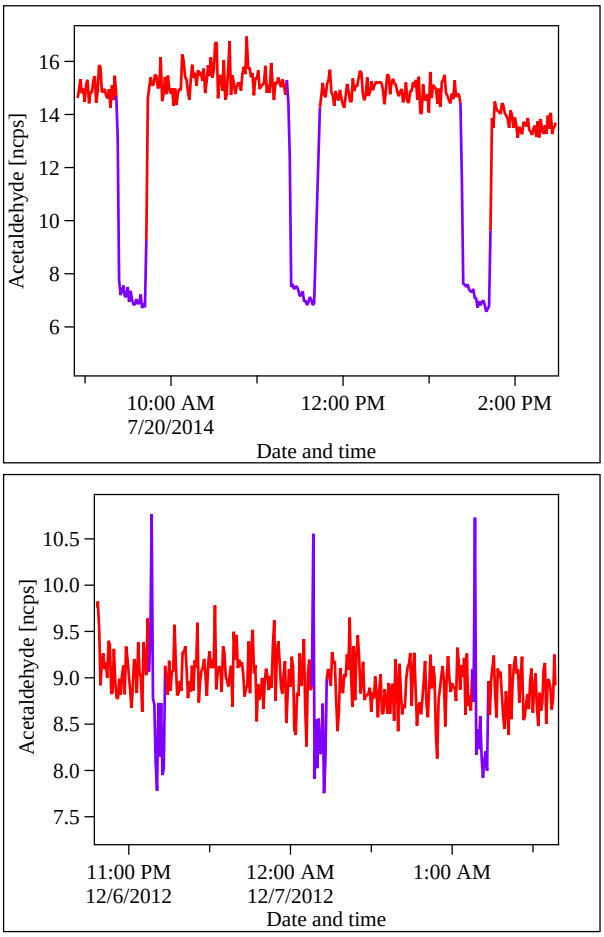

Figure 3.15.: Measurement of acetaldehyde in ambient air (red). In the upper panel the catalytic converter was permanently flushed and the background (purple) was measured for 20 min. The lower panel shows a background measurement of only 5 min without flushing the catalyst.

4. Volatile organic compounds (VOCs) in photochemically aged air from the Eastern and Western Mediterranean

4.1. Introduction

The island of Cyprus is situated on the Southeastern edge of the European Union. During the summer months the east-west pressure gradient between the quasi-permanent South Asian monsoon low, the Persian trough and the Azores high induces northerly winds (Etesians), that overcome the westerly flow, which is typical at temperate latitudes. The varying influences from the westerly and northerly winds make Cyprus an ideal vantage point to examine photochemically processed air from Eastern and Western Europe. Despite a modest population (1.15 million[1]) and little industrial emissions, the EU ozone air quality standard is regularly exceeded (Kourtidis et al., 2002; Kouvarakis et al., 2002; Gerasopoulos et al., 2005; Kalabokas et al., 2007, 2008, 2013; Doche et al., 2014; Kleanthous et al., 2014). The excess ozone is formed in sunlit conditions when NOx (NO + NO_2) and VOCs, emitted from countries to the north and west of Cyprus, are oxidized in the gas phase by the atmosphere's primary oxidant, the OH radical (Atkinson, 1990). In addition to ozone, numerous other secondary oxidants are formed including a suite of OVOCs, such as alcohols (e.g. methanol), carbonyls (e.g. acetone), and organic acids (e.g. acetic acid). During the summertime campaign CYPHEX (CYprus PHotochemical EXperiment), we exploit the location and dual meteorological flow regime to investigate the abundance, temporal behavior, dependence on origin and the marine influence on VOCs. Several extensive studies of VOC have been conducted previously in the Mediterranean area, which have highlighted the relevance of anthropogenic, biogenic and biomass burning sources for regional chemistry. Airborne measurements have shown that the Mediterranean atmosphere is a cross-road for global pollution, with boundary layer chemistry driven by emissions from the European mainland, whereas the mid-troposphere (4-8 km) is influenced by North American emissions and above this, monsoon outflow from Asia (Lelieveld et al., 2002). Measurements made on Crete approximately one day downwind of mainland Greece revealed the enormous complexity of VOCs in the region (Xu et al., 2003). Moreover, it has been shown that the mixing ratios of many VOCs, especially OVOCs, in the Mediterranean strongly depend on long distance transport and are periodically influenced by biomass burning (Salisbury et al., 2003; Holzinger et al., 2005). Reactive biogenic species such as isoprene have also been shown to be emitted from Mediterranean vegetation (Kesselmeier et al., 1996; Liakakou et al., 2007).
Here we examine the relative impacts of biogenic emissions and long distance pollutant transport from Eastern and Western Europe on trace gas levels, with particular emphasis on VOCs. Moreover, we exploit the island location to investigate the influence of the sea on VOCs, since air from Eastern and Western Europe was advected with variable trans-

[1]http://data.worldbank.org/country/cyprus; accessed on 4th of May 2016

port times to the site within the marine boundary layer. The effect of the ocean on many VOCs, particularly OVOCs, can be significant and variable in latitude (Yang et al., 2013, 2014), biological activity (Taddei et al., 2009) and time of the day (Sinha et al., 2007). To this end we have examined the behavior of an alcohol (methanol), a carbonyl (acetone), and an acid (acetic acid). These three compounds are described in detail in chapter 1. Using the rate coefficient (k) for each OVOC provided by IUPAC[2] and the diel mean OH concentration of 2×10^6 molec/cm^3 measured during the CYPHEX campaign, the following atmospheric lifetimes with respect to OH were calculated: 6 days for methanol, 32 days for acetone and 8 days for acetic acid.
The novelty of this campaign for VOC research was threefold: firstly Eastern and Western European outflow was chemically characterized and contrasted; secondly the relative local impacts of biogenic and transported VOC were assessed and thirdly the influence of summertime Mediterranean marine boundary layer transport on OVOC was investigated.

4.2. Experimental

4.2.1. Site

The measurement site (Ineia) is situated on the northwest coast of Cyprus at the top of a 650 m hill located ca. 10 km from the shoreline (34°57'N / 32°23'E). The surrounding area (5 km radius) is rural in character, comprising of farmland and a few small villages (e.g Ineia population 367). Extending 25 km to the northwest was the Akamas peninsula national park and to the northeast the terrain descended rapidly to the city of Polis (population 1975) at sea level. The vegetation is sparse and scrub like. Small trees such as the native pine (*Pinus brutia*), juniper (*Juniperus phoenicea*) and olives (*Olea europea*), Carob (*Ceratonea siliqua*) are interspersed amidst low lying bushes, such as *Inula viscosa* and *Foeniculum vulgare*. In addition small groves of vines, almonds and pomegranates are kept by some local farmers.
In summer, Cyprus is normally influenced by the Etesian winds, which bring air masses from the north (from Eastern Europe, and crossing Turkey and Greece). However, in 2014 a southward displacement of the storm track and associated synoptic weather systems weakened the east-west pressure gradient (Tyrlis et al., 2015) delaying the onset of the Etesian winds and causing periodic influence of air advected from the west over the Mediterranean Sea. Despite clear variation in air mass origin during this campaign (12$^{\text{th}}$ - 03$^{\text{rd}}$ August 2014), the local wind direction at the site was primarily SW (72 %, see Figure 4.1).

4.2.2. Instrumentation

Measurement instruments were installed in four air-conditioned laboratory containers, positioned in two stacks of two with a 8 m tall, 0.5 m diameter, high flow (10 m^3 min^{-1} common inlet situated between the stacks (see Figure 4.1). The common inlet was designed to minimize wall losses of species in air drawn from the 8 m high sampling point, and to avoid small scale measurement differences caused by individual inlet positioning. For the

[2]http://iupac.pole-ether.fr/index.html; accessed on 12$^{\text{th}}$ of July 2016

measurement of VOCs a slower subsample flow (5 L min^{-1} was drawn through insulated and heated (35 °C) Teflon (OD = 1.27 cm) lines installed perpendicular to the direction of main inlet flow and into the VOC group measurement container. This air was analyzed by a Proton Transfer Reaction-Time Of Flight-Mass Spectrometer (PTR-TOF-MS), an OH reactivity system, two Gas Chromatography systems with a Flame Ionization Detector (GC-FID) and one Gas Chromatography system combined with a Mass Spectrometer (GC-MS).

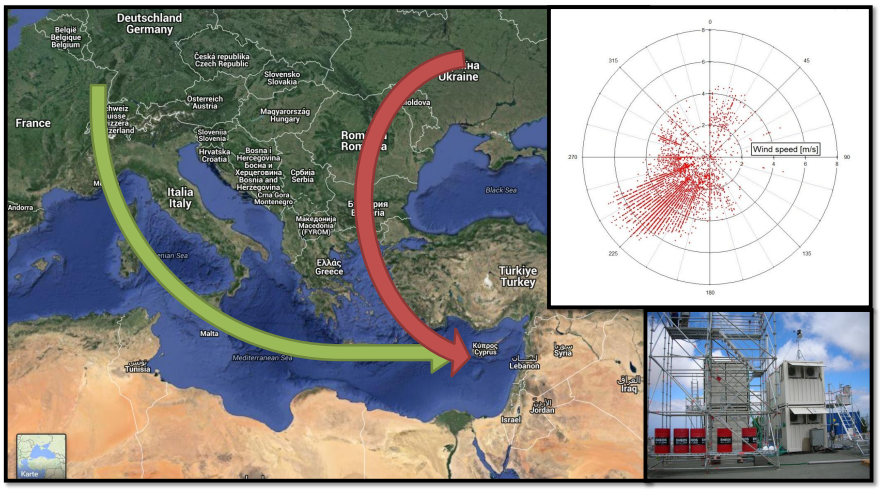

Figure 4.1.: Map of the Mediterranean Basin. The green arrow shows the inflow from western and the red the inflow from Eastern Europe. On the right hand side a wind rose displaying the dominant wind direction and a picture of the laboratory containers can be seen.

Proton Transfer Reaction-Time of Flight-Mass Spectrometer

On-line VOC measurements were performed with a PTR-TOF-MS (Ionicon Analytik GmbH, Innsbruck, Austria). This instrument has been described in detail in chapter 2. Post-acquisition data analysis was performed using the program "PTR-TOF DATA ANALYZER", which is detailed elsewhere (Müller et al., 2013). The time resolution of the measurements was 1 min and the background level was determined every two hours for twenty minutes by passing air through a catalytic converter containing platinum coated pellets heated to 320 °C. The drift pressure was maintained at 2.20 mbar and the drift voltage 600 V (E/N 137 Td). To perform mass scale calibration 1,3,5-trichlorobenzene was permanently bled into the sample stream as an internal standard. A comprehensive 4 point humidity dependent calibration of the instrument was performed at the beginning

and at the end of the campaign using a commercial gas standard (Apel-Riemer Environmental) containing 14 compounds. The sensitivity of the instrument, which was interpolated linearly over the campaign, decreased from between 0.6 ncps/ppbv (e.g. isoprene) and 3 ncps/ppbv (e.g. methanol). With increasing humidity the sensitivity, expressed in counts per second per ppbv, decreased exponentially for most species. Only isoprene and methanol did not show any humidity dependency. Calibration factors were applied by taking the time of the measurement as well as the humidity for each data point into account. Detection limits for each species quantified were determined by calculating three times the standard deviation of the background measurement, which resulted in between 15 pptv (e.g. acetonitrile) and 200 pptv (methanol). The total uncertainty varied between 10 and 15 %. Only methanol had a higher total uncertainty of 30 % due to problems during calibration (see section 3). Acetic acid was calibrated separately by the use of a permeation source, because it was not included in the pressurized gas standard. For the acid only one calibration was performed in the field with two different humidities. As found by Feilberg et al. (2012) the humidity dependency of acetic acid shows a linear behavior. After the campaign a second calibration was done in the laboratory at three different humidities. The calibration factors obtained in the field and in the laboratory differed by a factor of ca. 2.5. Also the slope of the linear interpolations between the calibration factors of different humidities measured in the laboratory and in the field varied. Therefore, the fit parameters of both linear regressions were averaged and the resulting mean fit function was used to calculate the calibration factor according to the humidity at the time. A high total uncertainty of 47 % was determined so that the discrepancy in the calibration factors was covered.
Acetic acid was measured at mass m/z 61.0284 amu, but its mixing ratios must be considered as upper limits, because the PTR-TOF-MS is not able to distinguish between acetic acid and its isomer glycolaldehyde (Baasandorj et al., 2014). Furthermore, fragments of peroxyacetic acid (PAA) and ethyl acetate can also be measured on the exact mass of acetic acid (Baasandorj et al., 2014). However, since the sources of ethyl acetate are mainly anthropogenic and the measurement site remote, we assume the influence of ethyl acetate was negligible. This assumption is supported by the finding that the signal at m/z 61.0284 amu was significantly reduced during periods when the site was impacted by fog, indicating that the responsible trace gas was highly soluble in water. The potentially interfering molecule ethyl acetate is not nearly as soluble: 0.059 $mol\,m^{-3}\,Pa^{-1}$ in comparison to 40 - 46 $mol\,m^{-3}\,Pa^{-1}$ for acetic acid, see Sander (2015).
The PTR-TOF-MS was not calibrated for PAA and monitored it only during a few days of the campaign at mass m/z 77.0233 amu. On these days the PAA signal in counts per second was very low (ca. 0.3 cps). Španěl et al. (2003) reported that 90 % of PAA are measured at the exact mass of acetic acid while 10 % are recorded at the mass of the mother ion (m/z 77.0233 amu). If this is taken into account PAA would still influence acetic acid only between 10 and 20 % because of the low count rates. But these numbers are based on the signal in counts only and can change if the sensitivity would also be considered. A Chemical Ionization Mass Spectrometer (CIMS) designed to measure PAA operated in two modes during the campaign (Phillips et al., 2013).
From $\sim 17^{th}$ - 24^{th} July the CIMS measured PAA only and found very low values, close to the detection limit. From $\sim 26^{th}$ July until the end of the campaign the collisional

dissociation parameters were adjusted and PAA and acetic acid were detected on the same mass (59 amu). During CYPHEX no attention was paid on the CIMS data for acetic acid. Relative sensitivity tests and approximate reprocessing of the data were done in 2015. For this reason, the data from the CIMS should be considered largely qualitative, but reveal that PAA levels were substantially lower than those of acetic acid.
Figure 4.2 displays the acetic acid and the peracetic acid traces as well as their correlation and it can be seen that the PAA data without accompanying detection of acetic acid showed very low values between 0 and 200 pptv from $\sim 17^{\text{th}}$ - 24^{th} July. The later period from $\sim$ 26^{th} July until 3^{rd} of August exhibited much higher signals due to the sum of PAA and acetic acid and the correlation in the CIMS and the PTR-TOF-MS time profiles suggest that most of this is due to acetic acid. This is confirmed by the high correlation factor of 0.74 between acetic acid and PAA during the later period.
The potential interference in the PTR-TOF-MS signal for acetic acid is thus covered by the 47 % total uncertainty in the acetic acid measurements. The main sources of glycolaldehyde are biomass burning and secondary production from isoprene and ethene degradation (Niki et al., 1981; Paulson and Seinfeld, 1992). Since the acetonitrile levels stayed low during the whole campaign we can exclude a significant influence of biomass burning. Furthermore, as will be shown in the results section, isoprene levels were low due to the scarce vegetation and low local anthropogenic emissions occurred. The atmospheric lifetime of glycolaldehyde was calculated taking the reaction with OH and photolysis into account. During the campaign an average OH concentration of $\sim 2 \times 10^6$ molec/cm^3 and an average photolysis rate of $\sim 3 \times 10^{-6}$ s^{-1} were determined. Using a reaction rate of 8.0×10^{-12} cm^3 molec^{-1} s^{-1}) provided by IUPAC[3] a lifetime of ∼15 h was calculated. Wet and dry deposition were not considered in this calculation and would reduce the lifetime even further. In most cases the air masses measured remained twelve or more hours over the Mediterranean Sea before reaching Cyprus. This would mean that some glycolaldehyde could survive transport, especially during night, but the amount is expected to be small. Since there is no known ocean source for glycolaldehyde, we can assume that this compound has only a minor effect on the acetic acid signal. In view of the discussion above, the acetic acid mixing ratios shown in the following analysis may be regarded as an upper limit.

Monoterpenes, ozone, CO and meteorological parameters

Monoterpenes measured by a commercial GC-MS system (MSD 5973; Agilent Technologies GmbH) combined with an air sampler and a thermal desorber unit (Markes International GmbH). The sample interval was 45 min, the total uncertainty roughly 20 % and the detection limit amounted to $\sim$ 1 pptv.
Ozone was monitored using a U.V. Photometric O_3-Analyzer (model 49, Thermo Environmental Instruments, U.S.) The detection limit was 2 ppbv and the overall uncertainty less than 5 %.
CO was monitored by a Room Temperature Quantum Cascade Laser (RT-QCL) (Li et al., 2012). The instrument uses wavelength modulation absorption spectroscopy (2190 cm^{-1}) over a path length of 36 m to measure CO at a time resolution of 1 s. The detection limit

[3]http://iupac.pole-ether.fr/index.html; accessed on 12^{th} of July 2016

was determined to be 0.4 ppbv and the overall uncertainty 14.4 %. For more information please refer to Li et al. (2012).
The weather station Vantage Pro2 (Davis Instruments Corp., Hayward, CA) was used to measure temperature, pressure, wind direction and speed, solar radiation and humidity with a time resolution of 1 minute.

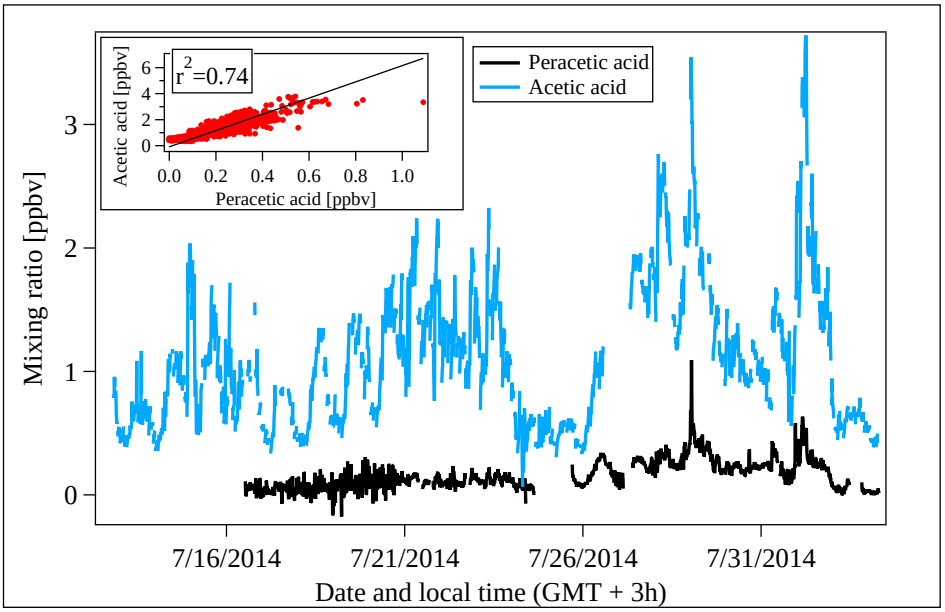

Figure 4.2.: Time trace of peracetic acid measured by CIMS and acetic acid measured by PTR-TOF-MS

4.2.3. Modeling

FLEXPART model

The dynamical transport history of air reaching Cyprus during the CYPHEX campaign was determined by using the Lagrangian particle dispersion model FLEXPART (Stohl et al., 2002, 2005, 2007). It computes trajectories of infinitesimally small air parcels (so-called particles) to describe the transport and diffusion of tracers (Stohl et al., 2005). Thereby mean winds interpolated from analysis fields and turbulence represented by random motions are used (Stohl et al., 2007).
In this study, FLEXPART was run backward in time from the measurement site driven with analyses from the ECMWF with $0.2\,^\circ \times 0.2\,^\circ$ horizontal resolution (derived from T799 spectral truncation), a vertical resolution of 137 model levels and temporal resolution of 1 hour, which is a combination of 6 h- analysis and short-term forecasts.
Backward simulations were made for 3 h time intervals between 12th of July 2014 and 03rd August 2014 and for each interval 10000 passive air tracer particles were released and followed backward in time for 120 h. The distribution of tracer particles is analyzed during the 120 h simulation and leads to a particle density distribution describing the residence

time in each cell of a defined geographical grid. Column-time integration of residence times results in a horizontal distribution indicating the total upwind area of influence. Regions of higher residence times during the simulation period identify major transport routes of air reaching the site.

CAABA/MECCA

To investigate photochemical processing over the ocean, the observations were compared to simulations with the chemical box model CAABA/MECCA (Sander et al., 2011). We used version 3.8, which includes the recently developed comprehensive organic reaction scheme MOM by Taraborrelli et al. (manuscript in preparation). Focusing on organics, we switched off halogen and sulfur chemistry, as well as heterogeneous and aqueous phase reactions in view of the low cloudiness and aerosol concentrations. Initial values were retrieved from the EMAC model (Jöckel et al., 2016) and are available in the appendix A. Photolysis rate coefficients were calculated for the latitude of Cyprus. The model simulated two diurnal cycles, starting on 19$^{\text{th}}$ July at 6 am and running for 48 h. No further emissions were injected during the model run, except ozone. Dry deposition as well as uptake by aerosols were not considered in this study. The results will be discussed in section 4.3.2.

4.3. Results and discussion

4.3.1. Biogenic compounds

In general, the mixing ratios of biogenic compounds measured at the site were low, with the sum of isoprene (m/z 69.0699) and monoterpenes (m/z 137.1325) never exceeding 0.5 ppbv and a campaign average daily maximum of $\sim$0.1 ppbv for both. This is in contrast to tropical forest regions where typical values of 8 ppbv isoprene have been reported recently (Yañez-Serrano et al., 2014), but consistent with levels reported from the Mediterranean areas (Liakakou et al., 2007; Davison et al., 2009). Comparable emission rates of isoprene and monoterpenes can be regarded as typical for the Mediterranean vegetation (Kesselmeier and Staudt, 1999). With regard to atmospheric lifetimes for isoprene and monoterpenes in the order of minutes to hours with respect to reaction with OH, we concluded that they must have been emitted from local vegetation. Figure 4.4 displays the campaign averaged, diel cycles of the sum of the monoterpenes and of isoprene. Both median diel cycles follow a roughly sinusoidal curve and were strongly light dependent. This finding is consistent with the literature, concerning isoprene and monoterpene emissions and atmospheric mixing ratios in the Mediterranean area (Kesselmeier et al., 1998; Liakakou et al., 2007; Davison et al., 2009).
Figure 4.3 shows the course of isoprene and the main monoterpene species as observed over the whole campaign detected by a GC-MS system with α-pinene being the dominant species among the monoterpenes quantified. At night the values were close to the detection limit of the PTR-TOF-MS, but the GC-MS data revealed that the mixing ratios of isoprene and monoterpenes decreased to nearly zero in almost all nights (see Figure 4.3). This light dependent behavior of the monoterpenes indicates that the vegetation is dominated by broad leaf species. Conifers, on the other hand, are able to store specific monoter-

penes and emit them also depending only on temperature or other stress (Kesselmeier and Staudt, 1999, and references therein) so that elevated levels could also be found at night (e.g. Davison et al., 2009; Staudt et al., 1997).

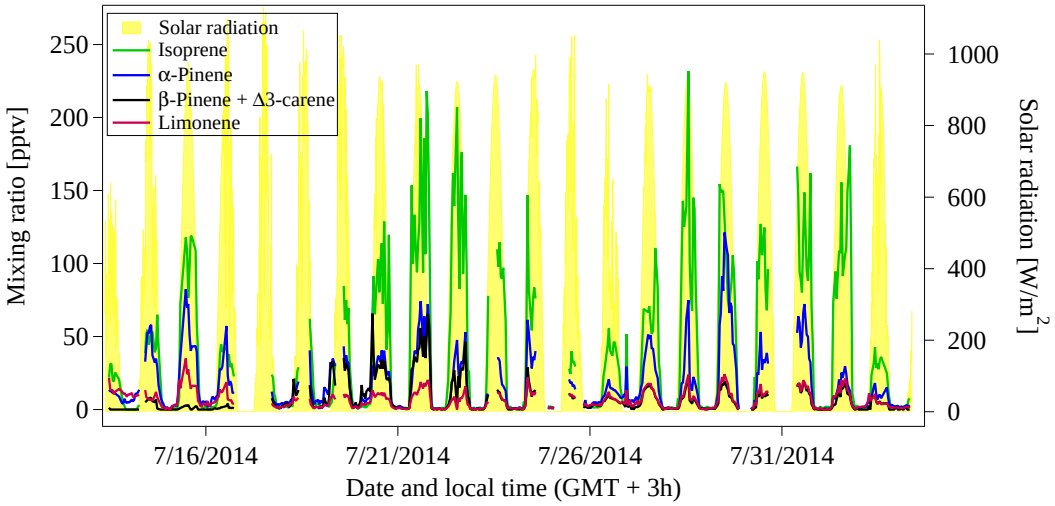

Figure 4.3.: Time traces of isoprene and different monoterpenes in pptv measured by GC-MS as well as solar radiation in Wm^{-2}

The isoprene mean data (Figure 4.4) show slightly elevated values in comparison to the median values in the morning and afternoon. A potential explanation can be found by considering the changes in meteorological conditions during these parts of the day, e.g. variation of the local boundary layer height relative to the hilltop site or the onset of the local sea breeze. The impact of these changes varied during the campaign, potentially causing the difference between median and mean values and motivates a closer look to single days. To illustrate this, isoprene from an example day has been plotted at 1 minute time resolution (Figure 4.5). On 22nd July at around 9:30 am local time the wind changed from N-NE to W-SW direction as accompanied by a sharp increase in relative humidity and in atmospheric dimethylsulfide (DMS), a species primarily emitted from marine sources (Cline and Bates, 1983; Mesarchaki et al., 2014). Before the wind direction changed, isoprene initially increased together with temperature. But as soon as the wind turned towards a direction reflecting a shorter distance between ocean and site, isoprene levels decreased rapidly. This behavior is consistent with the current understanding that the sea is only a weak source of isoprene and the main source is the local terrestrial vegetation (Bonsang et al., 1992; Broadgate et al., 1997; Palmer and Shaw, 2005; Arnold et al., 2009). However, isoprene did not always follow this pattern. On occasions isoprene levels stayed elevated in the morning despite a drop in temperature and associated increase in relative humidity and DMS. One explanation for this is an influence from a small forest upwind of the site. The Pikni forest 7 km to the southwest and some 300 m lower than the site can, given the right meteorological conditions, contribute to isoprene levels at the site despite its short lifetime (ca. 30 minutes with respect to OH, using a mean OH concentration of 5×10^6 molec/cm^3 measured between 6 am and 10 am). With an assumed average wind speed of 3.5 m/s

the transport time of isoprene from the forest to the site would amount to ~ 30 minutes. The same reasoning can be applied to the monoterpenes, because their lifetime amounts to ca. 60 minutes with respect to OH (calculated for α-pinene and an OH concentration of 5×10^6 molec/cm^3). But in contrast to the isoprene data the median and mean values of the monoterpenes showed less discrepancy, which might indicate differences concerning the source behavior. One possible explanation could be that species with different emission patterns for isoprene and for monoterpenes were not co-located. If the Pikni forest for example would be dominated by isoprene emitting plants, its irregular influence on the site could cause discrepancies between median and mean values of isoprene while the monoterpenes would remain unaffected. Other reasons supposably exist, such as a different emission regulation. However, direct measurements to demonstrate such different primary emissions were not performed and the atmospheric mixing ratio development indicates a clear light dependent emission regulation for monoterpenes as for isoprene with a very close relationship between isoprene and monoterpene production. In summary, the local vegetation produces modest emissions of reactive isoprene and monoterpenes. Their diel emission profiles are both light driven with a maximum around midday and slight variations can be traced back to changes in the local meteorology.

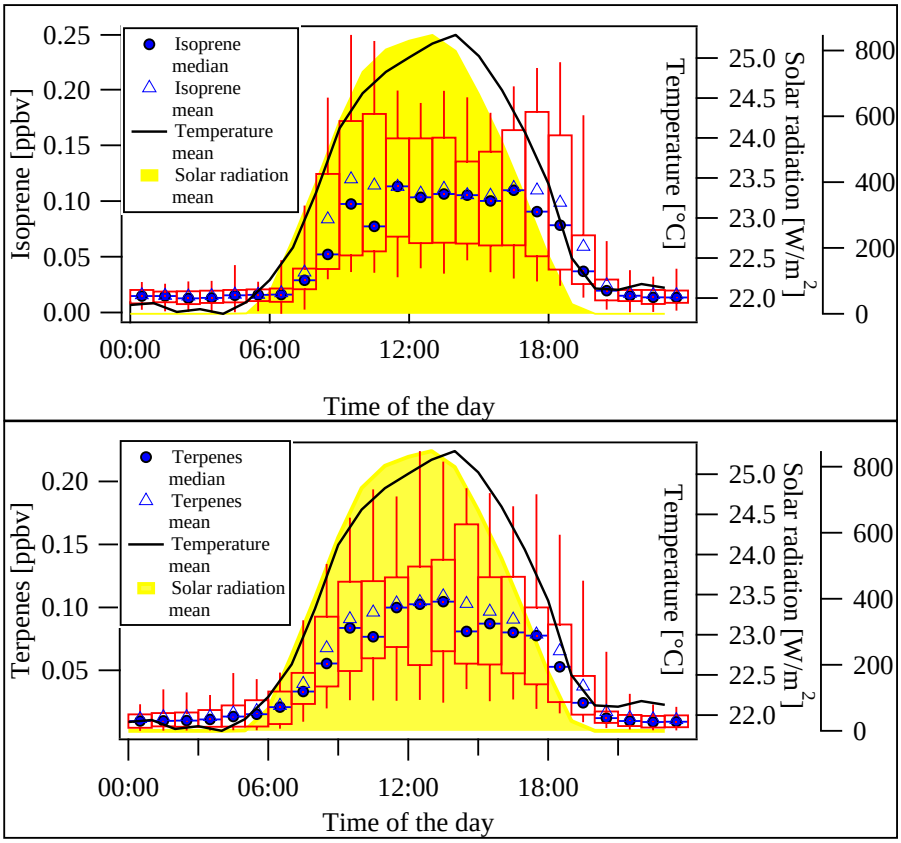

Figure 4.4.: Box and whiskers plot of isoprene and the sum of monoterpenes. The box contains 50 % of the data. 25 % of the data lie below the lower end of the box, 75 % below the upper end. The whiskers present the 5 - 95 % range of the data.

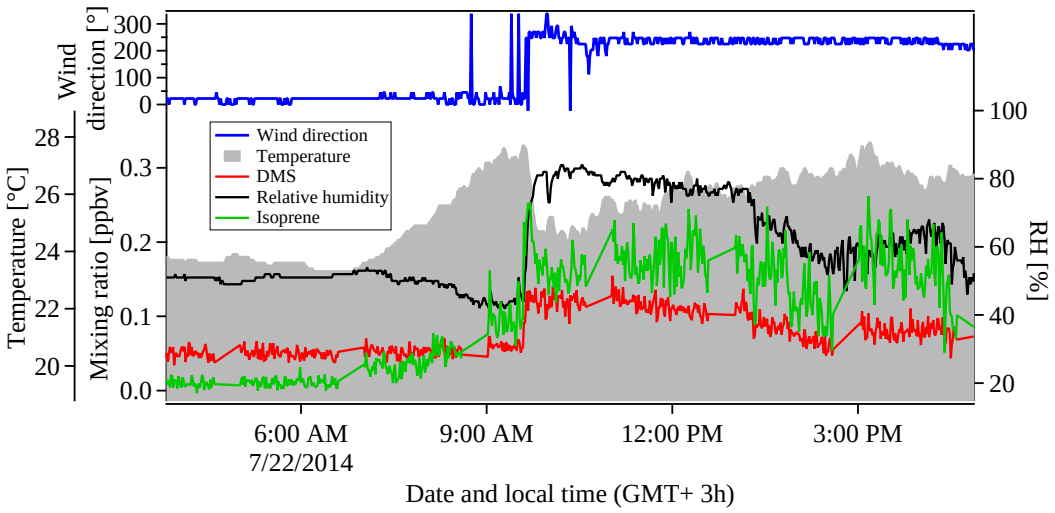

Figure 4.5.: Mixing ratios of isoprene and DMS in ppbv as well as wind direction, temperature and relative humidity over time with an one minute time resolution

4.3.2. Oxygenated volatile organic compounds (OVOCs)

Local impacts and transport processes

In contrast to the pronounced diel cycles and low mixing ratios found for the biogenic compounds the oxygenated VOCs showed relatively high values with comparatively little variation. Figure 4.6 displays the diel cycles of acetone, methanol and acetic acid. It becomes clear that the mean and median mixing ratios deviate in the morning and afternoon as already discussed for isoprene. The same reasoning is likely to apply: variable local meteorology leading to high values in the morning and afternoon on some days. Methanol exhibited a maximum mean and median mixing ratio in the early morning. Since vegetation is an important source of methanol this increase could be explained by sunlight dependant plant emissions or by evaporation of methanol collected in dew. The median mixing ratios of acetic acid indicate that a weak diel cycle is present. The acetic acid mixing ratios (humidity corrected) reveal a pronounced diel cycle between the 16$^{\text{th}}$ and 21$^{\text{th}}$ of July, which is displayed in Figure 4.7. In this part of the campaign a distinct anti-correlation between the acetic acid mixing ratio and humidity is apparent. Fog formation, which occurs under specific meteorological conditions (notably 100 % relative humidity (RH) in the presence of cloud condensation nuclei), leads to droplet sedimentation so that soluble gases are largely removed. Acetic acid is more strongly affected than acetone and methanol, because the latter are factor 143 and 22 less soluble, respectively. Uptake to droplets and sedimentation only occurs when 100 % relative humidity is reached and thus cannot explain the diel cycle of acetic acid at less than 100 %. Three other effects could play a role in this process: first, local photochemical production of acetic acid, second, in-mixing from the free troposphere by turbulence and third emission from and/or uptake by vegetation and soil.

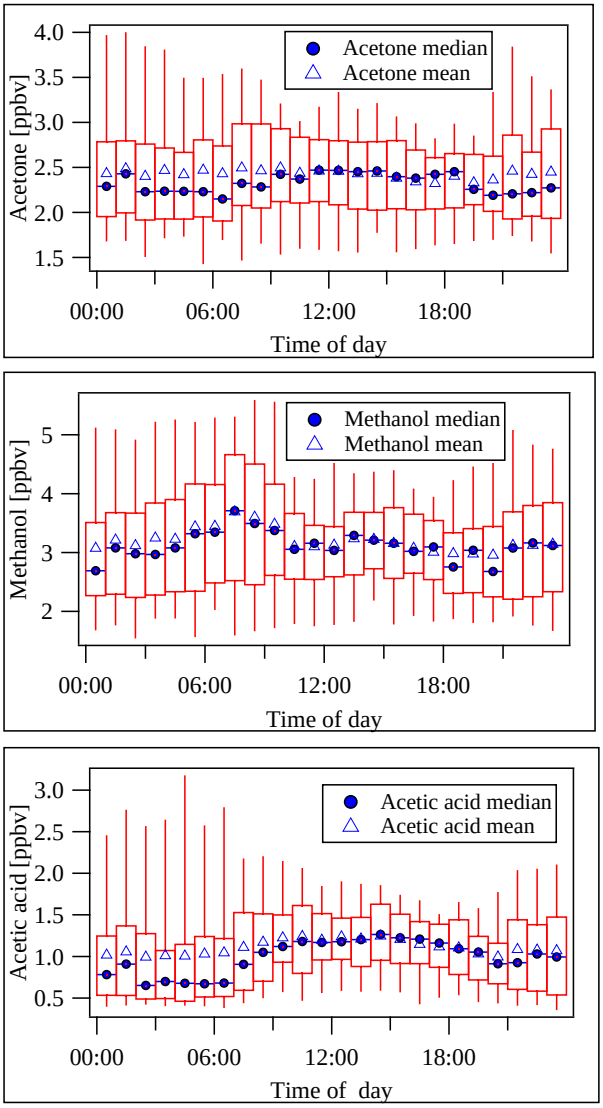

Figure 4.6.: Box and whiskers plot of acetone, methanol and acetic acid. The box contains 50 % of the data. 25 % of the data lie below the lower end of the box, 75 % below the upper end. The whiskers present the 5 - 95 % range of the data.

The measured production from 06:00 till 14:00 and the loss rate from 14:00 till 22:00 during the period from the 16th and 21th of July amounted roughly to 0.1 ppbv/h and 0.08 ppbv/h, respectively. Sanhueza and Andreae (1991) reported a daily average emission of acetic acid from savanna soil of 0.07 nmol m^{-2} s^{-1}. Assuming a PBL height of 500 m this would give a production rate of 0.012 ppbv/h. Although a direct comparison might be difficult, because the measurements were performed at different locations, the discrepancy of one order of magnitude strongly indicates that other processes than emission from soil played a role. According to Paulot et al. (2011) emissions from terrestrial vegetation account for 3 % of the total sources while photochemical production represents the major part of 69 %. However, in a remote site the contribution of secondary production is expected to be minor due

to a lack of precursors. Thus, it was concluded that in-mixing from the free troposphere contributed to the net, apparent production rate with the onset of turbulent mixing in the morning. It is assumed that, in comparison to the PBL, acetic acid levels are elevated in the free troposphere due to the high deposition rate of the acid within the PBL. The distinct diel cycles of acetic acid also coincided with a period of higher solar radiation (see Figure 4.7), which promoted turbulence.

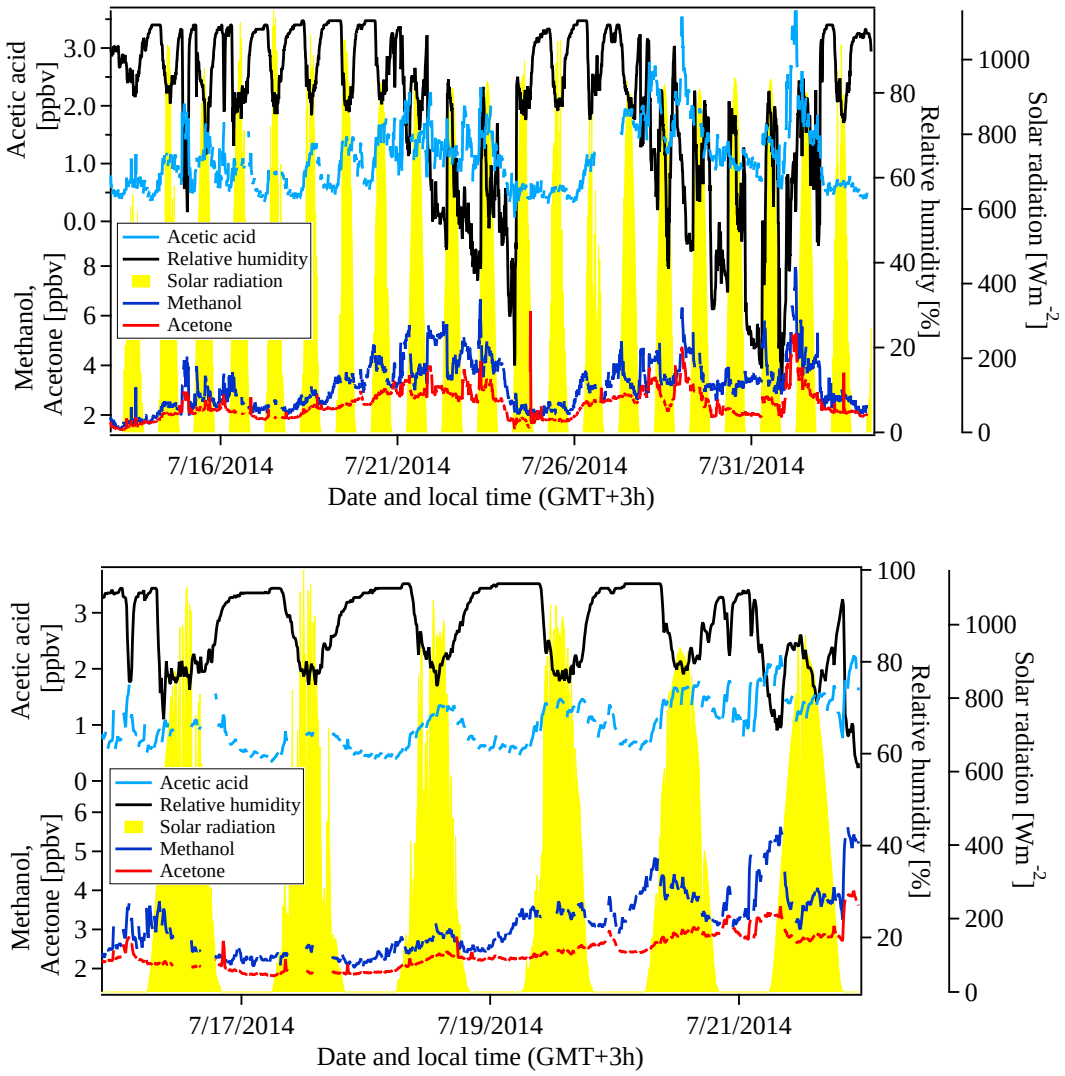

Figure 4.7.: Mixing ratios of acetic acid, acetone and methanol in ppbv, relative humidity in % and solar radiation in Wm^{-2} against time. The lower panel shows a detail from 16th to 21st of July.

Hartmann et al. (1991) determined a dry deposition rate of 0.5 - 1 cm/s for acetic acid in a savanna region. A boundary layer height of 500 m and an average acetic acid mixing ratio of 1 ppbv during the day would result in a loss rate of 0.04 - 0.07 ppbv/h. The measured loss rate in Cyprus (0.08 ppbv/h) was already quite close to this calculation,

which suggests that dry deposition is the major loss process of acetic acid. The reason why acetic acid did not display diel variability during the whole campaign is related to varying meteorological conditions, e.g. in the periods associated with strong decreases in humidity the site was likely within the free troposphere at night so that no distinct diel cycles could be established. Furthermore, long distance transport could have dominated over local processes.
To investigate the influence of transport processes the source regions and transport pathways of air arriving at the site were examined using the FLEXPART model. The area of influence of each single simulation can be described by the fraction of time the air has spent over different regions. For this study, the upwind region, namely the European continent, has been delineated into color coded sections, see Figure 4.8. Thus, the overall transport time for air masses reaching the site can be subdivided in specific colored fractions between 0 and 1. As one single colorbar characterizes the transport history of air at a certain time step, the combination of all colorbars of all single simulations weighted by time results in an overview of the evolution of transport patterns. This is shown in the upper panel of Figure 4.9. The lower-most panel of Figure 4.9 shows for each simulation the fraction of the time the air has spent within the planetary boundary layer ($\leq 30\,\%$), where surface processes, e.g. surface emissions or uptake of trace gases, can influence the air composition. To determine the footprint for a spatial and temporal variable layer as the PBL it was necessary to consider the PBL height over time at each single column within the area of influence. For example, the air mass that arrived on July 21st in Cyprus had spent 30 % of the last 120 hours within the PBL (see lower panel). Of this 30 %, two thirds were affected by Eastern Europe, marked in red, purple and pink. In contrast, on the 25th of July 35 % of the time the air was inside the PBL, whereof the main part was within the marine boundary layer (marked in blue). In the center section of the graph, mixing ratios of methanol, acetone and acetic acid are plotted on the same time scale. From Figure 4.9 it can be seen that the mixing ratios of all three compounds were higher when the air sampled came from Eastern Europe (red, purple, pink) and lower when arriving from western areas (green, yellow). Transport from the west to Cyprus entails longer transport times in the Mediterranean marine boundary layer than from the east. The trend implies that either the sources in Eastern Europe were stronger or loss rates were greater in air transported from the west. In Table 4.1 we list campaign averaged mixing ratios of different VOCs, O_3 and CO separated by eastern and western air flow. Consistent with methanol, acetone and acetic acid, other OVOCs like acetaldehyde and methylethylketone as well as O_3 and CO show higher mixing ratios in air masses with Eastern European origin. The mixing ratio of acetonitrile, a tracer for biomass burning, amounted to roughly 110 pptv in both flow regimes. These low mixing ratios and the lack of variability indicates that no air masses influenced by recent biomass burning reached Cyprus in the period of measurement. Anthropogenic tracers, such as the aromatic compounds benzene, toluene and the xylenes showed very low mixing ratios between 20 and 50 pptv, which confirms the remote location of the site and the minor influence of local anthropogenic emissions. This is also stressed by the small number of points which are above the detection limit (see Table 4.1). The high standard deviations of these aromatic compounds can be traced back to some rarely occurring spikes. The ozone mixing ratios of 60 - 70 ppbv are consistent with or even slightly higher than values found in Gerasopoulos et al. (2005) and Kleanthous et al. 2014.

The values measured during CYPHEX also exceed the European Air Quality Standard of 120 μg/m^3 (60 ppbv as a maximum daily 8 h mean)[4].
In the following section we examine the role of photochemical processes on the mixing ratios of the OVOC.

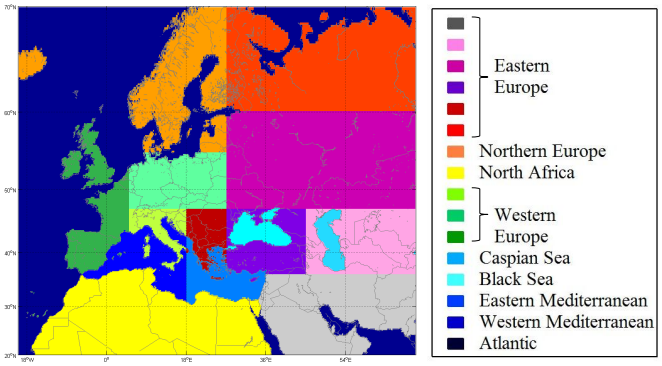

Figure 4.8.: Allocation of Europe into specific regions. The color scale refers also to Figure 4.9.

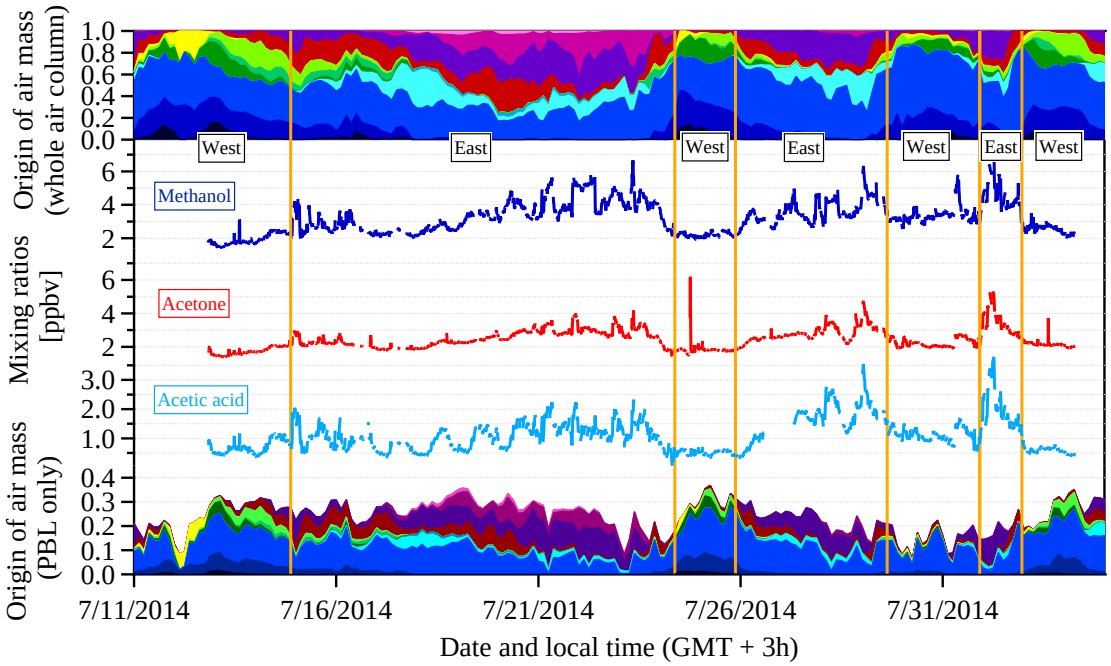

Figure 4.9.: Traces of methanol, acetone and acetic acid in ppbv as well as modeled data of the area of influence, given in fractions of 1. The color scale can be found in Figure 4.8

[4]http://ec.europa.eu/environment/air/quality/standards.htm; accessed 11th of July 2016

Table 4.1.: Averaged data of VOCs, O_3 and CO and their standard deviation in pptv for periods reached by air from eastern or western regions. For the calculation only data above the detection limit (3 σ) were used and n represents the number of points above this limit.

Compound	Eastern air mass	Standard deviation (east)	Western air mass	Standard deviation (west)
Methanol	3545 (n = 1687)	949	2571 (n = 908)	694
Acetonitrile	112 (n = 1695)	23	108 (n = 908)	29
Acetaldehyde	370 (n = 1625)	146	246 (n = 907)	92
Acetone	2659 (n = 1695)	576	1994 (n = 908)	342
Acetic acid	1280 (n = 1566)	598	778 (n = 851)	312
Dimethylsulfide	103 (n = 1695)	40	117 (n = 882)	60
Isoprene	101 (n = 941)	62	78 (n = 498)	55
Methylvinylketone	43 (n = 910)	31	41 (n = 348)	40
Methylethylketone	127 (n = 1695)	32	81 (n = 908)	21
Benzene	37 (n = 1515)	16	24 (n = 230)	11
Toluene	19 (n = 462)	21	17 (n = 72)	7
Xylenes	26 (n = 427)	33	49 (n = 99)	124
Trimethylbenzenes	19 (n = 223)	29	27 (n = 96)	74
Monoterpenes	65 (n = 1326)	56	49 (n = 736)	42
Ozone	73588	9441	61844	8627
CO	107274	9868	91361	6902

Investigation of photochemical processes using the CAABA/MECCA box model

The CAABA/MECCA box model was used to examine the photochemical processes influencing the mixing ratios of acetone, acetic acid and methanol. In order to simulate conditions in the MBL, where no major sources can be found, only initial values of precursors were set, with further emissions during the run deactivated. Dry deposition was also excluded, because this model run was intended to investigate photochemistry only. The trace gases included and their initial values, which originate from the Mainz Organics Mechanism, MOM, chemistry in the EMAC model, see Jöckel et al. (2016) can be found in the appendix. The model mixing ratios cannot be directly compared to the measured results, because processes like transport, ocean emission/uptake or dry deposition were not included in the box model. In Figure 4.10 the predicted mixing ratios of methanol, acetone and acetic acid, are displayed for a 48 h model run with an initial value for NOx of 2.4 ppbv. While methanol and acetic acid decrease, the mixing ratio of acetone increases. Figure 4.11 displays the rates of important reactions with a production or loss rate $\geq 10^{-16}$ mol/mol/s (0.36 pptv/h) impacting the budgets of the OVOCs. The main process affecting methanol is the degradation by OH radicals. For acetic acid production via the peroxy acetyl radical ($CH_3C(O)O_2$) is countered by its loss via reaction with OH. Net production of acetic acid was achieved only if enough organic precursors would be emitted at low NOx level (ca. 300 pptv), which reduces the OH mixing ratio. The modeled

behavior of acetone is more complex. Among the most important reactions were its loss by OH radical reaction or photolysis as well as its production via the reaction of different intermediates, mainly peroxy radicals, with NO or OH. Examples would be the reaction of isopropyl peroxy radicals ($iC_3H_7O_2$) with NO or the reaction of NO and $C_{10}H_{17}O_5$, which is an intermediate from β- pinene oxidation. In the model β - pinene had an initial value of 30 pptv. It can be concluded that secondary production in the MBL plays only a role for acetone while methanol and acetic acid are rather depleted.

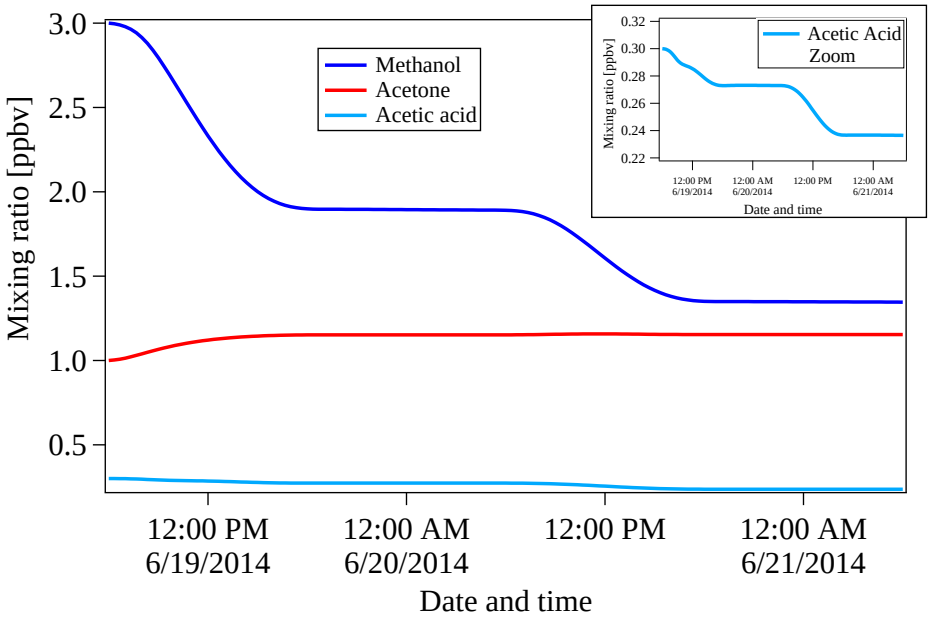

Figure 4.10.: Modeled mixing ratios of acetic acid, acetone and methanol over the period of 48 h starting at 6 am. Initial values originate from the MOM chemistry in the global model EMAC (Jöckel et al., 2016).

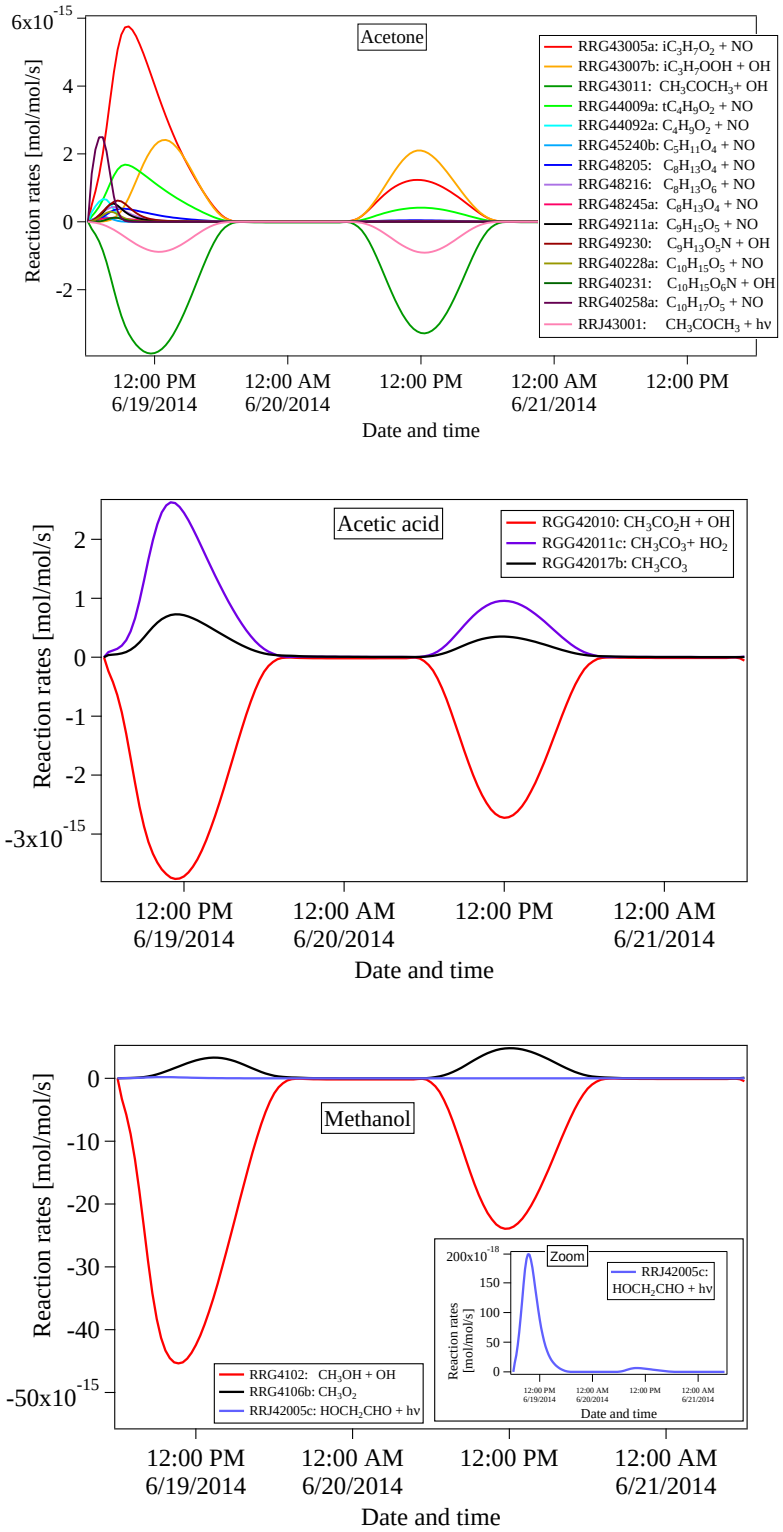

Figure 4.11.: Rates for reactions influencing mixing ratios of acetone, acetic acid and methanol. Further explanations of the reactions can be found in Taraborrelli et al. and Derstroff et al. (manuscripts in preparation).

Influence of marine boundary layer transport on OVOCs

In Figure 4.12, mixing ratios of methanol, acetone and acetic acid are plotted against the time the air spent in the marine boundary layer, calculated by adding up the FLEXPART modeled percentage of the influence of the Eastern and Western Mediterranean, the Black Sea, the Caspian Sea and the Atlantic Ocean. The summed percentage was then multiplied by the duration of the modeled backward trajectories (120 h). The data were separated into periods affected by Eastern and by Western Europe. The r^2 values vary from 0.2-0.5, but the slopes were consistently negative in all cases, and steeper for air masses from Eastern Europe. The OVOC loss rate values amounted to 0.1 ppbv/h for methanol, 0.06 ppbv/h for acetone and 0.05 ppbv/h for acetic acid for the eastern outflow and 0.06 ppbv/h for methanol, 0.02 ppbv/h for acetone and 0.03 ppbv/h for acetic acid for flow from the West. The net effect of transport over water for all three substances is a function of dilution (by vertical and horizontal mixing), photochemical degradation, uptake or emission by the ocean and production from the oxidation of larger organic molecules. As already mentioned, the atmospheric lifetimes with respect to OH were about 6 days for methanol, 32 days for acetone and 8 days for acetic acid. FLEXPART calculated transport times from Eastern Europe to Cyprus of roughly 1 - 2 day and from Western Europe to the site of around 2 - 5 days. Clearly the atmospheric lifetimes of acetone, methanol and acetic acid are all relatively long compared to the average transport time. This allows the influence of the MBL to be gauged. Only acetic acid was impacted by local effects in the period from 16^{th} - 21^{st} of July, because it showed a diel cycle. Since this period coincides with an eastern flow regime, only air masses from Western Europe are studied here. The loss rates of the three OVOCs were calculated using the following formula:

$$[RH]_t = [RH]_0 \times exp(-(k_{OH} \times [OH] + V_{dep}) \times t) \tag{4.1}$$

where $[RH]_t$ is the mixing ratio of the compound at a specific transport time t, $[RH]_0$ the initial mixing ratio, $[k]_{OH}$ the rate coefficient for reaction with OH radicals, [OH] the mixing ratio of OH and V_{dep} the dry deposition rate. Photolysis rates are so low that they can be neglected. The diel averaged OH mixing ratio at the site was measured as 2×10^6 molec/cm^3. k_{OH} values originate from IUPAC[5]. Since OH concentrations were constrained by measurement and the OH rate coefficients are well known, this loss term is assumed to be reasonably accurate. Dry deposition rates, on the other hand, represent a large uncertainty factor and dilution by vertical and horizontal mixing is not accounted for in the equation. We consider three different scenarios:

1. Dry deposition rates over the sea were taken from the global model EMAC (Jöckel et al., 2016) and amounted to 0.41 cm/s for acetic acid, 0.031 cm/s for acetone and 0 cm/s for methanol despite the higher solubility of methanol in comparison to acetone. An average PBL height of 500 m was assumed. The results can be found as light blue lines in Figure 4.12. The black lines represent the linear fit of the measured data. It becomes clear that acetic acid is well captured by the calculation while the measured net loss was greater than the calculated loss for methanol and acetone.

[5]http://iupac.pole-ether.fr/index.html; accessed on 12^{th} of July 2016

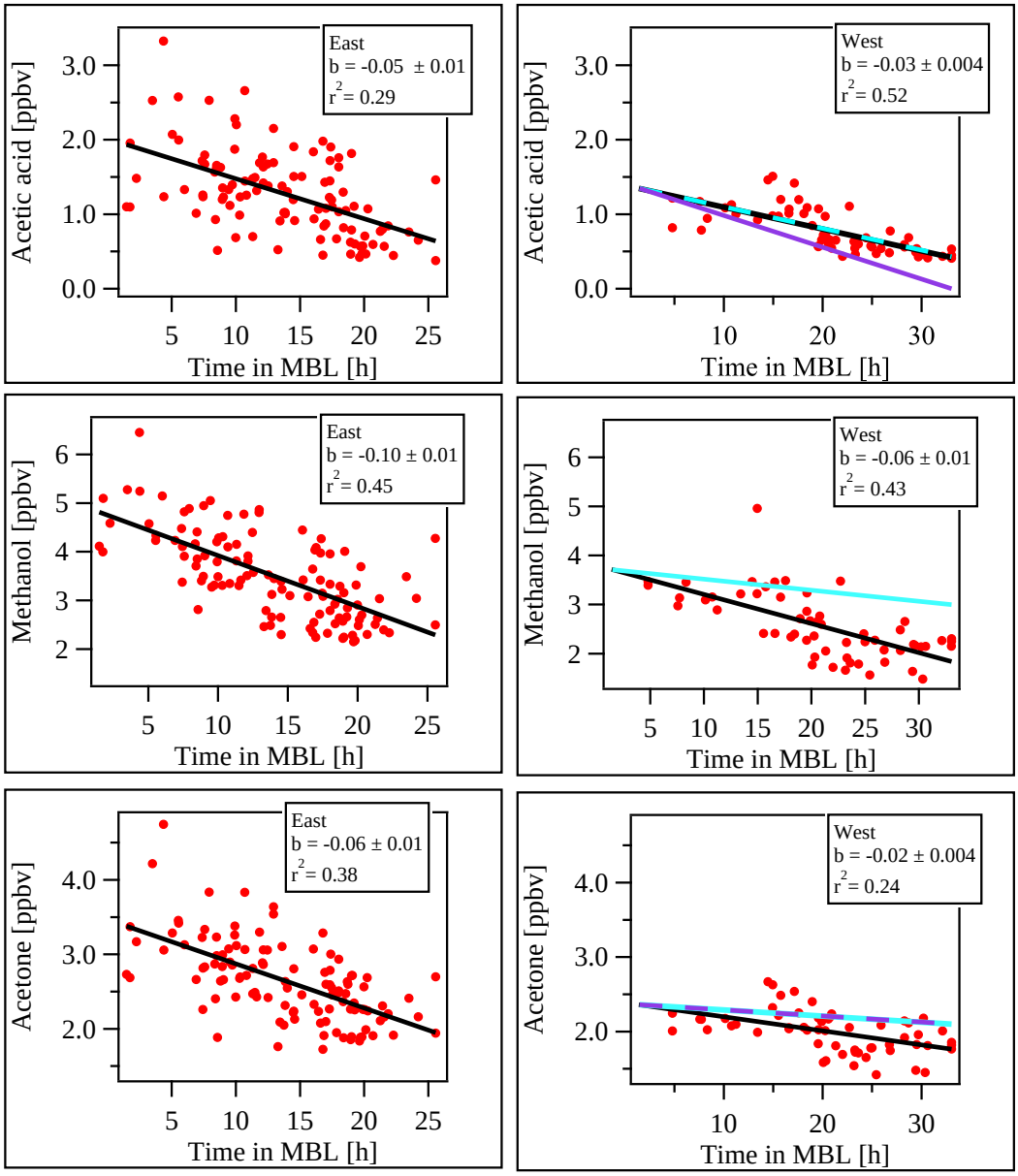

Figure 4.12.: Data of acetone, methanol and acetic acid separated by eastern and western air masses, plotted against the time in the MBL. The data were fitted using a linear fit algorithm (black line). The light blue lines refer to calculated loss rates using dry deposition rates from the EMAC model. The violet lines represent loss rates adjusted by solubility relative to methanol.

2. In the second scenario it was assumed that vertical in-mixing from above was low and the air masses are horizontally homogeneous. Without the process of dilution the dry deposition rate would be the only uncertain variable. Thus, dry deposition rates were adjusted so that the measured loss rates were reached. This method yielded a dry deposition rate coefficient of 0.21 cm/s for methanol, 0.10 cm/s for acetone and 0.42 cm/s for acetic acid, still assuming a PBL height of 500 m. These values do not reflect the relative solubilities. According to Sander (2015) methanol has a Henry's Law constant between 1.7 and 2.2 $mol\,m^{-3}\,Pa^{-1}$, acetone between 0.26 and 0.33 $mol\,m^{-3}\,Pa^{-1}$ and acetic acid between 40 and 46 $mol\,m^{-3}\,Pa^{-1}$. Based on solubility alone we would therefore expect the acetic acid loss rate to be much higher than that of acetone.

3. In the last scenario the dry deposition of methanol was adjusted so that the loss rate matches the measured one (0.21 cm/s). The dry deposition rates of acetic acid and acetone were set according to their relative solubilities: 4.4 cm/s for acetic acid and 0.031 cm/s for acetone. The results can be found as violet lines in Figure 4.12. Interestingly, the value for acetone gained by this method is the same as in the model and its loss rate is still underestimated. The loss rate of acetic acid is now even higher than the measured one.

Clearly, the measured loss rates of methanol and acetone are higher than expected. Although the acetic acid loss rate is nicely reproduced by the model, a higher loss rate would be anticipated owing to its solubility. Four possible explanations for this apparent anomaly will be considered here. The first is that vertical transport to the sea surface layer was a limiting factor so that turbulence rather than solubility defined the distribution. The second is that sea-water surface layer concentrations of acetic acid were high relative to methanol and acetone, compensating for the difference in solubilities. The third is that photochemical production of acetic acid in air was much more important than acetone and methanol. The fourth is that in-mixing of air from the free troposphere is significant. Although ocean concentrations and air-sea fluxes of acetone and methanol have been determined previously (Williams et al., 2004; Sinha et al., 2007), to our knowledge no equivalent measurements for acetic acid exist. Generally it has been found for methanol and acetone that the ocean and air are close to equilibrium on a global scale (Millet et al., 2008; Fischer et al., 2012), but that a significant aqueous phase production term exists for both species. Regionally, strong biological activity can drive a surface ocean oversaturation of acetone, that leads to its emission (Taddei et al., 2009). Dixon et al. (2014) have shown that in-ocean microbial acetone loss rates are highest in winter and that methanol is more efficiently consumed microbially than acetone (Dixon et al., 2014). These findings therefore do not appear to offer an explanation for the methanol and acetone ratio nor the relatively low loss rate of acetic acid.
In the case of in-situ photochemical production of methanol, acetone and acetic acid, several global estimates exist. As already mentioned, Millet et al. (2008) calculated that 37 Tg/yr of the total 242 Tg/yr global source budget of methanol was produced through the reaction of the CH_3O_2 radical. Fischer et al. (2012) calculated with the same model that 26 Tg/yr of acetone from global total 146 Tg/yr was from photooxidation of isoalkanes. In the case of acetic acid the 86 Tg/yr per year global budget is dominated by photochemical

production of 59 Tg/yr (Paulot et al., 2011). Therefore, on a global scale the fraction of the global budget attributable to photochemical production is larger for acetic acid (69 %) relative to methanol (15 %) and acetone (18 %). However, in order to compensate for solubility driven loss rates this photochemical production of acetic acid would have to be over 60 times more effective than methanol and acetone, which is unlikely in view of the budgets detailed above. Furthermore, the CAABA/MECCA box model indicates that acetic acid is depleted over the ocean rather than produced (see section 4.3.2). Another possible reason for the high loss rates could be in-mixing of acetone and methanol poor air from the free troposphere. That in-mixing took place or that the site was even within the free troposphere is confirmed by strong decreases in humidity levels (see Figure 4.7) and by the loss rate of CO. In general, no significant loss of CO is assumed over the ocean due to its long lifetime of 40 days with respect to OH and its negligible dry deposition. However, a loss rate of 0.65 ppbv/h, which is higher than expected, was determined. Thus, it can be concluded that entrainment of air from the free troposphere occurred. If dry deposition rates reflecting the solubilities are assumed it would therefore mean that acetic acid rich air caused a reduction of its net loss rate. As discussed above, a higher mixing ratio of acetic acid in the free troposphere is reasonable due to its high deposition loss rate in the PBL.
The most likely explanation for our observations are that loss of trace gases at the sea surface is limited by turbulence rather than by solubility and that vertical entrainment and horizontal dilution impact the mixing ratios measured downwind of the source regions.

Correlations between acetone, methanol, acetic acid, CO and ozone

Table 4.2 shows slopes, intercepts and correlation coefficients (r^2) from the bivariate fits between methanol, acetone, acetic acid, CO and ozone separated by eastern and western air masses. In the acetone data the two spikes occurring at the 24^{th} of July and 2^{nd} of August were removed, because they were most probably emerging from local sources. It can be seen that the correlations calculated from air masses originating in Eastern Europe are, on average, higher than the ones from Western Europe. As already mentioned horizontal or vertical dilution/ in-mixing, photochemical processes as well as emission or uptake by the ocean play important roles during transport. These effects can influence the various compounds to different degrees so that divergent correlation factors are expected.
Figure 4.13 displays the correlations between the OVOCs divided into eastern and western flow regimes. The decreasing correlation factors appear as higher scatter between the trace-gases measured in western air masses. The highest correlation is between acetone and acetic acid in the eastern flow ($r^2 = 0.81$) while the correlation between the same molecules, acetone and acetic acid, in the western flow is $r^2 = 0.52$, only. The slope between acetone and acetic acid, on the other hand, stayed almost the same for both flow regimes (~ 1). However, the graph referring to air coming from Western Europe shows two rather distinct branches. This can be understood if acetone and acetic acid were influenced by different loss and/or production processes, that led to the grouping of the data points along different correlation lines and the decreasing r^2 value. The longer the transport time the more important are the discrepancies between loss and production.

Table 4.2.: Slope, intercept and correlation coefficient (r^2) of different compounds separated in air masses from Eastern and Western Europe

Eastern air masses	Western air masses
Methanol vs. acetone $slope = 1.8, intercept = -1.1, r^2 = 0.76$	Methanol vs. acetone $slope = 2.8, intercept = -3.0, r^2 = 0.62$
Acetic acid vs. methanol $slope = 0.54, intercept = -0.64, r^2 = 0.53$	Acetic acid vs. methanol $slope = 0.37, intercept = -0.18, r^2 = 0.57$
Acetic acid vs. acetone $slope = 1.0, intercept = -1.5, r^2 = 0.81$	Acetic acid vs. acetone $slope = 1.1, intercept = -1.4, r^2 = 0.52$
Methanol vs. ozone $slope = 0.056, intercept = -0.60, r^2 = 0.32$	Methanol vs. ozone $slope = 0.022, intercept = 1.2, r^2 = 0.08$
Methanol vs. CO $slope = 0.065, intercept = -3.4, r^2 = 0.45$	Methanol vs. CO $slope = 0.067, intercept = -3.6, r^2 = 0.44$
Acetone vs. ozone $slope = 0.036, intercept = 0.017, r^2 = 0.36$	Acetone vs. ozone $slope = 0.0067, intercept = 1.6, r^2 = 0.04$
Acetone vs. CO $slope = 0.046, intercept = -2.3, r^2 = 0.61$	Acetone vs. CO $slope = 0.030, intercept = -0.80, r^2 = 0.52$
Acetic acid vs. ozone $slope = 0.032, intercept = -1.1, r^2 = 0.26$	Acetic acid vs. ozone $slope = 0.018, intercept = -0.35, r^2 = 0.25$
Acetic acid vs. CO $slope = 0.041, intercept = -3.1, r^2 = 0.46$	Acetic acid vs. CO $slope = 0.024, intercept = -1.4, r^2 = 0.28$
Ozone vs. CO $slope = 0.92, intercept = -25, r^2 = 0.30$	Ozone vs. CO $slope = 1.9, intercept = -110, r^2 = 0.14$

To a lesser degree, similar effects are found in the correlation between methanol and acetone. Here the correlation factors decreased from 0.76 (eastern flow) to 0.62 (western flow). In Figure 4.14 correlations between methanol and acetone as well as acetic acid from western flow regimes are color coded by relative humidity (RH) and O_3. The methanol vs. acetone as well as acetic acid vs. acetone plots color coded by RH reveal that the origin of the different branches is tied into high relative humidity and thus fog events (RH $> 90\,\%$, red dots). Since methanol and acetic acid are more soluble than acetone, these compounds are more efficiently removed by droplet sedimentation in foggy conditions. This leads to a decrease in the slope and therefore the formation of the lowest branch.
Furthermore, the acetic acid vs. acetone plot color coded by O_3 shows that higher ozone levels were correlated with higher acetic acid and/or lower acetone mixing ratios. The branching was most probably dominated by the relationship between acetic acid and ozone, because the correlation between acetone and ozone was weak in the western flow regime (r^2=0.04). Since ozone is in general generated by photochemical processes, the correlation may indicate that acetic acid is also generated photochemically. However, this would contradict the conclusions of the box-model study (see 4.3.2), in which acetic acid is lost rather than formed over the ocean due to a lack of precursors.

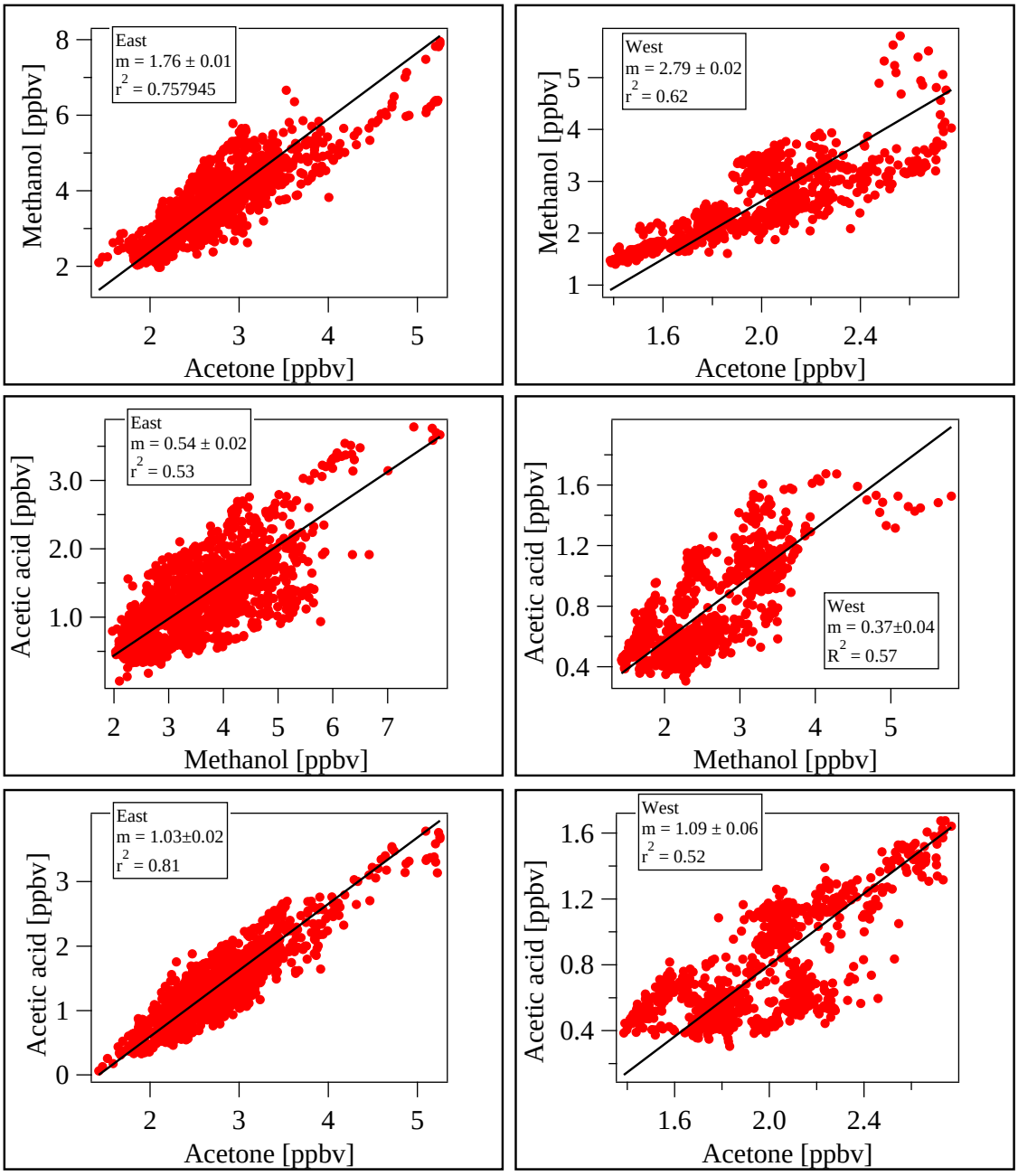

Figure 4.13.: Correlations between the OVOCs separated by eastern and western flow regimes. A bivariate fitting method was applied.

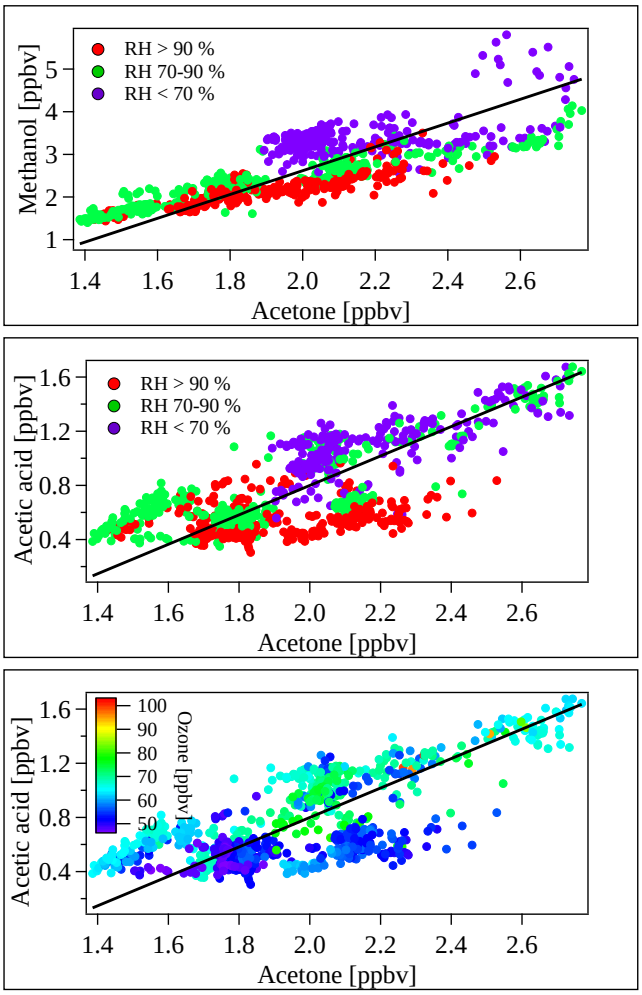

Figure 4.14.: Correlation plots exclusively from western air masses were color coded by ozone data and relative humidity to show different branches

Another reason for the correlation could be in-mixing of both compounds from the free troposphere as both acetic acid and O_3 mixing ratios are expected to decrease close to the ground due to high dry deposition rates. Another indication for the impact of air masses from the free troposphere is the low relative humidity. The high ozone mixing ratios (color coded in light green in the lower most panel of Figure 4.14) coincide with RH levels below 70 % (color coded in violet in the panels above), which can be interpreted that rather dry, but ozone rich air was influencing the site.
The correlation coefficients between acetic acid and methanol, listed in Table 4.2, showed no difference between eastern and western air masses, but the slope slightly decreased when changing from eastern to western flow regimes. If the loss rates over the ocean are taken into account (see Figure 4.12 and section 4.3.2) an increasing instead of decreasing slope would be expected, because acetic acid showed a weaker decline than methanol. The slope between methanol and acetone on the other hand increased when changing from eastern to western air masses, although a decrease would be expected. Hence, it can be concluded that not only the time over the ocean, but also other effects played an important role,

e.g. different emission ratios at the continent or local impacts like fog events or changing meteorological conditions. Especially acetic acid was biased by these local effects during an eastern flow regime which can be seen in the diel cycles between the 16th and 21th of July (see section 4.3.2).
Comparing the three OVOCs to CO (Table 4.2) shows that the correlation between methanol and CO remained remarkably constant between the western and eastern flow regimes (r^2=0.44 and 0.45). In contrast to acetic acid and acetone, this correlation appears to be insensitive to the combined processes of dilution, marine uptake/emission and photochemical aging for air masses in this region. The data can be compared to the MINOS campaign, which took place in Finokalia, Crete (Salisbury et al., 2003). One part of the MINOS campaign, with no biomass burning influence and an eastern flow regime ("period 1"), was the most appropriate to compare with the CYPHEX data. Interestingly the ratio between methanol and CO calculated from Salisbury et al. (2003) (0.02 for "period 1") is smaller than the one determined in this study (0.033). The reason for this is a lower CO mixing ratio (MINOS: 167 ppbv, CYPHEX: 107 ppbv) while the methanol values were similar in both campaigns (MINOS: 3.34 ppbv, CYPHEX: 3.54 ppbv). In the same way, the acetone/CO ratio measured in this study (0.025) for easterly conditions was larger than the one reported by Salisbury et al. (2003) (0.017, "period 1") due to lower CO mixing ratios. The decreased CO values might be traced back to the economic crisis in Greece, which led to a reduction of industrial production and therefore to decreasing emissions of anthropogenic compounds like CO.
Another interesting relationship arose between ozone and the OVOCs. Regarding western air masses the correlations between the OVOCs and ozone were extremely poor, the best being between acetic acid and O_3 (r^2=0.25) while the others were below r^2=0.01. In eastern flow regimes, on the other hand, the correlations were slightly stronger. If the correlation plots among the OVOCs from eastern air masses are color coded by ozone (Figure 4.15) it can be seen that all plots show the same pattern: the higher the ozone values the higher the OVOC mixing ratios. This can be explained by the shorter distance from Cyprus to the sources in Eastern Europe. Still it needs to be kept in mind that the sources for the four compounds are different, e.g. methanol is mainly biogenically produced while secondary production dominates for acetic acid over land. The reason for the correlation could simply be that the sources were co-located on the continent and due to the shorter transport time from Eastern Europe the various loss and production processes had a weaker impact than in air masses from western Europe.

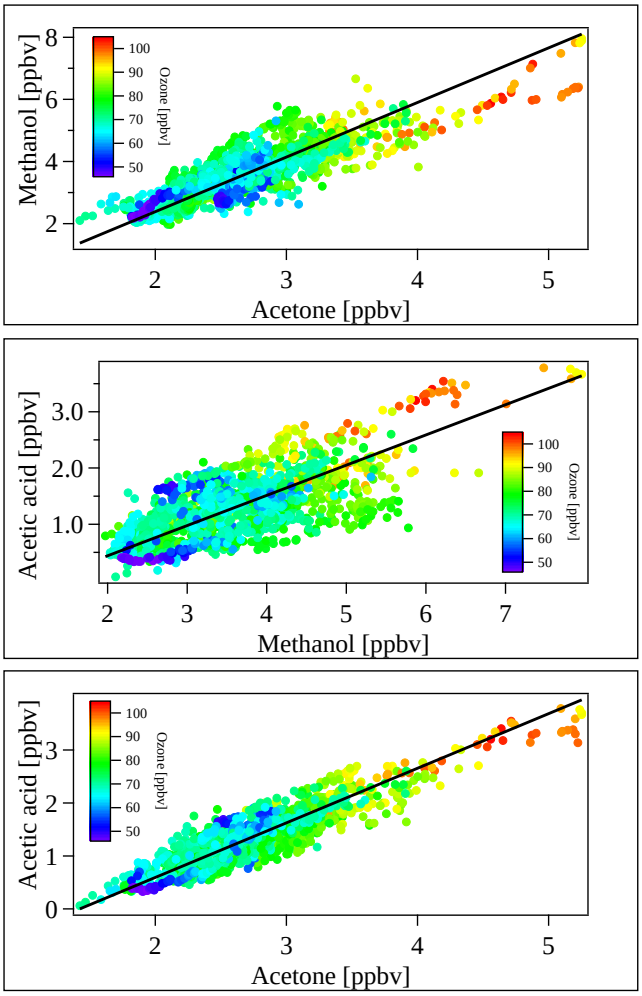

Figure 4.15.: Correlations plots solely from eastern flow regimes were color coded by ozone data

4.4. Conclusions

During the 2014 CYPHEX campaign, air masses from Eastern (67 % of the time) and Western Europe (33 % of the time) were measured. Since the transport routes of the air pass over the Mediterranean Sea, the impact of the marine boundary layer on VOCs and especially OVOCs could be investigated.
Due to the sparse vegetation local biogenic emissions of isoprene and the sum of the monoterpenes were weak (always < 350 pptv). These species showed typical diel cycles with the highest mixing ratios around midday. The difference in median and mean mixing ratios in the isoprene data could be explained by the boundary layer evolution, the onset of a local sea breeze system and the presence upwind of a small forest in the southwesterly wind direction.
The methanol and acetone mixing ratios revealed relatively little diel variation and higher absolute mixing ratios than isoprene and the monoterpenes, indicating that local emission

or production was less significant in comparison to long range transport. Only acetic acid followed a pronounced diel cycle during one period of the campaign, which is the result of various local effects like emission from soil, in-mixing from the free troposphere due to turbulence as well as dry and wet deposition over land. The lack of diel cycles during the rest of the campaign can be explained by a higher impact of transport processes and different meteorological conditions. To exclude these local phenomena only data measured from western air masses, where no diel cycles of acetic acid occurred, were used to investigate the influence of the MBL during transport. The methanol, acetone and acetic acid data showed that uptake to the sea surface was not defined solely by solubility and that vertical entrainment likely played an important role.
The correlation coefficients between the OVOCs were higher in eastern than in western air masses, which can be explained by the longer transport time over the ocean and thus stronger impacts of different production and loss processes as well as some local effects like fog formation. The ratios of methanol/CO and acetone/CO were higher in this work than in a study performed over a decade ago consistent with the lowering in the regional sources of CO. The results displayed here indicate that air reaching Cyprus from Eastern and Western Europe showed different OVOC characteristics due to different emission patterns, transport times as well as varying impact of photochemical processes, dilution and ocean uptake or emission.

5. Measurement of car exhaust fumes

5.1. Introduction

Emissions from vehicles have a major impact on air quality, human health and climate. Besides CO_2 car exhaust contains other greenhouse gases (GHG) like CH_4 or N_2O and a variety of VOCs. Vehicles release particulate matter ($PM_{2.5}$) and NOx, which in turn leads to an increase of tropospheric ozone. Since diesel engines are more energy efficient and diesel fuel has a higher heating value, one approach for the reduction of GHGs has been to increase the percentage of diesel cars in the vehicle fleet. This policy has been widely followed in Europe. From 1990 until 2010 45 million diesel cars were registered in Europe, which represents an increase from 10 % to 35.3 % of the total vehicle fleet (Cames and Helmers, 2013). The European Automobile Manufacturers' Association (ACEA) states that 2015 the share of diesel cars in Western Europe (EU15 + EFTA) amounted to 51.6 % [1]. In contrast, other countries have pursued different strategies. In 1995 the fraction of diesel cars in the vehicle fleet of Japan was still 10.8 %, but the numbers decreased to 1.4 % in 2011, because Japan facilitated hybrid cars (Japan Automobile Manufacturer Association, 2012; Cames and Helmers, 2013). In the US 218 million vehicles were registered in 2014, but only 4 % were diesel cars. However, regarding the large numbers of diesel vehicles in Europe, the increasing number of cars worldwide in general and the hazards emerging from the emissions the measurement of diesel exhaust gases represents an important research field. According to the IPCC report 2007 the number of light duty vehicles will increase to ca. 2 billion world wide by 2050. Not only the already mentioned hazardous compounds like GHGs, NOx and ozone need to be monitored, but also the full spectrum of emitted hydrocarbons, which can be air toxics or serve as precursors for the production of toxic compounds. An example would be the PAHs, some of which are classified as carcinogenic (Nisbet and LaGoy, 1992; Boström et al., 2002; Boffetta et al., 1997). Furthermore, the hydrocarbons can influence the oxidation capacity of the atmosphere by reacting with OH radicals and thereby lead to formation of SOA (Tkacik et al., 2012; Zhao et al., 2015). Diesel exhaust contains more IVOCs with a chain length between 10 and 20 carbon atoms than the emissions of gasoline vehicles. Short-chained VOCs in the range of C_1-C_{12} can easily be measured by GC methods. Already in 1966 Jacobs et al. (1966) and McEwen et al. (1966) investigated automotive exhaust gases using GC techniques. Schauer et al. (1999) measured diesel exhaust using a two-stage dilution source sampling system. Filters, cartridges and canisters were used and analyzed by gas and liquid chromatography. A similar approach using Tedlar bags, Tenax cartridges and subsequent GC analysis was

[1] http://www.acea.be/statistics/tag/category/share-of-diesel-in-new-passenger-cars
accessed on 1st of July 2016
EU15: Austria, Belgium, Denmark, Finland, France, Germany, Greece, Ireland, Italy, Luxembourg, Netherlands, Portugal, Spain, Sweden, United Kingdom
EFTA = European Free Trade Association: Iceland, Norway, Switzerland

performed by Siegl et al. (1998). Disadvantages of these methods are that offline sampling is prone to artifacts and has a high analyzation effort. Several studies with online measurement techniques exist as well, e.g. Smith et al. (2002, 2004) used a Selected Ion Flow Tube Mass Spectrometer (SIFT-MS) while Jobson et al. (2005) employed a PTR-MS for the measurement of car engine exhaust. In both methods the separation of the ions is performed by a quadrupole and thus one drawback of this approach is the quite low mass resolution of only 1 amu. Due to the complexity of the mixture, multiple peaks are expected on many of the masses. Hence, a PTR-TOF-MS was used in this work, because it represents an online technique with a high mass resolution so that the emissions can be monitored fast and efficiently. Another important advantage of the PTR-TOF-MS is that the transmission efficiency enhances with increasing mass of the sample molecule while it declines in a PTR-quadrupole-MS. Besides the application in research, the online method would be especially valuable for regulatory monitoring networks.

5.2. Instrumentation and setup

For comparison between diesel and gasoline exhaust fumes a Volkswagen transporter (diesel, Euro 5, 103 kW, 1968 cm^3 cylinder capacity, first registration in 2014) and a Toyota Yaris (gasoline, Euro 3, 50 kW, 998 cm^3 cylinder capacity, first registration in 2002) were used in idle mode when stationary. A very efficient dilution technique for the exhaust was necessary due to high particle concentration and high gas mixing ratios. The dilution was performed using a single stage diluter (model TD110HSS) by AirVac, Seymour, CT. A picture and a sketch of the diluter can be found in Figure 5.1. The car exhaust gases are drawn into the device by means of the low pressure produced by the high dilution flow. Nitrogen 6.0 was used as dilution gas instead of synthetic air to avoid side reactions between sample molecules and $O_2{}^+$. For the measurement of the Volkswagen transporter (VW bus) we placed an 1/8" (0.318 cm) swagelok fitting at the inlet side of the diluter. We applied a dilution air flow of 9 L/min, which created an inlet flow of 191 mL/min and led to a dilution of 1:47. Since the Toyota Yaris, which runs on gasoline, produced very high mixing ratios of VOCs, an even higher dilution was required. The diameter of the inlet part was further reduced to create a dilution of 1:125 (72 mL/min inlet flow at a dilution flow of 9 L/min).
Figure 5.2 displays the setup. The instrument was situated inside a garage while the car was placed outside. The teflon tubing preceding from the diluter into the garage had a large diameter of 1/2" (1.27 cm) to minimize wall losses. At right angles from this 1/8" (0.318 cm) PEEK tubing was led into the PTR-TOF-MS. Further information about the instrument can be found in chapter 2.
In addition a 1/4" (0.635 cm) teflon tubing connected a non-dispersive infrared CO_2 analyzer LI-7000 by LI-COR (LI-COR Inc., Lincoln, Nebraska) to the experiment. To avoid dilution by outside air, the exhaust pipe was connected to the dilution system via aluminium foil. During the experiments the diluter was heated to 80 °C, the 1/2" (1.27 cm) line to 50-70 °C, the TOF ion source to 70 °C and the TOF drift tube to 80 °C. The high temperatures were necessary to improve the transmission of the heavy molecules through the tubing. Still, the conditioning of the 1/2" (1.27 cm) teflon line took several hours.

During this time the mixing ratios not only increased, but more and more molecules with higher masses were recorded. After ca. 3 h masses up to m/z 350 could be measured.

Figure 5.1.: Ejector diluter by AirVac. Source:
http : //www.airvacpumps.com/TDstainless.html;
accessed on 15th of July 2016.

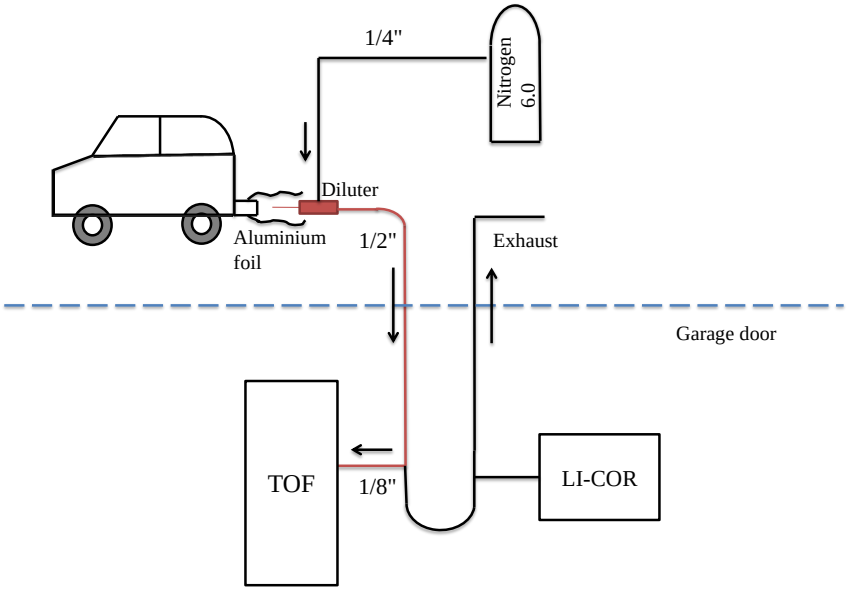

Figure 5.2.: Setup of the experiment to measure car exhaust. All parts marked in red were heated.

5.3. Transmission

In general, a PTR-TOF-MS has a better transmission for heavier than for lighter molecules. The reason is that one pulse of sample ions can only be injected as soon as the last ion from the previous pulse has reached the detector. Otherwise spectral overlap would occur. Until the next pulse the ions continue entering the modulator. Since lighter ions have a higher velocity in a monoenergetic beam, they scatter across a wider range than heavier ions. This causes a higher loss of lighter ions. In contrast, a PTR-quadrupole-MS has a weaker transmission for heavier compounds, because large molecules spend more time in the fringe field of the quadrupole filter, hence, the transmission efficiency decreases. For that reason, a PTR-TOF-MS is more suitable for the measurement of IVOC associated diesel exhaust. To calculate mixing ratios theoretically without calibration, the knowledge of the transmission rates are necessary. Therefore, the transmission curve of the instrument was determined by saturating the PTR-TOF-MS with different compounds, preferably of high mass. Saturation was achieved by measuring the head space of pure compounds. As soon as the signal of the primary ion reached zero, it was assumed that all H_3O^+ ions had transferred their proton to the sample molecules. If the transmission would be the same for primary ions and for the sample compound, then the same count number which was measured for the primary ion before would be detected on the mass of the compound. Since heavier molecules show better transmission rates, the recorded counts per second for the specific compound were larger. Three different compounds were measured, namely toluene, xylene and trichlorobenzene. For trichlorobenzene the isotopes were taken into account as well. Trichlorobenzene has such a low volatility that complete saturation could not be reached. In Fig. 5.3 the counts per second (cps) of the three substances as well as the primary ion were plotted against the mass. In this case, m/z 19 could be used, because the instrument was tuned in a way that only a very small amount of primary ions was produced. By means of this setting, the creation of full saturation was facilitated. A root function was used to fit the data points as it was recommended by the manufacturer. Despite the low counts of trichlorobenzene, the fit was reasonably accurate. Using the derived fit function, which can be found in the graph, the transmission of various compounds could be determined.

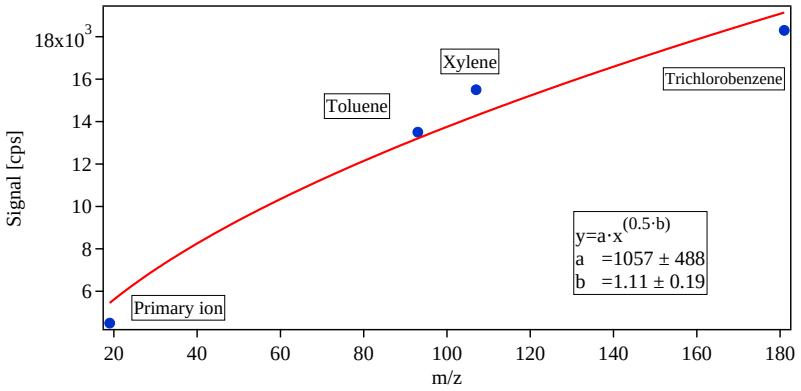

Figure 5.3.: Signal in cps of the primary ion, toluene, xylene and trichlorobenzene plotted against m/z. The fit is a root function.

5.4. Calculation of mixing ratios

If no calibration standard is available, the mixing ratios can be calculated by the use of a simplified kinetic approach. In the drift tube the primary ions H_3O^+ collide with neutral sample molecules R_i to form ions RH_i^+ and water:

$$R_i + H_3O^+ \rightleftharpoons RH_i^+ + H_2O \tag{5.1}$$

It can be seen in equation 5.1 that the decrease of the primary ions H_3O^+ coincide with the increase of the sum of the ions:

$$-\frac{d[H_3O^+]}{dt} = \sum_i \frac{d[RH_i^+]}{dt} = [H_3O^+] \cdot \sum_i (k_i \cdot [R_i]) \tag{5.2}$$

Here k_i is the rate coefficient of the reaction between H_3O^+ and R_i. Since the mixing ratio of the sample molecules R_i stays constant, the equation 5.2 represents a linear homogeneous differential equation. With $[H_3O^+]_0$ being the initial value at time $t = 0$, the following solution is gained:

$$[H_3O^+] = [H_3O^+]_0 \cdot \exp\left(-t \sum_i (k_i \cdot [R_i])\right) \tag{5.3}$$

Now one specific compound $[RH_j^+]$ is regarded:

$$\frac{d[RH_j^+]}{dt} = k_j \cdot [R_j] \cdot [H_3O^+] = k_j \cdot [R_j] \cdot [H_3O^+]_0 \cdot \exp\left(-t \cdot \sum_i (k_i \cdot [R_i])\right) \tag{5.4}$$

Integration leads to:

$$[RH_j^+] = \frac{k_j \cdot [R_j]}{\sum_i (k_i \cdot [R_i])} \cdot [H_3O^+]_0 \cdot \left(1 - \exp\left(-t \cdot \sum_i (k_i \cdot [R_i])\right)\right) \tag{5.5}$$

The following equations apply for the sum of all sample ions:

$$\sum_j [RH_j^+] = [H_3O^+]_0 \cdot \left(1 - \exp\left(-t \cdot \sum_i (k_i \cdot [R_i])\right)\right) = [H_3O^+]_0 - [H_3O^+] \tag{5.6}$$

Using equation 5.6 the sum in the exponent can be calculated:

$$\sum_i (k_i \cdot [R_i]) = -\frac{1}{t} \cdot \ln\left(\frac{[H_3O^+]}{[H_3O^+]_0}\right) \tag{5.7}$$

This term as well as equation 5.6 can be inserted into equation 5.5:

$$[RH_j^+] = -\frac{k_j \cdot [R_j] \cdot t}{\ln\left(\frac{[H_3O^+]}{[H_3O^+]_0}\right)} \cdot \sum_j [RH_j^+] \tag{5.8}$$

Solving the equation for $[R_j]$ leads to:

$$[R_j] = \frac{1}{k_j \cdot t} \cdot \frac{[RH_j^+]}{\sum_j [RH_j^+]} \cdot \ln\left(\frac{[H_3O^+]_0}{[H_3O^+]}\right) \tag{5.9}$$

$[H_3O^+]_0$ can be substituted:

$$\begin{aligned}[R_j] &= \frac{1}{k_j \cdot t} \cdot \frac{[RH_j^+]}{\sum_j [RH_j^+]} \cdot \ln\left(\frac{\sum_j [RH_j^+] + [H_3O^+]}{[H_3O^+]}\right) \\ &= \frac{1}{k_j \cdot t} \cdot \frac{[RH_j^+]}{\sum_j [RH_j^+]} \cdot \ln\left(1 + \frac{\sum_j [RH_j^+]}{[H_3O^+]}\right)\end{aligned}$$

A series can be used to replace the logarithmic function for $x \leq |1|$:

$$\ln(1+x) = x - \frac{x^2}{2} + \frac{x^3}{3} - ... \tag{5.10}$$

The higher terms can be neglected if the ratio $\sum_j [RH_j^+]/[H_3O^+]$ is small. This leads to the final equation

$$[R_j] = \frac{1}{k_j \cdot t} \cdot \frac{[RH_j^+]}{[H_3O^+]} \tag{5.11}$$

The mixing ratio of a sample compound $[R_{ppbv}]$ is defined as follows:

$$[R_{ppbv}] = \frac{[R] \cdot 10^9}{[air]} \cdot \frac{Tr_{H3O^+}}{Tr_{RH^+}} \tag{5.12}$$

while $Tr_{H_3O^+}/Tr_{RH^+}$ is the ratio of the transmission for H_3O^+ and the sample molecule. This ratio is derived from the measurement of the transmission curve. Since the primary ion is the reference for the transmission, $Tr_{H_3O^+}$ is set to 1. Further information can be found in section 5.3. $[R]$ is calculated via the equation 5.11 and $[air]$ represents the number density of air molecules in the volume of the drift tube.

$$[air] = \frac{N_0 \cdot T_0 \cdot p}{p_0 \cdot V_0 \cdot T} \tag{5.13}$$

while $N_0 = 6.022 \cdot 10^{23}$ is the number of particles at standard conditions
Standard conditions are defined as:
Temperature $T_0 = 273.15\ K$
Pressure $p_0 = 1013\ mbar$
Volume $V_0 = 22400\ cm^3$
T and p represent the temperature and pressure in the drift tube.
The reaction time t in equation 5.11 can be substituted by using the length of the drift tube L, the ion mobility μ and the drift voltage U:

$$t = \frac{L^2}{\mu \cdot U} = \frac{L^2 \cdot T_0 \cdot p}{T \cdot p_0 \cdot \mu_0 \cdot U} \tag{5.14}$$

while μ_0 is the reduced ion mobility at standard conditions.
The final equation is given as:

$$[R_{ppbv}] = \frac{[RH^+]}{[H_3O^+]} \cdot \frac{1}{Tr_{RH^+}} \cdot \frac{10^9 \cdot U \cdot \mu_0 \cdot V_0 \cdot p_0^2 \cdot T^2}{k \cdot L^2 \cdot p^2 \cdot N_0 \cdot T_0^2} \tag{5.15}$$

The only unknown in this equation is the reaction rate coefficient k. Various mathematical methods were developed to calculate the rate coefficients, e.g. the average dipole orientation theory by Su and Bowers (1973) or the calculation method via trajectories by Su and Chesnavich (1982). This trajectory method, in which an interaction potential affects the ion, regarded as a point charge, and the polar molecule, represented by a two-dimensional rigid rotor, is applied in this work (Su and Chesnavich, 1982). The result k_{cap} is linked to the classical Langevin capture rate coefficient k_L by a factor K_{cap} (Su and Chesnavich, 1982; Turulski and Niedzielski, 1994). Dipole moments and polarizabilities were necessary for the calculation and mainly taken from Zhao et al. (2004).

$$\frac{k_{cap}(\tau)}{k_L} = K_{cap}(\tau_R, I^*) \tag{5.16}$$

$$k_L = 2\pi \cdot q \cdot \sqrt{\frac{\alpha}{M}} \tag{5.17}$$

where τ is the total system angular momentum, q the charge of the ion, M the reduced mass and α the polarizability of the molecule.
K_{cap} depends on two reduced parameters which are defined as:

$$\tau_R = \frac{2\alpha \cdot k_b \cdot \tau}{\mu_D^2}$$

$$I^* = \frac{\mu_D \cdot I}{\alpha \cdot q \cdot M}$$

where μ_D is the dipole moment of the neutral, k_b is the Boltzmann constant and I the momentum of intertia of the neutral.
In this study k_{cap} was determined for the compounds for which the polarizability and the dipole moment are known. For all the other a k_{cap} value of $2 \times 10^{-9}\,cm^3/s$ was assumed (except for the alkane fragments, see section 5.7). One problem was that the formula 5.15 does not take the water cluster on mass m/z39 into account. But for low energies the cluster plays an important role, because the primary ions cluster to a higher degree and are therefore distributed to a large extent on m/z 39. Thus, the formula was altered to involve the water cluster. According to Hewitt et al. (2003) the k rates for the reactions of sample molecules with water cluster ions are lower than the ones with the primary ions, but often not reported. To simplify matters the same reaction rates for water cluster as well as primary ions were assumed here. The error made by this assumption is accounted for in the error calculation (see section 5.5.2) by applying a high uncertainty for the k rates.

$$[R_{ppbv}] = \frac{[RH^+]}{[H_3O^+] + 1/Tr_{H_5O_2^+} \cdot [H_5O_2^+]} \cdot \frac{1}{Tr_{RH^+}} \cdot \frac{10^9 \cdot U \cdot \mu_0 \cdot V_0 \cdot p_0^2 \cdot T^2}{k \cdot L^2 \cdot p^2 \cdot N_0 \cdot T_0^2} \tag{5.18}$$

For the data measured at 138 Td the inclusion of m/z 39 changed the results by 2-3 %, only. For the data recorded at 80 Td the difference lay between 50 and 80 %.

5.5. Error calculation

5.5.1. Error calculation for the calibration

The error calculation is explained in detail in chapter 2, section 2.2.6. However, for the exhaust experiment some changes needed to be applied. Since the experiment consisted only of short term measurements, no change of sensitivity over time was expected. Furthermore, the calibrations were performed only at one humidity, because, due to high dilution, the conditions were extremely dry. Variations in the water cluster ion can have several reasons and are detailed in section calcom. Thus, the parameters t (time dependence) and h (humidity dependence) were unnecessary. For the measurement of the Toyota Yaris at 80 Td the following equation for the systematic error was used:

$$Sys_{error}[\,\%] = \sqrt{a^2 + b^2 + c^2} \tag{5.19}$$

where a is the error of the calibration gas bottle stated by Apel Riemer Environmental Inc. (5 %), b is the error of the mass flow controller given by the producer (1 %) and c is the error of the calibration fit. For the Toyota no further term was needed, because the m/z 39: m/z 21 ratio was in good agreement with the calibration. The VW experiment, on the other hand, showed a high discrepancy between the m/z 39 : m/z 21 ratios so that a further term needed to be added. As the calibration was performed only at one m/z 39 value, no interpolation was possible. The largest difference of sensitivity due to humidity changes measured at 138 Td during the CYPHEX campaign was 20 %. Since no further data for 80 Td were available, 20 % was applied as additional error caused by different water cluster values in the drift tube:

$$Sys_{error}[\,\%] = \sqrt{a^2 + b^2 + c^2 + 0.2^2} \tag{5.20}$$

The experiments at 138 Td represent a special challenge, because the value of m/z 39 could not be determined due to fragmentation of higher masses on m/z 39. Thus, the m/z 39 value of the background measurement was used. To estimate the possible error caused by this effect the data were analyzed twice: Once using the water cluster data from the background measurement and once using the inseparable sum of m/z 39 and the fragment recorded during the experiment. The difference of both results $\Delta\, ppbv_{bias}$ was divided by the recorded value $ppbv$ calculated using the water cluster data from the background. This term was added to the formula:

$$Sys_{error}[\,\%] = \sqrt{a^2 + b^2 + c^2 + 0.2^2 + \left(\frac{\Delta\, ppbv_{bias}}{ppbv}\right)^2} \tag{5.21}$$

The statistical and the overall error were determined as already described in chapter 2. The total uncertainties for the Toyota measurement at 80 Td lay between 5 - 10 %, only

methanol gained a higher error of 25 % due to problems during calibration. The VW experiment at 80 Td yielded overall errors of 20 %, except methanol, which reached 30 %. The total uncertainties for the Toyota measurement at 138 Td lay between 20 and 25 %, only methanol reached 40 %. The VW analysis at 138 Td, on the other hand, showed 30 % overall error, with methanol having 45 %.

5.5.2. Error calculation for the theoretical approach

To calculate the error for the theoretical calculation of the mixing ratios the equation 5.18) was differentiated with respect to the variables which can be erroneous. These are the transmission rates for the specific compound ($\mathrm{Tr_{RH^+}}$) and for the water cluster ($\mathrm{Tr_{H_5O_2^+}}$), the temperature (T), the voltage (U) and the pressure (p) in the drift tube as well as the reaction rate coefficient (k). The equation of the Gauß' law of error propagation was applied:

$$\Delta[R_{ppbv}] = \sqrt{\left(\frac{\delta R_{ppbv}}{\delta Tr_{RH^+}} \cdot \Delta Tr_{RH^+}\right)^2 + \left(\frac{\delta R_{ppbv}}{\delta Tr_{H_5O_2^+}} \cdot \Delta Tr_{H_5O_2^+}\right)^2 + \left(\frac{\delta R_{ppbv}}{\delta T} \cdot \Delta T\right)^2 + \left(\frac{\delta R_{ppbv}}{\delta U} \cdot \Delta U\right)^2 + \left(\frac{\delta R_{ppbv}}{\delta p} \cdot \Delta p\right)^2 + \left(\frac{\delta R_{ppbv}}{\delta k} \cdot \Delta k\right)^2} \tag{5.22}$$

The variables ΔT, ΔU etc. represent the absolute errors of the specific quantity. Voltage, temperature and pressure were recorded by the instrument and their standard deviation was used. The errors of the transmission rates were derived from the error in the transmission fit function (see section 5.3). The Δk values were determined by comparing k rates which were calculated in two different ways. The ions have a high kinetic temperature in the drift tube due to the electrical gradient. In the first case this temperature, implied by ion velocity, is not thermally distributed through other molecular modes of motion (vibration, rotation). Applying these conditions as a basis, the "thermal" rate coefficients can be derived. In the second case, the effective temperature, at which an equal distribution arises, was used. The equations for the calculations can be found in Su et al. (1982). The highest discrepancy occurring due to the two different theoretical approaches amounted to 59 %. Therefore, this percentage was applied to calculate the absolute error Δk individually for each compound. The obtained overall uncertainties lay between 60 and 80 %.

5.5.3. Changing of chemistry and Townsend number

The PTR-TOF-MS 8000 used here is able to switch between the reagent ions H_3O^+, NO^+ and $O_2{}^+$. The advantage of this lies in the broader range of compounds that can be detected. In the H_3O^+ mode, only compounds with a higher proton affinity than water can be measured. When NO^+ or $O_2{}^+$ are used as precursor ions, mostly charge transfer takes place, which means that all substances with a lower ionization potential than the reagent ion can be recorded. In Table 5.1 and 5.2 various compounds are listed with

their proton affinity and ionization potential. In the H_3O^+ mode, small alkanes cannot be measured while higher alkanes ($\geq C_6$) can undergo adduct formation with H_3O^+ to make measurable ions (Spanel and Smith, 1998b). In the NO^+ mode, alkanes can be recorded more efficiently, because they undergo hydride transfer and to a smaller degree cluster formation.
As long as the ionization potential of the sample molecule is lower than the one of NO^+, then the following reaction occurs:

$$RH + NO^+ \rightarrow RH^+ + NO \tag{5.23}$$

But if the potential is higher, then a hydride ion transfer can take place:

$$RH + NO^+ \rightarrow R^+ + HNO \tag{5.24}$$

Furthermore, three body clustering reactions need to be taken into account, when the collision energy is very low:

$$RH + NO^+ \rightarrow RH \cdot NO^+ \tag{5.25}$$

Generally speaking, the mass recorded by the PTR-TOF-MS in the H_3O^+ mode is the molecular mass plus the mass of one proton (1.0079 amu) minus the mass of one electron (5.5×10^{-4} amu) (If the molecular mass is calculated from the masses of the respective atoms, the binding energy needs to be taken into account). In contrast, many molecules react via charge transfer with NO^+ so that they are monitored on their molecular mass minus the mass of one electron, only. Furthermore, some groups of molecules undergo cluster reactions with NO^+ and are found on their molecular mass plus the mass of NO^+ (m/z 29.9974) minus the mass of one electron.
One important advantage of the NO^+ mode is that isomeric molecules with different functional groups can be separated. Aldehydes mainly transfer a hydride ion to NO^+ (Spanel et al., 1997; Blake et al., 2006; Jordan et al., 2009) while ketones show a different behavior. Spanel et al. (1997) used a Selected Ion Flow Tube technique (SIFT) with rather low energies and found that ketones react mainly via molecule association. Blake et al. (2006), who used a Chemical Ion Reaction method (CIR), as did Jordan et al. (2009), report decreasing cluster production with increasing energy in the drift tube. The respective parent ions of the ketones produced via charge transfer can also be measured (Blake et al., 2006; Jordan et al., 2009). Due to the different reactions of aldehydes and ketones, isomeric compounds like acetone and propanal or butanone and butanal can be distinguished. Most alcohols transfer either a hydride or a hydroxy ion forming $[M\text{-}H]^+$ and HNO or $[M\text{-}OH]^+$ and HNO_2. The only exception is methanol, which produces a cluster with NO^+ (Spanel and Smith, 1997). Carboxylic acids, on the other hand, react either via cluster formation or hydroxide transfer (Spanel and Smith, 1998a). Aromatic compounds undergo charge transfer to form $[M]^+$ while aliphatic hydrocarbons mainly transfer hydride ions, but in some cases molecule association can also take place (Spanel and Smith, 1998b). Furthermore, the electric field strength per buffer gas number density E/N in the drift tube was switched between 138 and 82 (VW)/ 83 (Toyota) Townsend (Td) to create different cluster and fragmentation patterns. To simplify matters the lower energy mode will be referred to as "80 Td" in the following text.

Table 5.1.: Proton affinity values of different compounds in kcal/mol.
Source: *http://webbook.nist.gov/chemistry/*; accessed in April 2016.

Compound	Proton affinity [kJ/mol]
Helium	177.8
Oxygen	421.0
Hydrogen	422.3
Nitrogen	493.8
Carbondioxide	540.5
Carbonmonoxide	594.0
Ethane	596.3
Propane	625.7
Water	691.0
Formaldehyde	712.9
Formic acid	742.0
Benzene	750.4
Methanol	754.3
Acetaldehyde	768.5
Ethanol	776.4
Acetic acid	783.7
Toluene	780.0
Propanal	786.0
Naphthalene	802.9
Acetone	812.0
Isoprene	826.4
Methylethylketone	827.3
Dimethylsulfide	830.9

Table 5.2.: Ionization Potential of different compounds in eV.
Source: *http : //webbook.nist.gov/chemistry/*; accessed in April 2016.

Compound	Ionization Potential [eV]
Helium	24.59
Nitrogen	15.58
Carbonmonoxide	14.01
Carbondioxide	13.78
Methane	12.61
Water	12.62
Oxygen	12.07
Formic acid	11.33
Ethane	11.52
Propane	10.94
Formaldehyde	10.88
Methanol	10.80
Acetic acid	10.65
Ethanol	10.48
Acetaldehyde	10.23
Propanal	9.96
Acetone	9.70
NO	9.26
Benzene	9.24
Isoprene	8.86
Toluene	8.83
Dimethylsulfide	8.69
Naphthalene	8.14
Phenanthrene	7.89

5.6. Spectra

In Figure 5.4 two example spectra, one of a diesel exhaust and one of a gasoline exhaust measurement, are shown. Diiodobenzene was used as internal standard to perform mass scale calibration, but its peaks were removed in this graph. While the gasoline exhaust spectrum reached only up to m/z $\sim$ 220 the diesel exhaust spectrum showed m/z up to $\sim$ 350. In the range where no emissions occurred from gasoline cars, the diesel spectrum still revealed a large amount of compounds with a high signal intensity. Furthermore, the more volatile substances show higher signal intensities in the gasoline exhaust fumes. As an example the area between m/z 90 to m/z 130 is presented in the lower panel of Figure 5.4. The three largest peaks, which are marked by arrows and even reached saturation, were the well known aromatic compounds toluene (m/z 93.0699), the total xylenes (m/z 107.0855) and the total trimethylbenzenes (m/z 121.1012). In the diesel exhaust spectra these substances give a lower signal. The reason for that is simply that gasoline consists

of smaller, more volatile compounds than diesel fuel. Especially the diesel mass spectrum exhibits repeating patterns, which refer to groups of molecules (see Figure 5.5), that are explicitly analyzed in the next section.

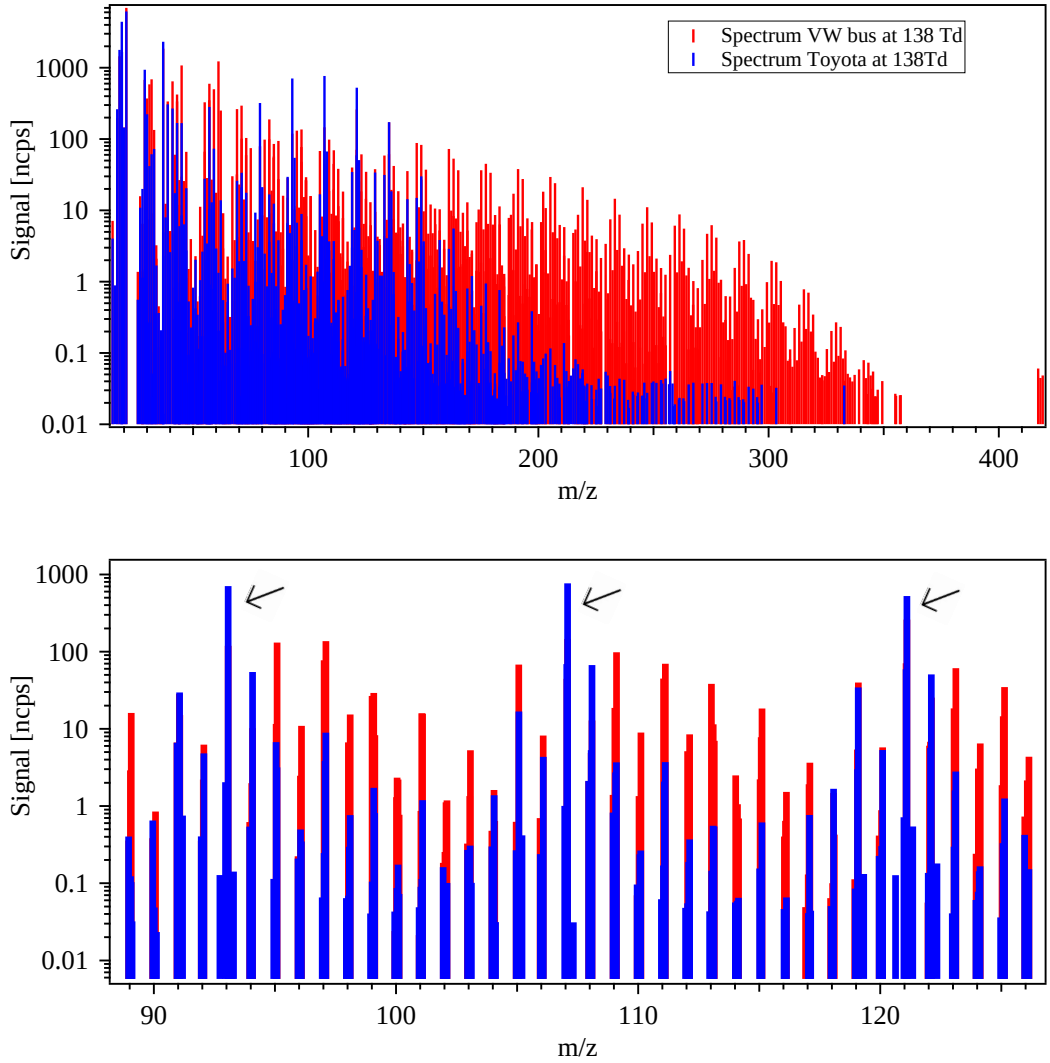

Figure 5.4.: Spectra of the measurement of diesel (red) and gasoline (blue) exhaust recorded at 138 Td are shown. The signal on the y axis is given in ncps while the x axis shows the mass to charge ratio. The peaks marked with an arrow in the lower panel refer to toluene (m/z 93.0699), total xylenes (m/z 107.0855) and total trimethylbenzenes (m/z 121.1012).

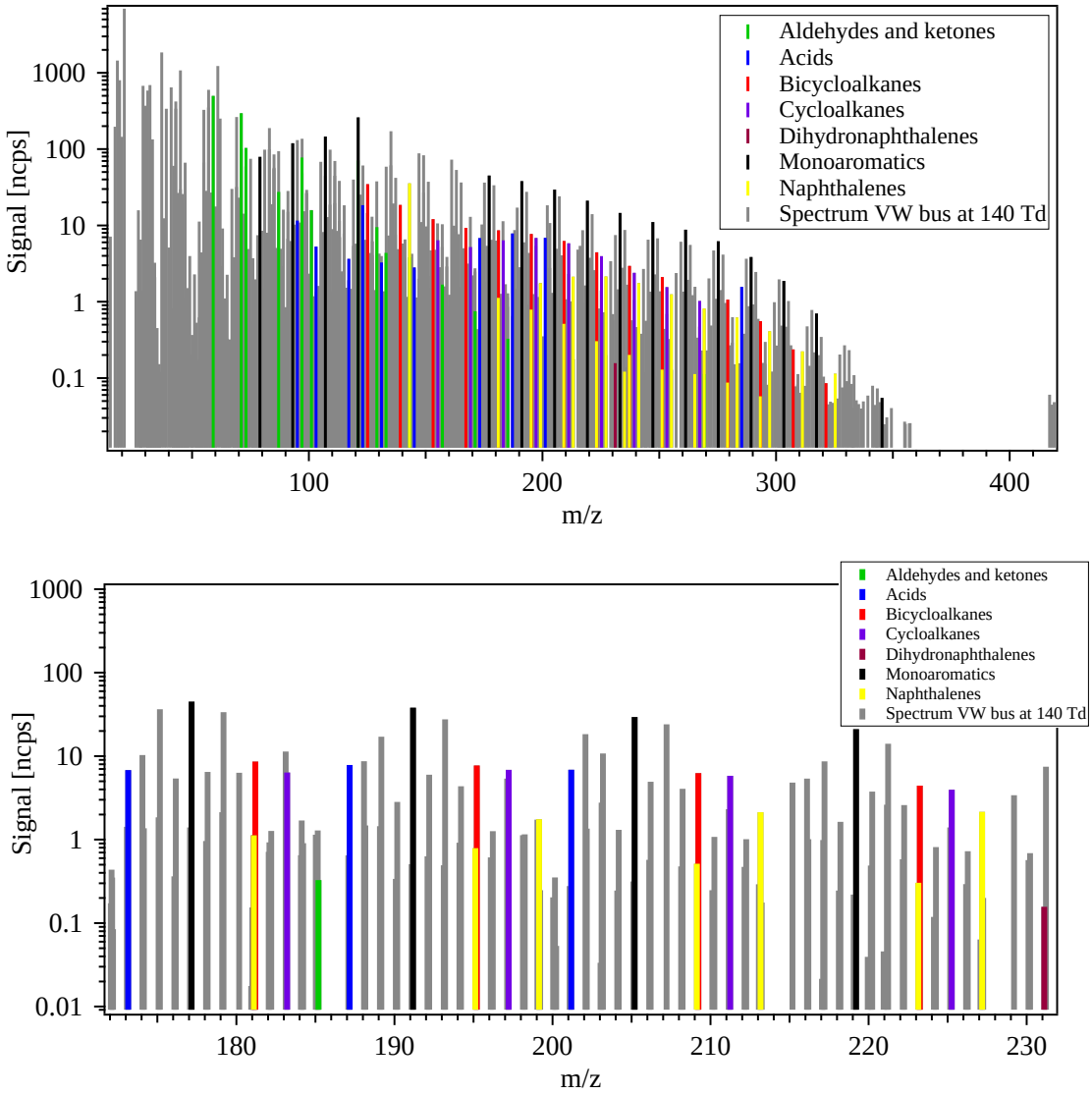

Figure 5.5.: The sprectrum of diesel exhaust at 138 Td is displayed in grey and the colors mark different groups of molecules

5.7. Peak identification

The measurement of diesel exhaust represents a complicated challenge, especially because of the enormous number of peaks recorded. In the following a method for peak identification is described.

A list of molecules which can possibly be found in the car exhaust gases was created together with the expected m/z value of the respective compound for the H_3O^+ mode based on Schauer et al. (1999) and Jobson et al. (2005). A subdivision into molecular classes was performed. In Table 5.3 the monoaromatic compounds and their masses are displayed as an example, while the tables of the other classes can be found in appendix B.

It needs to be kept in mind that most of the sum formulas represent not only one molecule,

Table 5.3.: List of monoaromatic compounds, their sum formula and their possible TOF mass

Carbon number	Name	Formula	TOF mass
6	Benzene	C_6H_6	79.0542
7	Toluene	C_7H_8	93.0699
8	Xylenes	C_8H_{10}	107.0855
9	C3-Alkylbenzene	C_9H_{12}	121.1012
10	C4-Alkylbenzene	$C_{10}H_{14}$	135.1168
11	C5-Alkylbenzene	$C_{11}H_{16}$	149.1325
12	C6-Alkylbenzene	$C_{12}H_{18}$	163.1481
13	C7-Alkylbenzene	$C_{13}H_{20}$	177.1638
14	C8-Alkylbenzene	$C_{14}H_{22}$	191.1794
15	C9-Alkylbenzene	$C_{15}H_{24}$	205.1951
16	C10-Alkylbenzene	$C_{16}H_{26}$	219.2107
17	C11-Alkylbenzene	$C_{17}H_{28}$	233.2264
18	C12-Alkylbenzene	$C_{18}H_{30}$	247.2420
19	C13-Alkylbenzene	$C_{19}H_{32}$	261.2577
20	C14-Alkylbenzene	$C_{20}H_{34}$	275.2733
21	C15-Alkylbenzene	$C_{21}H_{36}$	289.2890
22	C16-Alkylbenzene	$C_{22}H_{38}$	303.3046
23	C17-Alkylbenzene	$C_{23}H_{40}$	317.3203
24	C18-Alkylbenzene	$C_{24}H_{42}$	331.3359
25	C19-Alkylbenzene	$C_{25}H_{44}$	345.3516
26	C20-Alkylbenzene	$C_{26}H_{46}$	359.3672

but conceal various other isomeric structures. Without a calibration using a standard of the specific compound, no further identification can be made. All tables containing 175 compounds in total were combined to one "'master mass list"'. All together around 690 peaks were found in the raw data by the program PTR-TOF-DATA-ANALYZER, which is described elsewhere (Müller et al., 2013). After mass scale calibration these data were loaded into IGOR Pro 6.12A and compared to the master mass list. From the 175 sum formulas with known mass, 87 matches were found among the 690 peaks. The determined masses, their sum formula, their calculated mixing ratio and a possible identity can be found in Table 5.4, which is analyzed in more detail in the following sections. The compounds acetonitrile, acetone, acetic acid, MEK, total xylenes, total trimethylbenzenes and naphthalene are listed in the table with their exact mass, but were not correctly found on that mass, thus slightly shifted. One reason might be that the peaks were already in saturation due to the extremely high mixing ratios. Another explanation could be that the saturation did not occur due to the high amount of that compound, but due to another molecule/fragment emerging on almost the same mass and therefore increasing the peak up to saturation. In both cases the analysis program was not able to locate the peak correctly. Since the calibration gas contained many of these compounds, they were interesting

to compare. Therefore, the slightly shifted mass was assumed to be the specific compound and added to the list. The calculation of the mixing ratios is described in detail in the next section. Note that the given mass is not the one of the sum formula, but the one referring to the protonated molecule. The given identity arose from the generation of the list of molecular classes. In Table 5.4 only proton transfer reactions, which produce $[M+H]^+$ ions, are considered. However, Gueneron et al. (2015) report that some cycloalkanes and bicycloalkanes can also undergo hydride abstraction leading to $[M-H]^+$ ions. Cyclohexane (C_6H_{12}) for example was found to produce $[M+H]^+$ and $[M-H]^+$ ions at 80 Td, while at 120 Td $[M+H]^+$ ions, $[M-H]^+$ ions as well as several fragment ions of cyclohexane were recorded. This shows that the interpretation of a car exhaust spectrum represents a challenge. Therefore, the high uncertainty due to clustering and fragmentation should be kept in mind when regarding the mixing ratios given in this work.

Table 5.4.: Table of matching TOF masses (protonated), their sum formula, calculated mixing ratios of undiluted diesel (VW) and gasoline (Toyota) exhaust in ppbv at different energies and one suggested identity

Matching TOF mass	Sum formula	VW bus 138 Td [ppbv]	VW bus 80 Td [ppbv]	Toyota 138 Td [ppbv]	Toyota 80 Td [ppbv]	Possible identity
33.0335	CH_4O	3472.5	2313.3	4783.9	3294.4	Methanol
42.0338	C_2H_3N	816.0	387.3	159.4	308.6	Acetonitrile
45.0335	C_2H_4O	19665.2	12357.2	7659.1	5309.2	Acetaldehyde
47.0491	C_2H_6O	29.3	345.8	1404.1	8755.7	Ethanol
59.0491	C_3H_6O	10034.0	8549	3733.0	3464.9	Acetone
61.0280 ?	$C_2H_4O_2$	32691.8	23517.0	0.7	28.1	Acetic acid
71.0491	C_4H_6O	4674.5	3826.4	849.1	831.5	MVK
73.029	$C_3H_4O_2$	1851.2	3121.3	not found	not found	Methylgyoxal
73.0648	C_4H_8O	1798.4	2201.3	784.3	593.9	MEK
79.0542	C_6H_6	2493.9	6532.6	25987.2	8288.8	Benzene
87.0441	$C_4H_6O_2$	2940.9	3092	not found	not found	Biacetyl
87.0804	$C_5H_{10}O$	859.2	1576.2	301.3	397.8	Pentanal
93.0699	C_7H_8	3398.6	838.2	51573.4	24528.2	Toluene
95.0491	C_6H_6O	277.9	190.2	405.9	213.5	Phenol
97.028	$C_5H_4O_2$	2421.0	1555.6	14.2	3.9	Furfural
103.0754	$C_5H_{10}O_2$	159.9	178.3	not found	not found	Pentanoic acid
107.0855	C_8H_{10}	3911.6	1715.2	52673.5	31692.8	Total xylenes
117.091	$C_6H_{12}O_2$	109.5	105.9	not found	not found	Caprioc acid
121.0648	C_8H_8O	2212.8	1712.5	4707.1	3673.2	Acetophenone
121.1012	C_9H_{12}	6574.2	3560.7	33926.2	20989.4	Total trimethylbenzenes
123.0441	$C_7H_6O_2$	570.9	436.8	17.7	22.6	Benzoic acid
125.1325	C_9H_{16}	1087.3	1937.4	97.5	274.7	C_9-Bicycloalkane
129.0699	$C_{10}H_8$	910.4	529.3	2093.4	1054.8	Naphthalene

129.1274	$C_8H_{16}O$	295.5	638.1	not found	not found	Octanal
131.1067	$C_7H_{14}O_2$	99.5	66.8	not found	not found	Enanthic acid
133.0648	C_9H_8O	135.9	170.2	not found	not found	Indanone
139.1481	$C_{10}H_{18}$	579.5	1787.8	23.0	86.7	C_{10}-Bicycloalkane
143.0855	$C_{11}H_{10}$	796.6	438	817.5	441.7	C_1-Naphthalene
143.143	$C_9H_{18}O$	117.5	252	not found	not found	Nonanal
145.1223	$C_8H_{16}O_2$	85.1	46.9	not found	not found	Caprylic acid
153.1638	$C_{11}H_{20}$	377.5	1307.1	8.7	32.5	C_{11}-Bicycloalkane
155.1794	$C_{11}H_{22}$	199.1	737.1	7.2	50.4	Cycloundecane
157.1587	$C_{10}H_{20}O$	50.3	110.5	not found	not found	Decanal
167.1794	$C_{12}H_{22}$	289.5	995.1	4.5	17.4	C_{12}-Bicycloalkane
169.1951	$C_{12}H_{24}$	162.0	649.5	6.3	37.2	Cyclododecan
171.1743	$C_{11}H_{22}O$	21.1	41.4	not found	not found	Undecanal
173.1536	$C_{10}H_{20}O_2$	212.6	143.2	not found	not found	Capric acid
177.1638	$C_{13}H_{20}$	1410.1	951.6	72.6	61.7	C_7-Alkylbenzene
181.1012	$C_{14}H_{12}$	26.3	45	1.9	1.9	C_1-Fluorene
181.1951	$C_{13}H_{24}$	269.4	918.2	1.8	6.1	C_{13}-Bicycloalkane
183.2107	$C_{13}H_{26}$	198.3	733.2	4.3	18.2	Cyclotridecane
185.19	$C_{12}H_{24}O$	8.3	22.9	2.9	6.5	Dodecanal
187.1693	$C_{11}H_{22}O_2$	245.3	185.8	not found	not found	Undecylic acid
191.1794	$C_{14}H_{22}$	1191.4	788.9	20.4	16.2	C_8-Alkylbenzene
195.1168	$C_{15}H_{14}$	23.7	35.7	not found	not found	C_2-Fluorene
195.2107	$C_{14}H_{26}$	241.8	803.8	0.9	2.4	C_{14}-Bicycloalkane
197.2264	$C_{14}H_{28}$	213.8	762	not found	not found	Cyclotetradecane
199.1481	$C_{15}H_{18}$	54.1	30.1	3.0	2.9	C_5-Naphthalene
201.1809	$C_{12}H_{24}O_2$	214.5	162.3	not found	not found	Lauric acid
205.1951	$C_{15}H_{24}$	922.8	610.4	5.7	5.4	C_9-Alkylbenzene
209.1325	$C_{16}H_{16}$	15.1	18.7	not found	not found	C_3-Fluorene
209.2264	$C_{15}H_{28}$	195.5	695.9	0.4	1.3	C_{15}-Bicycloalkane
211.242	$C_{15}H_{30}$	181.8	665.1	not found	not found	Cyclopentadecane
213.1638	$C_{16}H_{20}$	66.0	35.8	not found	not found	C_6-Naphthalene
219.2107	$C_{16}H_{26}$	659.4	459.3	2.3	2.5	C_{10}-Alkylbenzene
223.1481	$C_{17}H_{18}$	8.6	11.6	not found	not found	C_4-Fluorene
223.242	$C_{16}H_{30}$	138.7	492.2	0.3	1.2	C_{16}-Bicycloalkane
225.2577	$C_{16}H_{32}$	123.3	449.4	0.2	1.1	Cyclohexadecane
227.1794	$C_{17}H_{22}$	66.9	35.5	not found	not found	C_7-Naphthalene
231.1168	$C_{18}H_{14}$	4.3	10.5	0.8	0.5	Dihydrotetracene
233.2264	$C_{17}H_{28}$	455.6	324.8	0.5	1.1	C_{11}-Alkylbenzene
235.1481	$C_{18}H_{18}$	3.2	6.2	not found	not found	C_4-Anthracene
237.1638	$C_{18}H_{20}$	5.7	7.4	not found	not found	C_5-Fluorene
237.2577	$C_{17}H_{32}$	91.9	314.1	1.1	1.4	C_{17}-Bicycloalkane
239.2733	$C_{17}H_{34}$	74.5	228.1	not found	0.4	Cycloheptadecane

241.1951	$C_{18}H_{24}$	54.7	26.6	not found	not found	C_8-Naphthalene
247.242	$C_{18}H_{30}$	346.4	238.3	0.2	0.6	C_{12}-Alkylbenzene
251.1794	$C_{19}H_{22}$	3.5	4.3	not found	not found	C_6-Fluorene
251.2733	$C_{18}H_{34}$	65.7	204	not found	not found	C_{18}-Bicycloalkane
253.289	$C_{18}H_{36}$	48.3	129.3	not found	not found	Cyclooctadecane
255.2107	$C_{19}H_{26}$	38.5	18.8	not found	not found	C_9-Naphthalene
261.2577	$C_{19}H_{32}$	274.8	179.1	not found	0.3	C_{13}-Alkylbenzene
265.1951	$C_{20}H_{24}$	3.0	3.1	not found	not found	C_7-Fluorene
267.3046	$C_{19}H_{38}$	31.6	71.3	1.0	1.2	Cyclononadecane
269.2264	$C_{20}H_{28}$	25.2	10.9	not found	not found	C_{10}-Naphthalene
269.2839	$C_{18}H_{36}O$	3.2	4.4	not found	not found	Octadecanal
275.2733	$C_{20}H_{34}$	193.9	122.1	1.0	1.2	C_{14}-Alkylbenzene
279.2107	$C_{21}H_{26}$	2.2	2.4	not found	not found	C_8-Fluorene
279.3046	$C_{20}H_{38}$	33	88.1	not found	not found	C_{20}-Bicycloalkane
283.242	$C_{21}H_{30}$	18.9	9.2	not found	not found	C_{11}-Naphthalene
285.2788	$C_{18}H_{36}O_2$	48.4	19	1.0	0.9	Stearic acid
293.2264	$C_{22}H_{28}$	1.4	1.7	not found	not found	C_9-Fluorene
293.3203	$C_{21}H_{40}$	17.1	51.8	1.0	1.1	C_{21}-Bicycloalkane
297.2577	$C_{22}H_{32}$	12.2	6.1	not found	not found	C_{12}-Naphthalene
303.3046	$C_{22}H_{38}$	58.1	47.6	1.0	0.9	C_{16}-Alkylbenzene
307.3359	$C_{22}H_{42}$	6.9	25.4	not found	not found	C_{22}-Bicycloalakne
311.2733	$C_{23}H_{34}$	6.5	3.7	not found	not found	C_{13}-Naphthalene
317.3203	$C_{23}H_{40}$	21.4	22.2	not found	not found	C_{17}-Alkylbenzene
321.3516	$C_{23}H_{44}$	2.2	9.5	not found	not found	C_{24}-Bicycloalkane
325.289	$C_{24}H_{36}$	3.1	2.1	not found	not found	C_{14}-Naphthalene
345.3516	$C_{25}H_{44}$	1.2	2.4	not found	not found	C_{19}-Alkylbenzene

As already mentioned the identity is only one suggestion out of many possible molecules. For example the sum formulas of the listed aldehydes could as well refer to the isomeric ketones. The measurements recorded in the NO^+ mode can serve to differentiate between the aldehydes and the ketones, because they react differently with NO^+ (see section 5.5.3). The Figures 5.6, 5.7 and 5.8 show peaks possibly related to isomeric aldehydes and ketones from diesel exhaust fumes. In the following, the peaks will be discussed as examples for the separation of these two molecular classes in the NO^+ mode: The upper panel of Figure 5.6 exhibits a NO^+ as well as a H_3O^+ spectrum in the range of m/z 57 - m/z 59. Using H_3O^+ as a primary ion, isomeric compounds cannot be separated, which means that on m/z 59.0491 the sum of acetone and propanal is recorded (marked with the blue dotted line). In the NO^+ mode, on the other hand, acetone either loses an electron, which would lead to m/z 58.0413 or builds a molecule association with NO^+, which gives m/z 88.0393, shown in the lower panel. Propanal, on the other hand, looses a hydride ion so that it is recorded on m/z 57.0335. The lower panel reveals the differences due to variation of the Townsend number. At lower energies there is a higher probability of cluster production while at higher Townsend numbers clusters are more easily destroyed due to higher collision

energy. The graph shows two spectra recorded in the NO^+ mode, one at 138 the other at 80 Td. It can be seen that at lower energies the peak of the cluster marked with the orange dotted line is considerably larger than at higher energies. By changing the energy the existence of molecule associations can be proven. It can be concluded that the diesel exhaust contained both propanal as well as acetone. In Figure 5.7 the the same kind of graphs are shown for pentanal and its isomers. In the same way as for acetone, the sum of aldehyde and ketone isomers can be discovered in the H_3O^+ spectrum (m/z 87.0804) while in the NO^+ spectrum the aldehydes and the ketones can be found separately (m/z 85.0648 and m/z 86.0726). This illustrates that C_5-aldehyde as well as C_5-ketone isomers were most probably present in the diesel vehicle emissions. The lower panel reveals that the interpretation of the spectra is challenging due to overlapping peaks. Still, a shoulder can be seen, that coincides with the mass of the ketone NO^+ cluster. The last Figure 5.8 shows the peak corresponding to octanal and its isomers at m/z 127.1117 in the NO^+ spectrum, but the peak of the ketone isomers, expected at m/z 128.1196 in the NO^+ mode, is missing. Several peaks were measured on the mass of the cluster (expected at m/z 158.1176), but they were so close together that a proper separation is impossible at this mass resolution. Therefore, no specific information can be given about the occurrence of C_8-ketones in the diesel exhaust gases. However, the missing peak of the ketone at m/z 128.1196 is a strong hint that the aldehyde was the dominant form. In general, no quantitative statements can be made, because no calibration is available for these compounds.

Sum formulas containing two oxygen atoms were identified here as organic acids. These formulas could as well refer to substances with a carbonyl as well as a hydroxyl group, or to ester compounds. In the literature Schauer et al. (1999) also report higher organic acids from vehicle exhaust.

Alkanes are one of the main compounds in car emissions (Siegl et al., 1999; Schauer et al., 1999), but the PTR-TOF-MS is not able to record short-chained alkanes in the H_3O^+ mode due to their low proton affinity. Larger alkanes, on the other hand, are expected to fragment in the drift tube (Arnold et al., 1998). Jobson et al. (2005) identified alkyl fragments which correspond to alkanes with more than 10 carbon atoms. Their integer mass can be calculated from the formula $14n + 1$ with n lying between 3 and 8 (Jobson et al., 2005). Fragments corresponding to C_5 to C_9 n-aldehydes were reported as well (Spanel et al., 1997; Jobson et al., 2005; Jordan et al., 2009). Using the known sum formula of the fragments, their mass expected from the PTR-TOF-MS measurement could be calculated. For the aldehyde fragments a reaction rate coefficient of $2 \times 10^{-9}\,cm^3/s$ was assumed. Alkanes, on the other hand, have lower reaction rates due to their low proton affinities. Arnold et al. (1998) report an overall reaction rate coefficient of $9.9 \times 10^{-10}\,cm^3/s$ for the alkane n-$C_{10}H_{22}$ at 300 K. This value was used to calculate the mixing ratios of the alkane fragments. The exact masses were not always found in the spectra produced here due to slight shifts in the mass scale. Hence, the peaks being closest to the actual mass were used. A strong hint for the correctness of this assumption is that these peaks showed high count rates, which was expected because of the high amounts of alkanes in the exhaust. The results of these fragments from this work can be found in Table 5.5.

Interestingly, the peaks in the spectra reached up to a mass of ~ 350 and then faded, but at m/z 417.0780 another peak occurred. A suggestion would be that the peak could belong to the group of hopanes or steranes, because these compounds have very high molecular

masses and were already measured in diesel exhaust (Schauer et al., 1999). But their masses do not match the exact value of the peak, they are slightly lighter. One possible sum formula would be $C_{33}H_{21}^{+}$, which could refer to a structure similar to octacene, but with a ring of 5 C atoms at one end. The expected mass in the PTR-TOF-MS for this molecule would be m/z 417.1638. The discrepancy between the expected and the measured peak can either mean that the masses were shifted and could not be corrected due to a missing internal standard at such high masses or that the peak referred to yet another compound.

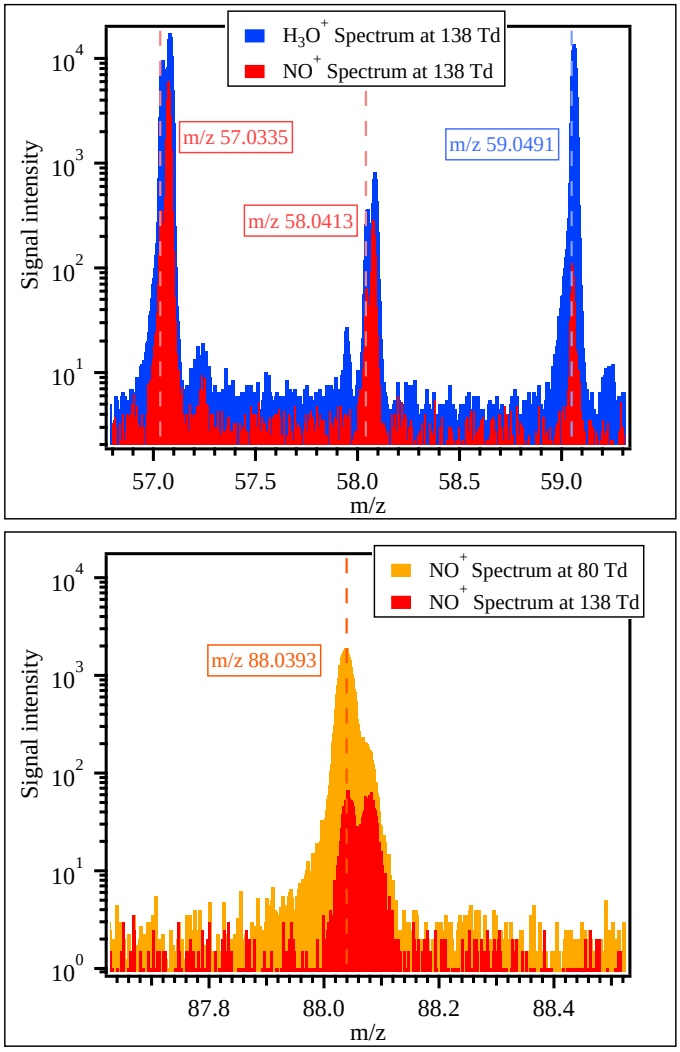

Figure 5.6.: In the upper panel the NO^{+} spectrum at 138 Td (red) and the H_3O^{+} spectrum from the diesel exhaust measurement at 138 Td (blue) are shown in the range of m/z 57 - m/z 59. Marked by red dotted lines are the expected masses measured in the NO^{+}: m/z 57.0335 being propanal and m/z 58.0413 being acetone. The blue dotted line shows the sum of acetone and propanal measured in the H_3O^{+} mode at m/z 59.0491. The lower panel displays NO^{+} spectra at 138 Td and 80 Td at m/z 88. The orange dotted line refers to the cluster of acetone and NO^{+} at mass 88.0393.

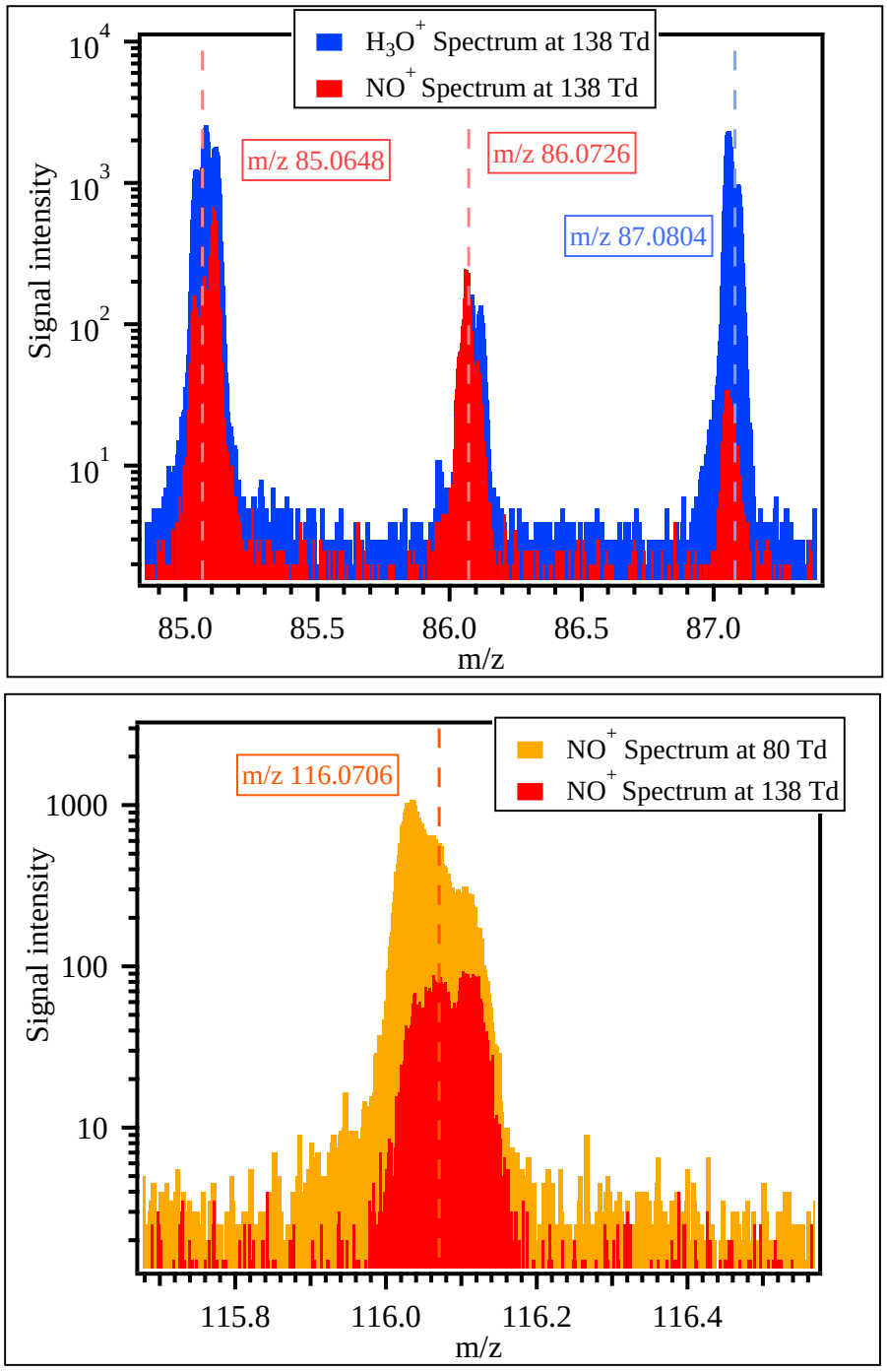

Figure 5.7.: The NO^+ spectrum at 138 Td (red) and the H_3O^+ spectrum from the diesel exhaust measurement at 138 Td (blue) are displayed in the range of m/z 85 - m/z 87 in the upper panel. Red dotted lines show the expected masses measured in the NO^+: m/z 85.0648 being the aldehyde isomers and m/z 86.0726 referring to the ketone isomers . The blue dotted line mark the sum of aldehyde and ketone isomers measured in the H_3O^+ mode at m/z 87.0804. The lower panel displays NO^+ spectra at 138 Td and 80 Td at m/z 116. Marked in orange is the mass of the ketone cluster with NO^+ at m/z 116.0706.

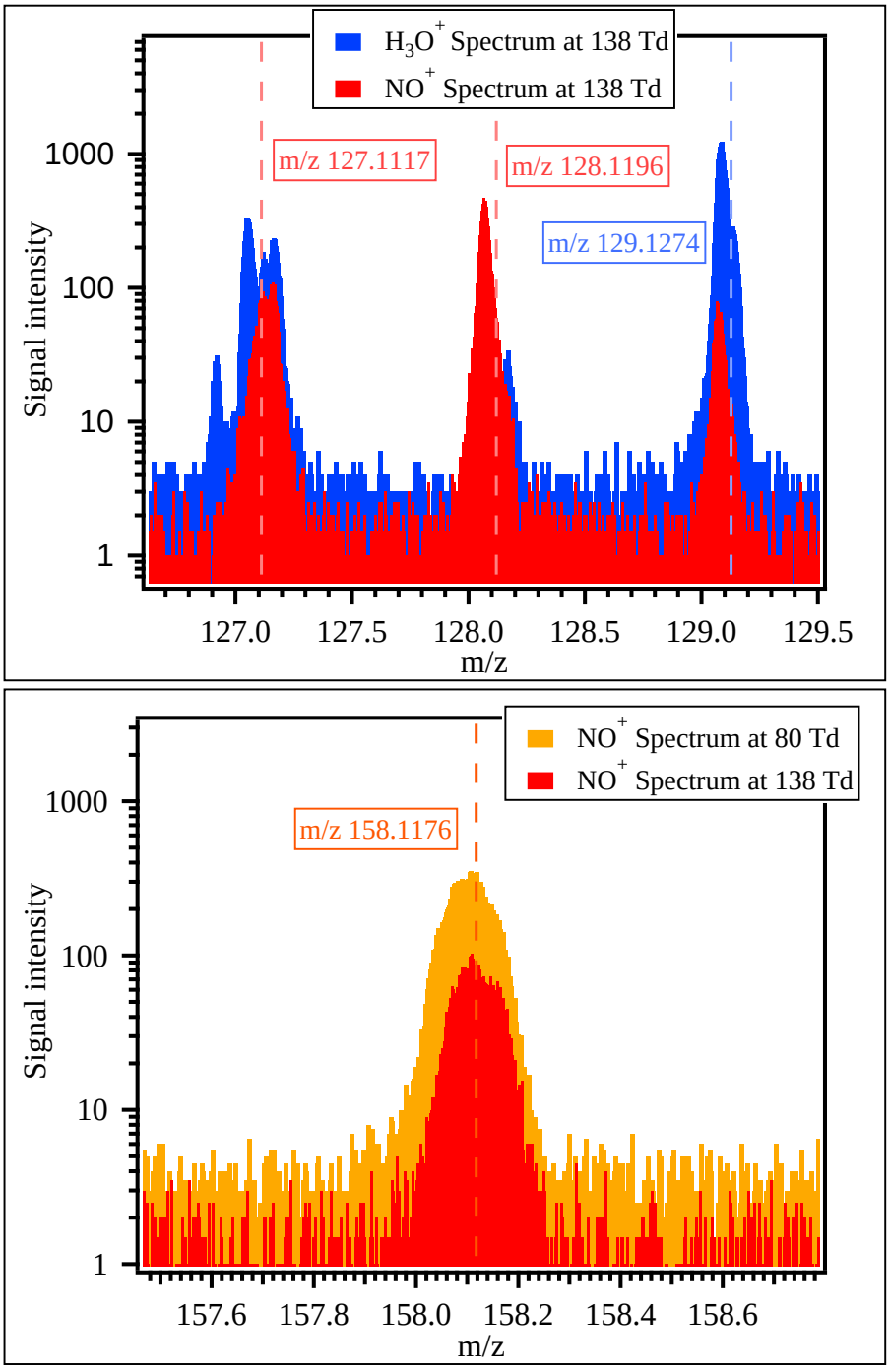

Figure 5.8.: In the upper panel the NO^+ spectrum at 138 Td (red) and the H_3O^+ spectrum from the diesel exhaust measurement at 138 Td (blue) are graphed in the range of m/z 127 - m/z 129. Red dotted lines mark the expected masses 127.1117, which refers to the aldehyde-isomers, and m/z 128.1196, which represents the ketone isomers measured in the NO^+ mode. The blue dotted line marks the sum of the aldehyde and ketone isomers measured in the H_3O^+ at m/z 129.1274. The lower panel shows NO^+ spectra at 138 Td and 80 Td at m/z 158. The mass of the ketone cluster with NO^+ at m/z 158.1176 is marked with a dotted orange line.

Table 5.5.: Fragments of alkanes and aldehydes, their matching TOF masses, sum formula, mixing ratios of undiluted diesel (VW) and gasoline (Toyota) exhaust in ppmv at different energies

	Matching TOF mass	Sum formula	Calculated [ppmv] VW bus 138 Td	Calculated [ppmv] VW bus 80 Td	Calculated [ppmv] Toyota 138 Td	Calculated [ppmv] Toyota 80 Td
Alkanes	41.0386	$C_3H_5^+$	40.7	0.6	43.4	1.1
	43.0542	$C_3H_7^+$	21.4	5.5	27.2	24.8
	57.0699	$C_4H_9^+$	37.8	7.5	45.6	42.4
	71.0855	$C_5H_{11}^+$	6.4	5.5	5.4	17.2
	85.1012	$C_6H_{13}^+$	3.6	4.8	2.0	8.4
	99.1168	$C_7H_{15}^+$	0.5	1.3	0.1	0.9
Sum			110.4	25.2	123.7	94.8
Aldehydes	69.0699	$C_5H_9^+$	8.2	0.8	2.1	1.7
	83.0855	$C_6H_{11}^+$	5.9	1.0	1.3	1.8
	97.1012	$C_7H_{13}^+$	4.3	1.6	0.7	1.1
	111.1168	$C_8H_{15}^+$	2.2	1.6	0.3	0.7
Sum			20.6	5.0	4.4	5.3

5.8. Comparison between high and low energy settings

Despite the consideration of the different water cluster values, the differences between the high and low energy mode were striking: For example the total xylenes (m/z 107.0855) and the total trimethylbenzenes (m/z 121.1012) showed ca. 2 times larger values at higher energy for the measurement of diesel exhaust gases. This can be interpreted as larger molecules fragmenting on to the masses of the xylenes and trimethylbenzenes. The fragmentation process does not necessarily have to yield the exact mass, but can also lead to a mass being so close to the actual compound that the instrument is not able to resolve the two peaks. Another example would be benzene, which behaves the other way round, namely having a ca. 2.5 times higher result at lower energy in diesel exhaust. Here enhanced clustering at lower energies is the most likely explanation. Figure 5.9 shows the calculated mixing ratios of the m/z 79.0542, m/z 61.0311 and m/z 43.0203. While m/z 79.0542 is the exact mass of benzene, the other two values can not definitively be assigned. With a high probably m/z 61.0331 refers to acetic acid, which has the expected mass of 61.0284. The slight shift might have its origin in the saturation of the peak. The mass 43.0203 represents most probable the fragment $C_2H_3O^+$, which could refer to protonated acetic acid minus one water molecule. If this fragment would cluster with two water molecules, it would be measured on m/z 79.0390. A resolution of more than 5000 would be necessary to separate this peak from the peak of benzene. Since the resolution during measurement was only 3500, the sum of the cluster and benzene was detected on the same

mass, which, most probably, was the reason for the much higher benzene mixing ratio at 80 Td. Figure 5.9 displays the trends of the mixing ratios given in ppmv. Mass 43.0203 decreased while benzene increased when the energy had been reduced. This behavior can either be interpreted that m/z 43.0203 formed a higher amount of clusters with two water molecules at lower energy so that the peak of benzene increased. It could also mean that at 80 Td acetic acid fragmented less so that less m/z 43.0203 was produced. But the latter effect would result in an increase of m/z 61.0331 at lower energy due to reduced fragmentation. Figure 5.9 shows the opposite trend. The decline in acetic acid is remarkable and difficult to explain. One reason could be that m/z 43.0203 was not only produced from acetic acid but also by the fragmentation of larger molecules. Clustering of m/z 43.0203 might take place at 138 Td as well as 80 Td, but at lower energies m/z 43.0203 might prefer to cluster with two water molecules instead of one to give more m/z 79.0390 and less m/z 61.0331. Since m/z 61.0331 is not the correct mass of acetic acid, it could also be that the peak itself is biased by fragments. This would explain the decrease of m/z 61.0331 at lower energies. For that reason, the acetic acid data in Table 5.4 were given a question mark and need to be handled with caution. For benzene the more reliable value might therefore be ca. 2.5 ppmv measured at 138 Td. Gueneron et al. (2015) found that aromatic compounds containing alkyl side chains can fragment of the mass of benzene and toluene at 120 Td. This would mean that the real value of benzene would be lower than 2.5 ppmv.
Toluene (m/z 93.0699), on the other hand, gained lower mixing ratios at 80 Td than at 138 Td in diesel exhaust. The high mixing ratio of ca. 3.4 ppmv at high Townsend number is most probable the result of fragmentation of heavier compounds on the mass of toluene. The gasoline exhaust showed 2 to 3 times higher values of benzene and toluene at 138 Td than at 80 Td. Fragmentation can be considered as an explanation here as well. These examples prove that the comparison between different energies represents a challenge, especially for the measurement of highly polluted air. If clustering and fragmentation would not occur, the measurements at high and low energies should yield the same results. As a consequence of these processes, the reported mixing ratios need to be treated with caution and as long as no calibration with the same matrix of gases exists no exact quantitative statements can be made. Favorable operating conditions would be a low energy setting to reduce fragmentation and a removal of water vapor to minimize clustering.

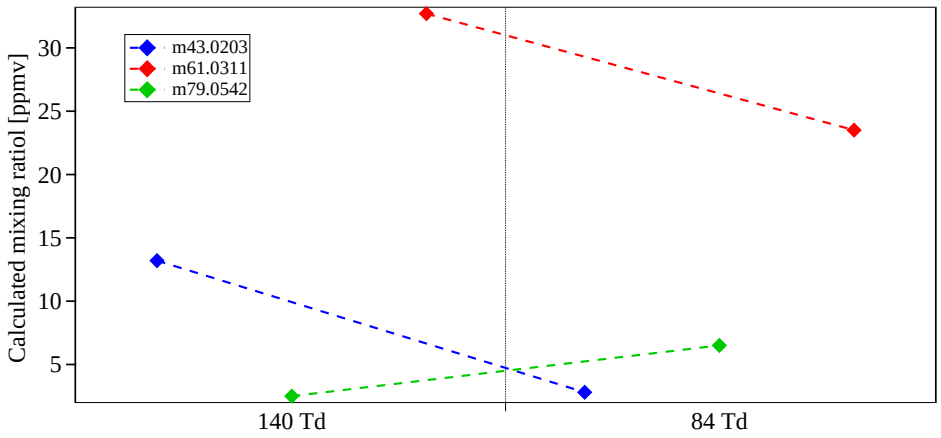

Figure 5.9.: Calculated mixing ratios of the masses 43.0203, 61.0311, 79.0542 during the measurement of VW bus exhaust at 138 Td (left part) and 80 Td (right part). The recorded masses are given. m/z 79.0542 represents benzene, the others most probably refer to acetic acid (exact m/z 61.0280) and the fragment $C_2H_3O^+$ (exact m/z 43.0178).

5.9. Calculated values: Analysis and comparison between VW bus and Toyota

The calculated mixing ratios of the compounds identified in the mass spectrum can be found in Table 5.4. The results of diesel (VW bus) as well as gasoline exhaust (Toyota) measured at high and low energies are shown. It becomes clear that far fewer compounds were recorded during the measurement of the gasoline vehicle. Especially high masses were either measured in very low mixing ratios or were not found at all. This was expected, because gasoline contains smaller molecules, e.g. shorter chained alkanes. The high number of masses found in the diesel exhaust gases does not only mean that it consists of more components, but the reason can also be the fragmentation of larger molecules, especially long-chained alkanes, onto multiple lower masses.
Table 5.6 contains main compound groups and their percentages in diesel and gasoline exhaust fumes. The values were determined by using the calculated data in ppbv. It should be noted that the numbers do not sum up to 100 %, because some compounds were included in the total amount, but not in the different groups, such as aliphatic compounds with carbon numbers larger than 20 and some were assigned to two groups, e.g. phenol is an aromatic as well as oxygenated species, or the aldehydes were determined as an extra group, but were also included into the oxygenated compounds.
It becomes clear that the main components of diesel exhaust were the oxygenated substances as well as the alkanes (43 and 45 % at 138 Td, respectively). At 80 Td the values shifted towards the oxygenated compounds due to less fragmentation. In emissions from gasoline vehicles, on the other hand, aromatic compounds dominated the exhaust mixture (40-50 %). This can be traced back to the high amount of light aromatics like benzene in gasoline even before combustion. Benzene, toluene or the total xylenes occurred in one

magnitude higher values in the gasoline than in the diesel exhaust fumes. At 138 Td the xylenes for example showed a value of around 53 ppmv in gasoline, but only 4 ppmv in diesel car emissions. Ethanol is included in gasoline to a high amount, which can be seen in the ca. 50 times higher gasoline exhaust value at 138 Td in comparison to diesel exhaust. Mass 61.0284 (found on m/z 61.0331) showed a much higher value in the diesel exhaust (ca. 33 ppmv at 138 Td) and was very low in the gasoline vehicle emissions (around 0.7 ppbv at 138 Td). This result is quite striking, because acetic acid is expected to be present in car exhaust (e.g. Kawamura et al., 1985; Zervas et al., 1999). Two possible explanations can be considered: Either the mass actually represents acetic acid and the Toyota emitted much less acid under these conditions or as already mentioned, problems occurred during the measurement of the gasoline exhaust like clustering or scavenging of the acid so that it was either measured on another mass or not captured at all. Further tests would be necessary to make a clear statement.
While m/z 143.0855, which might refer to C_1-naphthalene, revealed similar values for VW bus and Toyota emissions (around 800 - 820 ppbv at 138 Td), all masses being higher than m/z 143.0855 displayed much higher values in diesel exhaust gases. Many of the masses were not even found in the exhaust of gasoline vehicles. IVOCs (C_{10}-C_{20} account for 5 % of the total mass signal at 138 Td in diesel exhaust, but only for 1 % in emissions from gasoline cars. The masses higher than m/z 140 sum up to $\sim$11 ppmv from VW bus emissions and only $\sim$1 ppmv from Toyota emissions at 138 Td. In the next section the calculated results will be compared to the calibrated data.

Table 5.6.: Percentages of different compound groups in diesel (VW bus) and gasoline (Toyota) exhaust at high and low energies. The value for the oxygenated compounds includes the aldehyde fragments.

Group	VW bus 138 Td [%]	VW bus 80 Td [%]	Toyota 138 Td [%]	Toyota 80 Td [%]
Oxygenated	43	56	9	15
Aromatics	12	17	54	42
Alkane fragments	45	19	39	44
Aldehyde fragments	8	4	1	2
IVOCs C_{10}-C_{20}	5	14	1	1

5.10. Calibrated compounds

The instrument was calibrated using an Apel Riemer Environmental Inc. gas standard containing 14 compounds. Calibrations were performed for H_3O^+ as well as for NO^+ primary ions at two different energy settings (138 Td and ca. 80 Td), respectively. The calibration was carried out under dry conditions, because the exhaust was expected to be very dry due to the high dilution (50 to 100 times) with dry nitrogen. However, high count rates on the water cluster isotope m/z 39 occurred during measurement. This phenomenon can be traced back to three possible reasons: First, when the energy in the drift tube is reduced,

weaker collisions between the molecules take place so that clustering is favored. Therefore, m/z 39 increased, when the Townsend number was switched from 138 Td to 80 Td. Second, during the high energy setting the m/z 39 peak was broader and showed a lower resolution, which is a strong hint that a second peak, probably a fragment, was lying directly under the m/z 39 peak. The instrument was not able to resolve the two peaks so that their sum was measured. Since m/z 39 is necessary for normalization (see chapter 2), the value for it was taken from the background measurement, where no fragments were present. This effect was only a problem at high energies, where fragmentation is promoted. The application of the water cluster value of the background can cause an error, which is accounted for in the error calculation. Third, alkanes, which occurred in high amounts in the exhaust, catalyze the production of water clusters by ligand switching reactions (see Gueneron et al., 2015). The last two effects only took place during measurement, because the exhaust represented a matrix of various compounds which influenced the water cluster. These conditions could not be completely reproduced during the calibration so that the m/z 39 : m/z 21 ratio differed. A comparison of the ratios at 138 Td is very difficult, because the m/z 39 peak was biased by a fragment. On the other hand, the m/z 39 value of the background at 138 Td is most probably too low, because ligand switching reactions only occur during exhaust and not during the background measurement. Therefore, it is difficult to make a statement for the high energy case and the error can only be estimated. For the low energy case the water cluster could be measured so that a comparison is possible: The calibration and the Toyota measurement at 80 Td agreed well with a m/z 39 : m/z 21 ratio of 1.5 and 1.6 respectively. In contrast, the ratio was twice as high (3.0) for the measurement of the VW exhaust at 80 Td. The clustering effect due to low energy should be the same for the Toyota and the VW bus experiment. In addition in both measurements at 80 Td the m/z 39 peak was a single peak, so likely not influenced by a fragment. Hence, the only reason for the discrepancy can be the higher amount of alkanes in diesel exhaust, which led to water cluster production due to ligand switching reactions. The error is accounted for in the error calculation. The Tables 5.7 and 5.8 show the calculated and calibrated results in ppmv for 10 different compounds from the exhaust measurement of the VW bus and of the Toyota Yaris respectively, at two different energy settings. A comparison between diesel and gasoline can be found in the previous chapter. Here only the differences between calibrated and calculated results shall be delineated. At 138 Td the discrepancies lay between 15 and 80 % while at 80 Td the differences showed values between 2 and 40 %. The percentages were calculated by dividing the difference between both values by the average value and they were the same for Toyota and VW, because the same procedures for the theoretical calculation were used. Since the error of the calculated data reached from 60 to 80 %, the results lay within the error range. Still, it is striking that the uncertainties at 138 Td were for some substances twice as high as at 80 Td. Fragmentation and clustering processes should not play a role here, because the calibrated as well as the calculated results were based on the same raw data. The differences must therefore either emerge from a deficient calibration factor or from uncertainties in the theoretical approach such as an erroneous reaction rate coefficient k. In general, the energy in the drift tube determines the reaction time, but should not influence the reaction rate coefficients k. Thus, it is legitimate to use the same k values for the high and the low energy mode. This means that the theoretical method is the same for both E/N values and consequently it can not

be the reason for the larger discrepancy. The only explanation is therefore an insufficiently accurate calibration at 138 Td. The calibration for car exhaust gases generally represents a challenge, because the gas matrix during calibration differs quite strikingly from the one during measurement. Especially processes like ligand switching only occur in the complex mixture of the car exhaust. Furthermore, it might be possible that the ratio between the water cluster and the primary ion changes in the transfer region between the drift tube and the mass spectrometer. Hence, it could be concluded that at higher energies these effects and differences play a more important role than at low energies and thus cause the larger divergence.

Table 5.7.: Undiluted mixing ratios of the calibrated compounds in ppmv for the VW bus at different Townsend numbers

Compound	VW 138 Td calibrated	VW 138 Td calculated	VW 80 Td calibrated	VW 80 Td calculated
Methanol	3.0 ± 1.3	3.5 ± 2.1	3.1 ± 1.0	2.3 ± 1.4
Acetonitrile	0.7 ± 0.2	0.8 ± 0.5	0.4 ± 0.08	0.4 ± 0.2
Acetaldehyde	14.1 ± 3.9	19.7 ± 11.9	11.9 ± 2.5	12.4 ± 7.6
Acetone	5.1 ± 1.4	10.0 ± 6.2	5.7 ± 1.2	8.5 ± 5.4
MVK	3.2 ± 0.9	4.7 ± 3.0	3.2 ± 0.7	3.8 ± 2.4
MEK	1.1 ± 0.3	1.8 ± 1.1	1.6 ± 0.3	2.2 ± 1.4
Benzene	1.2 ± 0.3	2.5 ± 1.6	5.6 ± 1.2	6.5 ± 4.2
Toluene	1.5 ± 0.4	3.4 ± 2.2	0.6 ± 0.1	0.8 ± 0.6
Total xylenes	1.7 ± 0.5	3.9 ± 2.6	1.3 ± 0.3	1.7 ± 1.2
Total trimethyl-benzenes	2.9 ± 0.9	6.5 ± 4.5	2.7 ± 0.6	3.6 ± 2.4

Table 5.8.: Undiluted mixing ratios of the calibrated compounds in ppmv for the Toyota Yaris at different Townsend numbers

Compound	Toyota 138 Td calibrated	Toyota 138 Td calculated	Toyota 80 Td calibrated	Toyota 80 Td calculated
Methanol	4.1 ± 1.7	4.8 ± 2.9	4.4 ± 1.1	3.3 ± 2.0
Acetonitrile	0.1 ± 0.03	0.2 ± 0.1	0.3 ± 0.02	0.3 ± 0.2
Acetaldehyde	5.5 ± 1.2	7.7 ± 4.7	5.1 ± 0.3	5.3 ± 3.2
Acetone	1.9 ± 0.4	3.7 ± 2.3	2.3 ± 0.1	3.5 ± 2.2
MVK	0.6 ± 0.1	0.8 ± 0.5	0.7 ± 0.04	0.8 ± 0.5
MEK	0.5 ± 0.1	0.8 ± 0.5	0.4 ± 0.02	0.6 ± 0.4
Benzene	12.2 ± 2.7	26.0 ± 16.7	7.2 ± 0.4	8.3 ± 5.3
Toluene	23.2 ± 5.2	51.6 ± 33.8	19.0 ± 1.0	24.5 ± 16.1
Total xylenes	22.8 ± 5.4	52.7 ± 35.1	23.3 ± 1.6	31.7 ± 21.2
Total trimethyl-benzenes	14.8 ± 3.9	33.9 ± 23.0	16.3 ± 1.9	21.0 ± 14.3

5.11. Comparison with literature

A direct comparison with literature values turns out to be quite difficult, because the studies were performed at different conditions. Siegl et al. (1999) as well as Schauer et al. (1999) were using a chassis dynamometer and emission rates were reported. Erickson et al. (2014) state data in ppbv, but only for exhaust of unknown dilution and the measurement took place under engine load. In contrast, the emissions in this work were measured while the car was stationary and idling. Jobson et al. (2005) measured a diesel vehicle under idle conditions as well so that a comparison is possible. Table 5.9 shows some compounds measured by Jobson et al. (2005) and reported in this work. The dilution was unknown in the study of Jobson et al. (2005), but an estimation was 70:1. Therefore, the values given by Jobson et al. (2005) were multiplied by the dilution factor so that the data can be compared, but the quite high uncertainty needs to be kept in mind. Since Jobson et al. (2005) were applying an energy of 150 Td in the drift tube, the calculated values of the VW bus measured at 138 Td from this study were used here. The sum of acetone and propanal showed a very nice agreement between both studies while methanol, acetaldeyhde, benzene, toluene and the sum of the aldehyde fragments were in the same order of magnitude. The sum of the alkane fragments as well as the values for naphthalene and phenol displayed 2-15 times higher values in the study of Jobson et al. (2005). Besides different cars and measurement conditions, the reason could be that Jobson et al. (2005) used a PTR-MS quadrupole, which has a resolution of 1 amu, only. If several peaks occur on one integer mass, then the quadrupole detects the sum. The spectrum recorded by the PTR-TOF-MS revealed that on the integer masses of the alkane fragments, naphthalene and phenol at least 2 peaks were measured, which means that the quadrupole overestimated these values. If all the peaks found on the integer masses of the alkane fragments in the PTR-TOF-MS spectrum would be summed up, the result would be 191.8 ppmv. This is still lower than

the value reported by Jobson et al. (2005), but if an error of 60 % is assumed (see section 5.5.2), the results would match within the error range.

Table 5.9.: Measured diesel exhaust values in [ppmv] by Jobson et al. (2005) and from this study

Compound	Jobson et al. (2005)	This study
Alkane fragments	261.2	110.4
Aldehyde fragments	23.8	20.6
Methanol	5.7	3.5
Acetaldehyde	29.8	19.7
Acetone/propanal	9.2	10.0
Benzene	3.3	2.5
Toluene	1.8	3.4
Phenol	4.2	0.3
Naphthalene	3.1	0.9

5.12. Summary

In consideration of the large fleet of diesel cars in Europe, a regular monitoring of VOCs and IVOCs would be preferable for the benefit of the environment, air quality and human health.
Gasoline emissions contain a large amount of VOCs, some of which are highly toxic, e.g. benzene. Furthermore, the exhaust has a high potential to increase tropospheric ozone. Diesel fuel, on the other hand, is more efficient, which means less CO_2 is produced. However, diesel exhaust contains a higher amount of IVOCs, which are known to produce secondary organic aerosol, than gasoline emissions. The thus increased particle concentration in the air strongly affects human health and leads to more premature deaths (Lelieveld et al., 2015). In addition diesel exhaust gases contribute to tropospheric ozone by compounds, which are not usually monitored. The PTR-TOF-MS opens a window on a new research field as it is capable of measuring these compounds simultaneously and online. Hence, it is particularly useful for studying car emissions.
In this work it was determined that diesel emissions mainly consisted of oxygenated compounds (43% at 138 Td) and alkanes (45% at 138 Td) while gasoline exhaust was dominated by aromatic species (54% at 138 Td). The diesel exhaust spectra ranged up to m/z ∼350 and the IVOCs represented 5% of the total diesel emissions. Gasoline exhaust, on the other hand, showed masses up to 220, only, and light aromatic compounds occurred in very high mixing ratios of 20 - 50 ppmv at 138 Td.
A separation of aldehydes and ketones was possible by using NO^+ as primary ions. It was found that the C_3-isomers were present in the aldehyde (propanal) as well as ketone (acetone) form in diesel exhaust while for the C_8-equivalent only the aldehyde form was detected. Furthermore, large discrepancies were determined between the measurements at high and low energies. Possible reasons were clustering and fragmentation processes,

which occurred to a different degree depending on the energy set in the drift tube.
Measurements of diesel exhaust fumes from Jobson et al. (2005) were compared to the values from this work and for some compounds, such as benzene or acetone, satisfactory results were gained. Others, like the sum of the alkane fragments, showed a larger inconsistency. One explanation for this could be the lower mass resolution of a PTR-quadrupol-MS used by Jobson et al. (2005). While the PTR-TOF-MS is able to resolve isobaric masses, the PTR-quadrupol-MS measures the sum. If multiple peaks occur, this leads to an overestimation.
The study described here was a first attempt at our institute and further research would be desirable and could pave the way for the PTR-TOF-MS being implemented as a standard device in regulatory monitoring networks.

6. Conclusion

The studies described within this work show the broad field of application and versatility of the PTR-TOF-MS instrument.
During the OVOC-inter-comparison campaign in Hohenpeißenberg good agreements were found between the three participating PTR-TOF-MS instruments. The only problematic compounds were methanol due to its high polarity and acetaldehyde partly due to its production inside the tubing and partly due to as yet undiscovered reasons. Depending on the environment, where the measurement takes place, interferences between isomeric compounds need to be kept in mind, e.g. between acetone and propanal or MEK and butanal. Since PTR-TOF-MS instruments are not able to separate these compounds, a comparison with a GC system is recommended. In general, it was concluded that clean background measurements and elaborate humidity dependent calibrations are essential. After the campaign improvements were undertaken, such as establishing the continual flushing of the catalytic converter or the reduction and heating of the lines in the calibration system, however, only minor improvements were achieved. Therefore, further investigations and comparisons, especially regarding these two compounds, would be of advantage.
The results from the field campaign on the island of Cyprus (CYPHEX) revealed insights in local Mediterranean emission patterns as well as long distance transport processes. Biogenic VOCs like isoprene and monoterpenes occurred in low atmospheric mixing ratios, reflecting the sparse vegetation, and they showed well defined diel cycles. The oxygenated VOCs methanol, acetone and acetic acid were used to investigate the impact of the marine boundary layer during transport, because they have long atmospheric lifetimes. Acetic acid was measured for the first time with the instrument of our group and further tests to identify artifacts and to improve the calibration would be of value for future campaigns. While methanol and acetone were not influenced by local emissions, acetic acid showed a diel cycle, but only during one part of the CYPHEX campaign. Local secondary production, soil emission or vertical in-mixing from the free troposphere were suggested as three possible reasons for this behavior, but further examinations would be required to narrow the possibilities further down. Flux measurements from different soil types as well as airborne measurements at various heights would be crucial to draw more specific conclusions. Furthermore, the ocean represents an interesting research field, because currently little is known about its role in the budgets of the three OVOCs, especially of acetic acid. During the CYPHEX campaign it was found that the measured loss rates of acetone, methanol and acetic acid did not follow the solubility or OH rate pattern. To explain these loss rates further investigations of the dry deposition rates and the fluxes over the ocean would be necessary and could be gained by a ship campaign on the Mediterranean Sea.
The measurement of car exhaust fumes stresses the diversity of applications of the PTR-TOF-MS. Regarding the increasing number of diesel vehicles in Europe, a monitoring system for VOCs, especially IVOCs, is needed. Proton Transfer Reaction - Time of Flight - Mass Spectrometry represents a powerful technique for this purpose because of its high

mass and time resolution. The measurements gave an insight into the composition of vehicle exhaust gases and comparisons between gasoline and diesel engine emissions as well as between calibrated and calculated mixing ratios were possible. It was found that the main components of diesel exhaust were OVOCs and alkanes while gasoline engine emissions were dominated by aromatic species. Masses higher than m/z 138 revealed ca. 10 times higher mixing ratios in diesel than in gasoline exhaust, because diesel fuel contains a much higher amount of long-chained components compared to gasoline. Due to the high uncertainties, the calculated and calibrated values matched within the error bars, but quite large discrepancies occurred. Since this study was a first attempt to measure car exhaust with our PTR-TOF-MS, improvements are yet to be achieved. Despite the gentle protonation process, fragmentation of long-chained compounds was determined and in addition clustering occurred at lower energy settings. Additionally, alkanes underwent ligand switching reactions, which increased the count rates of the water cluster. All these processes complicate the interpretation of the MS spectra. Thus, a calibration gas standard which resembles the complex mixture of vehicle exhaust would be helpful to make not only qualitative but also quantitative statements and would facilitate the comparison to calculated values. Furthermore, the dilution system needs improvement to prevent the saturation of the detector. A higher mass resolution would be of advantage as well due to the isobaric peak overlapping. To achieve this a larger flight path within the instrument, gained by running the instrument in the so called W-mode, would be necessary. Coupling with a GC system would also enhance the measurements, because a pre-separation of the compounds would reduce the complexity of the mass spectra. For future measurements using a chassis dynamometer, which enables the characterization of car exhaust at different engine loads, or field measurements, e.g. in an automobile tunnel or using portable measurement devices would be of great interest.
Proven by the manifold applications, the PTR-TOF-MS represents a valuable tool for the measurement of VOCs in a large dynamic range of mixing ratios and under various conditions.

Bibliography

Akagi, S. K., Yokelson, R. J., Wiedinmyer, C., Alvarado, M. J., Reid, J. S., Karl, T., Crounse, J. D., and Wennberg, P. O.: Emission factors for open and domestic biomass burning for use in atmospheric models, Atmos. Chem. Phys., 11, 4039–4072, doi:10.5194/acp-11-4039-2011, URL http://www.atmos-chem-phys.net/11/4039/2011/, 2011.

Amelynck, C., Schoon, N., Kuppens, T., Bultinck, P., and Arijs, E.: A selected ion flow tube study of the reactions of H_3O^+, NO^+ and $O_2{}^+$ with some oxygenated biogenic volatile organic compounds, Int. J. Mass spectrom., 247, 1–9, doi:10.1016/j.ijms.2005.08.010, URL http://www.sciencedirect.com/science/article/pii/S1387380605002010, 2005.

Andreae, M. O. and Merlet, P.: Emission of trace gases and aerosols from biomass burning, Global Biogeochem. Cy., 15, 955–966, doi:10.1029/2000GB001382, URL http://dx.doi.org/10.1029/2000GB001382, 2001.

Andreae, M. O., Talbot, R. W., Andreae, T. W., and Harriss, R.: Formic and acetic acids over the central Amazon region, Brazil: 1. Dry season, J. Geophys. Res., 93, 1616–1624, 1988.

Arey, J., Crowley, D. E., Crowley, M., Resketo, M., and Lester, J.: Hydrocarbon emissions from natural vegetation in California's South Coast Air Basin, Atmos. Environ., 29, 2977 – 2988, doi:10.1016/1352-2310(95)00137-N, URL http://www.sciencedirect.com/science/article/pii/135223109500137N, 1995.

Arnold, S. R., Spracklen, D. V., Williams, J., Yassaa, N., Sciare, J., Bonsang, B., Gros, V., Peeken, I., Lewis, A. C., Alvain, S., and Moulin, C.: Evaluation of the global oceanic isoprene source and its impacts on marine organic carbon aerosol, Atmos. Chem. Phys., 9, 1253–1262, doi:10.5194/acp-9-1253-2009, URL http://www.atmos-chem-phys.net/9/1253/2009/, 2009.

Arnold, S. T., Viggiano, A. A., and Morris, R. A.: Rate Constants and Product Branching Fractions for the Reactions of H_3O^+ and NO^+ with C_2-C_{12} Alkanes, J. Phys. Chem. A, 102, 8881–8887, doi:10.1021/jp9815457, URL http://dx.doi.org/10.1021/jp9815457, 1998.

Atkinson, R.: Gas-phase tropospheric chemistry of organic compounds: A review, Atmos. Environ., 24, 1–41, doi:10.1016/0960-1686(90)90438-S, URL http://www.sciencedirect.com/science/article/pii/096016869090438S, 1990.

Baasandorj, M., Millet, D. B., Hu, L., Mitroo, D., and Williams, B. J.: Measuring acetic and formic acid by proton transfer reaction-mass spectrometry: sensitivity, humidity dependence, and quantifying interferences, Atmospheric Measurement

Techniques Discussions, 7, 10 883–10 930, doi:10.5194/amtd-7-10883-2014, URL http://www.atmos-meas-tech-discuss.net/7/10883/2014/, 2014.

Benner Jr., B. A., Gordon, G. E., and Wise, S. A.: Mobile sources of atmospheric polycyclic aromatic hydrocarbons: a roadway tunnel study, Environ. Sci. Technol., 23, 1269–1278, doi:10.1021/es00068a014, URL http://dx.doi.org/10.1021/es00068a014, 1989.

Blake, R. S., Wyche, K. P., Ellis, A. M., and Monks, P. S.: Chemical ionization reaction time-of-flight mass spectrometry: Multi-reagent analysis for determination of trace gas composition, Int. J. Mass spectrom., 254, 85–93, doi:10.1016/j.ijms.2006.05.021, URL http://www.sciencedirect.com/science/article/pii/S1387380606002776, 2006.

Blitz, M. A., Heard, D. E., Pilling, M. J., Arnold, S. R., and Chipperfield, M. P.: Pressure and temperature-dependent quantum yields for the photodissociation of acetone between 279 and 327.5 nm, Geophys. Res. Lett., 31, doi:10.1029/2003GL018793, URL http://dx.doi.org/10.1029/2003GL018793, 2004.

Boffetta, P., Jourenkova, N., and Gustavsson, P.: Cancer risk from occupational and environmental exposure to polycyclic aromatic hydrocarbons, Cancer Causes & Control, 8, 444–472, doi:10.1023/A:1018465507029, URL http://dx.doi.org/10.1023/A:1018465507029, 1997.

Bon, D. M., Ulbrich, I. M., de Gouw, J. A., Warneke, C., Kuster, W. C., Alexander, M. L., Baker, A., Beyersdorf, A. J., Blake, D., Fall, R., Jimenez, J. L., Herndon, S. C., Huey, L. G., Knighton, W. B., Ortega, J., Springston, S., and Vargas, O.: Measurements of volatile organic compounds at a suburban ground site (T1) in Mexico City during the MILAGRO 2006 campaign: measurement comparison, emission ratios, and source attribution, Atmos. Chem. Phys., 11, 2399–2421, doi:10.5194/acp-11-2399-2011, URL http://www.atmos-chem-phys.net/11/2399/2011/, 2011.

Bonsang, B., Polle, C., and Lambert, G.: Evidence for marine production of isoprene, Geophysical Research Letters, 19, 1129–1132, doi:10.1029/92GL00083, URL http://dx.doi.org/10.1029/92GL00083, 1992.

Borbon, A., Gilman, J. B., Kuster, W. C., Grand, N., Chevaillier, S., Colomb, A., Dolgorouky, C., Gros, V., Lopez, M., Sarda-Esteve, R., Holloway, J., Stutz, J., Petetin, H., McKeen, S., Beekmann, M., Warneke, C., Parrish, D. D., and de Gouw, J. A.: Emission ratios of anthropogenic volatile organic compounds in northern mid-latitude megacities: Observations versus emission inventories in Los Angeles and Paris, J. Geophys. Res. - Atmos., 118, 2041–2057, doi:10.1002/jgrd.50059, URL http://dx.doi.org/10.1002/jgrd.50059, 2013.

Boström, C.-E., Gerde, P., Hanberg, A., Jernström, B., Johansson, C., Kyrklund, T., Rannug, A., Törnqvist, M., Victorin, K., and Westerholm, R.: Cancer Risk Assessment, Indicators, and Guidelines for Polycyclic Aromatic Hydrocarbons in the Ambient Air., Environmental Health Perspectives Supplements, 110, 451, URL http://search.ebscohost.com/login.aspx?direct=true&db=aph&AN=8602442&site=ehost-live&scope=site, 2002.

Broadgate, W. J., Liss, P. S., and Penkett, S. A.: Seasonal emissions of isoprene and other reactive hydrocarbon gases from the ocean, Geophysical Research Letters, 24, 2675–2678, doi:10.1029/97GL02736, URL http://dx.doi.org/10.1029/97GL02736, 1997.

Buhr, K., van Ruth, S., and Delahunty, C.: Analysis of volatile flavour compounds by Proton Transfer Reaction-Mass Spectrometry: fragmentation patterns and discrimination between isobaric and isomeric compounds, Int. J. Mass Spectrom., 221, 1 – 7, doi:http://dx.doi.org/10.1016/S1387-3806(02)00896-5, URL http://www.sciencedirect.com/science/article/pii/S1387380602008965, 2002.

Calvert, J. G. and Stockwell, W. R.: Acid generation in the troposphere by gas-phase chemistry, Environ. Sci. Technol., 17, 428A–443A, doi:10.1021/es00115a727, URL http://dx.doi.org/10.1021/es00115a727, 1983.

Cames, M. and Helmers, E.: Critical evaluation of the European diesel car boom - global comparison, environmental effects and various national strategies, Env. Sci. Eur., 25, 1–22, doi:10.1186/2190-4715-25-15, URL http://dx.doi.org/10.1186/2190-4715-25-15, 2013.

Chan, A. W. H., Kreisberg, N. M., Hohaus, T., Campuzano-Jost, P., Zhao, Y., Day, D. A., Kaser, L., Karl, T., Hansel, A., Teng, A. P., Ruehl, C. R., Sueper, D. T., Jayne, J. T., Worsnop, D. R., Jimenez, J. L., Hering, S. V., and Goldstein, A. H.: Speciated measurements of semivolatile and intermediate volatility organic compounds (S/IVOCs) in a pine forest during BEACHON-RoMBAS 2011, Atmos. Chem. Phys., 16, 1187–1205, doi:10.5194/acp-16-1187-2016, URL http://www.atmos-chem-phys.net/16/1187/2016/, 2016.

Charlson, R. J., Lovelock, J. E., Andreae, M. O., and Warren, S. G.: Oceanic phytoplankton, atmospheric sulphur, cloud albedo and climate, Nature, 326, 655–661, 1987.

Christian, T. J., Kleiss, B., Yokelson, R. J., Holzinger, R., Crutzen, P. J., Hao, W. M., Saharjo, B. H., and Ward, D. E.: Comprehensive laboratory measurements of biomass-burning emissions: 1. Emissions from Indonesian, African, and other fuels, J. Geophys. Res. - Atmos., 108, n/a–n/a, doi:10.1029/2003JD003704, URL http://dx.doi.org/10.1029/2003JD003704, 4719, 2003.

Cline, J. D. and Bates, T. S.: Dimethyl sulfide in the Equatorial Pacific Ocean: A natural source of sulfur to the atmosphere, Geophys. Res. Lett., 10, 949–952, doi:10.1029/GL010i010p00949, URL http://dx.doi.org/10.1029/GL010i010p00949, 1983.

Davison, B., Taipale, R., Langford, B., Misztal, P., Fares, S., Matteucci, G., Loreto, F., Cape, J. N., Rinne, J., and Hewitt, C. N.: Concentrations and fluxes of biogenic volatile organic compounds above a Mediterranean macchia ecosystem in western Italy, Biogeosciences, 6, 1655–1670, doi:10.5194/bg-6-1655-2009, URL http://www.biogeosciences.net/6/1655/2009/, 2009.

de Gouw, J., Warneke, C., Holzinger, R., Klüpfel, T., and Williams, J.: Inter-comparison between airborne measurements of methanol, acetonitrile and acetone using two differently configured PTR-MS instruments, Int. J. Mass Spectrom., 239, 129 – 137, doi:http://dx.doi.org/10.1016/j.ijms.2004.07.025, URL http://www.sciencedirect.com/science/article/pii/S1387380604003513, 2004.

de Gouw, J. A., Goldan, P. D., Warneke, C., Kuster, W. C., Roberts, J. M., Marchewka, M., Bertman, S. B., Pszenny, A. A. P., and Keene, W. C.: Validation of proton transfer reaction-mass spectrometry (PTR-MS) measurements of gas-phase organic compounds in the atmosphere during the New England Air Quality Study (NEAQS) in 2002, J. Geophys. Res. - Atmos., 108, doi:10.1029/2003JD003863, URL http://dx.doi.org/10.1029/2003JD003863, 4682, 2003.

de Gouw, J. A., Middlebrook, A. M., Warneke, C., Goldan, P. D., Kuster, W. C., Roberts, J. M., Fehsenfeld, F. C., Worsnop, D. R., Canagaratna, M. R., Pszenny, A. A. P., Keene, W. C., Marchewka, M., Bertman, S. B., and Bates, T. S.: Budget of organic carbon in a polluted atmosphere: Results from the New England Air Quality Study in 2002, J. Geophys. Res.-Atmos., 110, doi:10.1029/2004JD005623, URL http://dx.doi.org/10.1029/2004JD005623, d16305, 2005.

Dillon, T. J. and Crowley, J. N.: Direct detection of OH formation in the reactions of HO_2 with $CH_3C(O)O_2$ and other substituted peroxy radicals, Atmos. Chem. Phys., 8, 4877–4889, doi:10.5194/acp-8-4877-2008, URL http://www.atmos-chem-phys.net/8/4877/2008/, 2008.

Dixon, J. L., Beale, R., Sargeant, S. L., Tarran, G. A., and Nightingale, P. D.: Microbial acetone oxidation in coastal seawater, Frontiers in Microbiology, 5, doi:10.3389/fmicb.2014.00243, URL http://doi.org/10.3389/fmicb.2014.00243, 2014.

Doche, C., Dufour, G., Foret, G., Eremenko, M., Cuesta, J., Beekmann, M., and Kalabokas, P.: Summertime tropospheric-ozone variability over the Mediterranean basin observed with IASI, Atmos. Chem. Phys., 14, 10 589–10 600, doi:10.5194/acp-14-10589-2014, URL http://www.atmos-chem-phys.net/14/10589/2014/, 2014.

Dufour, G., Boone, C. D., Rinsland, C. P., and Bernath, P. F.: First space-borne measurements of methanol inside aged southern tropical to mid-latitude biomass burning plumes using the ACE-FTS instrument, Atmos. Chem. Phys., 6, 3463–3470, 2006.

Erickson, M. H., Gueneron, M., and Jobson, B. T.: Measuring long chain alkanes in diesel engine exhaust by thermal desorption PTR-MS, Atmos. Mech. Tech., 7, 225–239, doi:10.5194/amt-7-225-2014, URL http://www.atmos-meas-tech.net/7/225/2014/, 2014.

Fall, R. and Benson, A. A.: Leaf methanol - the simplest natural product from plants, Trends Plant Sci., 1, 296 – 301, doi:10.1016/S1360-1385(96)88175-0, URL http://www.sciencedirect.com/science/article/pii/S1360138596881750, 1996.

Feilberg, A., Liu, D., Adamsen, A. P. S., Hansen, M. J., and Jonassen, K. E. N.: Odorant Emissions from Intensive Pig Production Measured by Online Proton-Transfer-Reaction

Mass Spectrometry, Environ. Sci. Technol., 44, 5894–5900, doi:10.1021/es100483s, URL http://dx.doi.org/10.1021/es100483s, 2010.

Fernandes, M., Sicre, M.-A., Boireau, A., and Tronczynski, J.: Polyaromatic hydrocarbon (PAH) distributions in the Seine River and its estuary, Marine Pollution Bulletin, 34, 857 – 867, doi:http://dx.doi.org/10.1016/S0025-326X(97)00063-5, URL http://www.sciencedirect.com/science/article/pii/S0025326X97000635, 1997.

Finlayson-Pitts, B. J. and Pitts, J. J. N.: Chemistry of the Upper and Lower Atmosphere, Academic Press, 1 edn., 2000.

Fischer, E. V., Jacob, D. J., Millet, D. B., Yantosca, R. M., and Mao, J.: The role of the ocean in the global atmospheric budget of acetone, Geophys. Res. Lett., 39, doi:10.1029/2011GL050086, 2012.

Galbally, I. and Kirstine, W.: The Production of Methanol by Flowering Plants and the Global Cycle of Methanol, J. Atmos. Chem., 43, 195–229, doi:10.1023/A:1020684815474, URL http://dx.doi.org/10.1023/A%3A1020684815474, 2002.

Galbally, I. E., Lawson, S. J., Weeks, I. A., Bentley, S. T., Gillett, R. W., Meyer, M., and Goldstein, A. H.: Volatile organic compounds in marine air at Cape Grim, Australia, Envir. Chem., 4, 178–182, doi:10.1071/EN07024, URL http://www.publish.csiro.au/paper/EN07024, 2007.

Gerasopoulos, E., Kouvarakis, G., Vrekoussis, M. and. Kanakidou, M., and Mihalopoulos, N.: Ozone variability in the marine boundary layer of the eastern Mediterranean based on 7-year observations, J. Geophys. Res., 110, doi:10.1029/2005JD005991, 2005.

Goldan, P. D., Kuster, W. C., Fehsenfeld, F. C., and Montzka, S. A.: Hydrocarbon measurements in the southeastern United States: The Rural Oxidants in the Southern Environment (ROSE) Program 1990, J. Geophys. Res. - Atmos., 100, 25 945–25 963, doi:10.1029/95JD02607, URL http://dx.doi.org/10.1029/95JD02607, 1995.

Goldan, P. D., Kuster, W. C., Williams, E., Murphy, P. C., Fehsenfeld, F. C., and Meagher, J.: Nonmethane hydrocarbon and oxy hydrocarbon measurements during the 2002 New England Air Quality Study, J. Geophys. Res. Atmos., 109, doi:10.1029/2003JD004455, URL http://dx.doi.org/10.1029/2003JD004455, d21309, 2004.

Goldstein, A. H. and Schade, G. W.: Quantifying biogenic and anthropogenic contributions to acetone mixing ratios in a rural environment, Atmos. Environ., 34, 4997 – 5006, doi:10.1016/S1352-2310(00)00321-6, URL http://www.sciencedirect.com/science/article/pii/S1352231000003216, 2000.

Grazyna E. Orzechowska, G. E. and Paulson, S. E.: Photochemical Sources of Organic Acids. 1. Reaction of Ozone with Isoprene, Propene, and 2-Butenes under Dry and Humid Conditions Using SPME, J. Phys. Chem. A, 109, 5358–5365, doi:10.1021/jp050166s, URL http://dx.doi.org/10.1021/jp050166s, 2005.

Grosjean, D.: Organic acids in Southern California air: ambient concentrations, mobile source emissions, in situ formation and removal processes, Environ. Sci. Technol., 23, 1506–1514, doi:10.1021/es00070a009, URL http://dx.doi.org/10.1021/es00070a009, 1989.

Grosjean, D.: Formic and Acetic Acid: Emissions, Atmospheric Formation and Dry Deposition at two Southern California Locations, Atmos. Environ., 26A, 3279–3286, doi:10.1016/0960-1686(92)90343-J, URL http://www.sciencedirect.com/science/article/pii/096016869290343J, 1992.

Grosjean, D., Grosjean, E., and L., W. E.: Atmospheric chemistry of olefins: a product study of the ozone-alkene reaction with cyclohexane added to scavenge hydroxyl radical, Environ. Sci. Technol., 28, 186–196, doi:10.1021/es00050a026, URL http://dx.doi.org/10.1021/es00050a026, 1994.

Groß, C. B. M., Dillon, T. J., Schuster, G., Lelieveld, J., and Crowley, J. N.: Direct Kinetic Study of OH and O_3 Formation in the Reaction of $CH_3C(O)O_2$ with HO_2, J. Phys. Chem., 118, 974–985, doi:dx.doi.org/10.1021/jp412380z, 2014.

Gueneron, M., Erickson, M. H., VanderSchelden, G. S., and Jobson, B. T.: PTR-MS fragmentation patterns of gasoline hydrocarbons, Int. J. Mass. Spectrom., 379, 97 – 109, doi:http://dx.doi.org/10.1016/j.ijms.2015.01.001, URL http://www.sciencedirect.com/science/article/pii/S1387380615000196, 2015.

Hartmann, W. R., Andreae, M. O., and Helas, G.: Measurements of organic acids over central Germany, Atmos. Environ., 23, 1531 – 1533, doi:http://dx.doi.org/10.1016/0004-6981(89)90412-5, URL http://www.sciencedirect.com/science/article/pii/0004698189904125, 1989.

Hartmann, W. R., Santana, M., Hermoso, M., Andreae, M. O., and Sanhueza, E.: Diurnal cycles of formic and acetic acids in the northern part of the Guayana shield, Venezuela, J. Atmos. Chem., 13, 63–72, doi:10.1007/BF00048100, URL http://dx.doi.org/10.1007/BF00048100, 1991.

Heikes, B. G., Chang, W. N., Pilson, M. E. Q., Swift, E., Singh, H. B., Guenther, A., Jacob, D. J., Field, B. D., Fall, R., Riemer, D., and Br and, L.: Atmospheric methanol budget and ocean implication, Global Biogeochem. Cycles, 16, 2002.

Helmig, D., Klinger, L. F., Guenther, A., Vierling, L., Geron, C., and Zimmerman, P.: Biogenic volatile organic compound emissions (BVOCs) I. Identifications from three continental sites in the U.S., Chemosphere, 38, 2163 – 2187, doi:10.1016/S0045-6535(98)00425-1, URL http://www.sciencedirect.com/science/article/pii/S0045653598004251, 1999.

Hewitt, C. N., Hayward, S., and Tani, A.: The application of proton transfer reaction-mass spectrometry (PTR-MS) to the monitoring and analysis of volatile organic compounds in the atmosphere, J. Environ. Monit., 5, 1–7, doi:10.1039/B204712H, 2003.

Holloway, A. M. and Wayne, R. P.: Atmospheric Chemistry, RSC Publishing, 2010.

Holzinger, R., Warneke, C., Hansel, A., Jordan, A., Lindinger, W., Scharffe, D. H., Schade, G., and Crutzen, P. J.: Biomass burning as a source of formaldehyde, acetaldehyde, methanol, acetone, acetonitrile, and hydrogen cyanide, Geophysi. Res. Lett., 26, 1161–1164, doi:10.1029/1999GL900156, URL http://dx.doi.org/10.1029/1999GL900156, 1999.

Holzinger, R., Jordan, A., Hansel, A., and Lindinger, W.: Methanol measurements in the lower troposphere near Innsbruck (047°16'N; 011°24'E) , Austria, Atmos. Environ., 35, 2525 – 2532, doi:10.1016/S1352-2310(00)00430-1, URL http://www.sciencedirect.com/science/article/pii/S1352231000004301, 2001.

Holzinger, R., Williams, J., Salisbury, G., Klüpfel, T., de Reus, M., Traub, M., Crutzen, P. J., and Lelieveld, J.: Oxygenated compounds in aged biomass burning plumes over the Eastern Mediterranean: evidence for strong secondary production of methanol and acetone, Atmos. Chem. Phys., 5, 39–46, doi:10.5194/acp-5-39-2005, URL http://www.atmos-chem-phys.net/5/39/2005/, 2005.

IPCC report
Kahn Ribeiro, S., Kobayashi, S., Beuthe, M., Gasca, J., Greene, D., Lee, D. S., Muromachi, Y., Newton, P. J., Plotkin, S., Sperling, D., Wit, R., and Zhou, P. J.: Transport and its infrastructure. In Climate Change 2007: Mitigation, Tech. rep., URL http://www.ipcc.ch/pdf/assessment-report/ar4/wg3/ar4-wg3-chapter5.pdf, 2007.

Jacob, D. J.: Introduction to Atmospheric Chemistry, Princeton University Press, 1 edn., 1999.

Jacob, D. J., Field, B. D., Jin, E. M., Bey, I., Li, Q., Logan, J. A., Yantosca, R. M., and Singh, H. B.: Atmospheric budget of acetone, J. Geophys. Res. - Atmos., 107, ACH 5–1–ACH 5–17, doi:10.1029/2001JD000694, URL http://dx.doi.org/10.1029/2001JD000694, 2002.

Jacob, D. J., Field, B. D., Li, Q., Blake, D. R., de Gouw, J., Warneke, C., Hansel, A., Wisthaler, A., Singh, H. B., and Guenther, A.: Global budget of methanol: Constraints from atmospheric observations, J. Geophys. Res, 110, doi:10.1029/2004JD005172, URL http://dx.doi.org/10.1029/2004JD005172, 2005.

Jacobs, E. S.: Rapid Gas Chromatographic Determination of C1 to C10 Hydrocarbons in Automotive Exhaust Gas., Anal. Chem., 38, 43–48, doi:10.1021/ac60233a011, URL http://dx.doi.org/10.1021/ac60233a011, 1966.

Japan Automobile Manufacturer Association, I.: Motor Vehicle Statistics Japan, Tech. rep., 2012.

Jardine, K., Yañez Serrano, A., Arneth, A., Abrell, L., Jardine, A., Artaxo, P., Alves, E., Kesselmeier, J., Taylor, T., Saleska, S., et al.: Ecosystem-scale compensation points of formic and acetic acid in the central Amazon, Biogeosciences, 8, 3709–3720, doi:10.5194/bg-8-3709-2011, URL http://www.biogeosciences.net/8/3709/2011/, 2011.

Jobson, B. T., Alexander, M. L., Maupin, G. D., and Muntean, G. G.: On-line analysis of organic compounds in diesel exhaust using a proton transfer reaction mass spectrometer (PTR-MS), Int. J. Mass Spectrom., 245, 78–89, doi:10.1016/j.ijms.2005.05.009, URL http://www.sciencedirect.com/science/article/pii/S1387380605001703, 2005.

Jöckel, P., Tost, H., Pozzer, A., Kunze, M., Kirner, O., Brenninkmeijer, C. A. M., Brinkop, S., Cai, D. S., Dyroff, C., Eckstein, J., Frank, F., Garny, H., Gottschaldt, K.-D., Graf, P., Grewe, V., Kerkweg, A., Kern, B., Matthes, S., Mertens, M., Meul, S., Neumaier, M., Nützel, M., Oberländer-Hayn, S., Ruhnke, R., Runde, T., Sander, R., Scharffe, D., and Zahn, A.: Earth System Chemistry integrated Modelling (ESCiMo) with the Modular Earth Submodel System (MESSy) version 2.51, Geosci. Model Dev., 9, 1153–1200, doi:10.5194/gmd-9-1153-2016, URL http://www.geosci-model-dev.net/9/1153/2016/, 2016.

Jordan, A., Haidacher, S., Hanel, G., Hartungen, E., Herbig, J., Märk, L., Schottkowsky, R., Seehauser, H., Sulzer, P., and Märk, T.: An online ultra-high sensitivity Proton-transfer-reaction mass-spectrometer combined with switchable reagent ion capability (PTR + {SRI} - MS), Int. J. Mass spectrom., 286, 32 – 38, doi:10.1016/j.ijms.2009.06.006, URL http://www.sciencedirect.com/science/article/pii/S1387380609002036, 2009.

Kalabokas, P., Mihalopoulos, N., Ellul, R., Kleanthous, S., and Repapis, C.: An investigation of the meteorological and photochemical factors influencing the background rural and marine surface ozone levels in the Central and Eastern Mediterranean, Atmos. Environ., 42, 7894–7906, doi:10.1016/j.atmosenv.2008.07.009, 2008.

Kalabokas, P. D., Volz-Thomas, A., Brioude, J., Thouret, V., Cammas, J.-P., and Repapis, C. C.: Vertical ozone measurements in the troposphere over the Eastern Mediterranean and comparison with Central Europe, Atmos. Chem. Phys., 7, 3783–3790, doi:10.5194/acp-7-3783-2007, URL http://www.atmos-chem-phys.net/7/3783/2007/, 2007.

Kalabokas, P. D., Cammas, J.-P., Thouret, V., Volz-Thomas, A., Boulanger, D., and Repapis, C. C.: Examination of the atmospheric conditions associated with high and low summer ozone levels in the lower troposphere over the eastern Mediterranean, Atmos. Chem. Phys., 13, 10 339–10 352, doi:10.5194/acp-13-10339-2013, URL http://www.atmos-chem-phys.net/13/10339/2013/, 2013.

Karl, T. G., Christian, T. J., Yokelson, R. J., Artaxo, P., Hao, W. M., and Guenther, A.: The Tropical Forest and Fire Emissions Experiment: method evaluation of volatile organic compound emissions measured by PTR-MS, FTIR, and GC from tropical biomass burning, Atmos. Chem. Phys., 7, 5883–5897, doi:10.5194/acp-7-5883-2007, URL http://www.atmos-chem-phys.net/7/5883/2007/, 2007.

Kawamura, K., Ng, L. L., and Kaplan, I. R.: Determination of organic acids (C1-C10) in the atmosphere, motor exhausts, and engine oils, Environ. Sci. Technol., 19, 1082–1086, doi:10.1021/es00141a010, URL http://dx.doi.org/10.1021/es00141a010, 1985.

Keene, W. C. and Galloway, J. N.: Organic acidity of precipitation of North America, Atmos. Environ., 18, 2491–2497, 1984.

Keene, W. C. and Galloway, J. N.: The biogeochemical cycling of formic and acetic acids through the troposphere: an overview of current understanding, Tellus 40B, 40B, 322–334, doi:10.1111/j.1600-0889.1988.tb00106.x, URL http://dx.doi.org/10.1111/j.1600-0889.1988.tb00106.x, 1988.

Kesselmeier, J.: Exchange of Short-Chain Oxygenated Volatile Organic Compounds (VOCs) between Plants and the Atmosphere: A Compilation of Field and Laboratory Studies, J. Atmos. Chem., 39, 219–233, doi:10.1023/A:1010632302076, URL http://dx.doi.org/10.1023/A:1010632302076, 2001.

Kesselmeier, J. and Staudt, M.: Biogenic Volatile Organic Compounds (VOC): An Overview on Emission, Physiology and Ecology, J. Atmos. Chem., 33, 23–88, doi:10.1023/A:1006127516791, URL http://dx.doi.org/10.1023/A:1006127516791, 1999.

Kesselmeier, J., Schäfer, L., Ciccioli, P., Brancaleoni, E., Cecinato, A., Frattoni, M., Foster, P., Jacob, V., Denis, J., Fugit, J., Dutaur, L., and Torres, L.: Emission of monoterpenes and isoprene from a Mediterranean oak species Quercus ilex L. measured within the BEMA (Biogenic Emissions in the Mediterranean Area) project, Atmos. Environ., 30, 1841–1850, doi:10.1016/1352-2310(95)00376-2, URL http://www.sciencedirect.com/science/article/pii/1352231095003762, 1996.

Kesselmeier, J., Bode, K., Schäfer, L., Schebeske, G., Wolf, A., Brancaleoni, E., Cecinato, A., Ciccioli, P., Frattoni, M., Dutaur, L., Fugit, J. L., Simon, V., and Torres, L.: Simultaneous field measurements of terpene and isoprene emissions from two dominant Mediterranean oak species in relation to a North American species, Atmos. Environ., 32, 1947–1953, 1998.

Khalili, N. R., Scheff, P. A., and Holsen, T. M.: {PAH} source fingerprints for coke ovens, diesel and, gasoline engines, highway tunnels, and wood combustion emissions, Atmos. Environ., 29, 533 – 542, doi:10.1016/1352-2310(94)00275-P, URL http://www.sciencedirect.com/science/article/pii/135223109400275P, 1995.

Khan, M., Cooke, M., Utembe, S., Archibald, A., Maxwell, P., Morris, W., Xiao, P., Derwent, R., Jenkin, M., Percival, C., Walsh, R., Young, T., Simmonds, P., Nickless, G., O'Doherty, S., and Shallcross, D.: A study of global atmospheric budget and distribution of acetone using global atmospheric model STOCHEM-CRI, Atmos. Environ., 112, 269 – 277, doi:http://dx.doi.org/10.1016/j.atmosenv.2015.04.056, URL http://www.sciencedirect.com/science/article/pii/S1352231015300595, 2015.

Kiehl, J. T. and Trenberth, K. E.: Earth's annual global mean energy budget, B. Am. Meteorol. Soc., 78, 197–208, doi:10.1175/1520-0477(1997)078⟨0197:EAGMEB⟩2.0.CO;2, URL http://dx.doi.org/10.1175/1520-0477(1997)078<0197:EAGMEB>2.0.CO;2, 1997.

Kleanthous, S., Vrekoussis, M., Mihalopoulos, N., Kalabokas, P., and Lelieveld, J.: On the temporal and spatial variation of ozone in Cyprus, Sci. total Environ., 476-477, 677 – 687, doi:10.1016/j.scitotenv.2013.12.101, URL http://www.sciencedirect.com/science/article/pii/S0048969713015842, 2014.

König, G., Brunda, M., Puxbaum, H., Hewitt, C. N., Duckham, S. C., and Rudolph, J.: Relative contribution of oxygenated hydrocarbons to the total biogenic {VOC} emissions of selected mid-European agricultural and natural plant species, Atmos. Environ., 29, 861 – 874, doi:10.1016/1352-2310(95)00026-U, URL http://www.sciencedirect.com/science/article/pii/135223109500026U, 1995.

Kourtidis, K., Zerefos, C., Rapsomanikis, S., Simeonov, V., Balis, D., Perros, P. E., Thompson, A. M., Witte, J., Calpini, B., Sharobiem, W. M., Papayannis, A., Mihalopoulos, N., and Drakou, R.: Regional levels of ozone in the troposphere over eastern Mediterranean, J. Geophys. Res., 107, doi:10.1029/2000JD000140, 2002.

Kouvarakis, G., Vrekoussis, M., Mihalopoulos, N., Kourtidis, K., Rappenglueck, B., Gerasopoulos, E., and Zerefos, C.: Spatial and temporal variability of tropospheric ozone (O3) in the boundary layer above the Aegean Sea (eastern Mediterranean), J. Geophys. Res., 107, doi:10.1029/2000JD000081, 2002.

Lawrence, M. G., Jöckel, P., and von Kuhlmann, R.: What does the global mean OH concentration tell us?, Atmospheric Chemistry and Physics, 1, 37–49, doi:10.5194/acp-1-37-2001, URL http://www.atmos-chem-phys.net/1/37/2001/, 2001.

Legreid, G., Balzani Lööv, J., Staehelin, J., Hueglin, C., Hill, M., Buchmann, B., Prevot, A. S., and Reimann, S.: Oxygenated volatile organic compounds (OVOCs) at an urban background site in Zürich (Europe): Seasonal variation and source allocation, Atmos.Environ., 41, 8409 – 8423, doi:http://dx.doi.org/10.1016/j.atmosenv.2007.07.026, URL http://www.sciencedirect.com/science/article/pii/S135223100700619X, 2007.

Lelieveld, J., Berresheim, H., Borrmann, S., Crutzen, P. J., Dentener, F. J., Fischer, H., Feichter, J., Flatau, P. J., Heland, J., Holzinger, R., Korrmann, R., Lawrence, M. G., Levin, Z., Markowicz, K. M., Mihalopoulos, N., Minikin, A., Ramanathan, V., de Reus, M., Roelofs, G. J., Scheeren, H. A., Sciare, J., Schlager, H., Schultz, M., Siegmund, P., Steil, B., Stephanou, E. G., Stier, P., Traub, M., Warneke, C., Williams, J., and Ziereis, H.: Global Air Pollution Crossroads over the Mediterranean, Science, 298, 794–799, doi:10.1126/science.1075457, 2002.

Lelieveld, J., Evans, J. S., Fnais, M., Giannadaki, D., and Pozzer, A.: The contribution of outdoor air pollution sources to premature mortality on a global scale, Nature, 525, 367–371, doi:10.1038/nature15371, URL http://dx.doi.org/10.1038/nature15371, 2015.

Lewis, A. C., Hopkins, J. R., Carpenter, L. J., Stanton, J., Read, K. A., and Pilling, M. J.: Sources and sinks of acetone, methanol, and acetaldehyde in North Atlantic marine air,

Atmos. Chem. Phys., 5, 1963–1974, doi:10.5194/acp-5-1963-2005, URL http://www.atmos-chem-phys.net/5/1963/2005/, 2005.

Li, J., Parchatka, U., Königstedt, R., and Fischer, H.: Real-time measurements of atmospheric CO using a continuous-wave room temperature quantum cascade laser based spectrometer, Opt. Express, 20, 7590–7601, doi:10.1364/OE.20.007590, URL http://www.opticsexpress.org/abstract.cfm?URI=oe-20-7-7590, 2012.

Liakakou, E., Vrekoussis, M., Bonsang, B., Donousis, C., Kanakidou, M., and Mihalopoulos, N.: Isoprene above the Eastern Mediterranean: Seasonal variation and contribution to the oxidation capacity of the atmosphere, Atmos. Environ., 41, 1002–1010, doi:10.1016/j.atmosenv.2006.09.034, 2007.

Louie, P. K. K., Ho, J. W. K., Tsang, R. C. W., Blake, D. R., Lau, A. K. H., Yu, J. Z., Yuan, Z., Wang, X., Shao, M., and Zhong, L.: VOCs and OVOCs distribution and control policy implications in Pearl River Delta region, China, Atmos. Environ., 76, 125 – 135, doi:10.1016/j.atmosenv.2012.08.058, URL http://www.sciencedirect.com/science/article/pii/S1352231012008436, 2013.

MacDonald, R. C. and Fall, R.: Detection of substantial emissions of methanol from plants to the atmosphere, Atmos.Environ. A-Gen., 27, 1709 – 1713, doi:10.1016/0960-1686(93)90233-O, URL http://www.sciencedirect.com/science/article/pii/0960168693902330, 1993.

Madronich, S. and Calvert, J. G.: Permutation reactions of organic peroxy radicals in the troposphere, J. Geophys. Res. - Atmos., 95, 5697–5715, doi:10.1029/JD095iD05p05697, URL http://dx.doi.org/10.1029/JD095iD05p05697, 1990.

Marandino, C. A., De Bruyn, W. J., Miller, S. D., Prather, M. J., and Saltzman, E. S.: Oceanic uptake and the global atmospheric acetone budget, Geophys. Res. Lett., 32, 2005.

McEwen, D. J.: Automobile Exhaust Hydrocarbon Analysis by Gas Chromatography., Anal. Chem., 38, 1047–1053, doi:10.1021/ac60240a023, URL http://dx.doi.org/10.1021/ac60240a023, 1966.

McKenzie, L. M., Hao, W. M., Richards, G. N., and Ward, D. E.: Quantification of major components emitted from smoldering combustion of wood, Atmos. Environ., 28, 3285 – 3292, doi:10.1016/1352-2310(94)00158-H, URL http://www.sciencedirect.com/science/article/pii/135223109400158H, 1994.

Mesarchaki, E., Yassaa, N., D., H., Lutterbeck, H. E., Zindler, C., and Williams, J.: A novel method for the measurement of VOCs in seawater using needle trap devices and GC-MS, Mar. Chem., 149, 1–8, doi:10.1016/j.marchem.2013.12.001, 2014.

Millet, D. B., Jacob, D. J., Turquety, S., Hudman, R. C., Wu, S., Fried, A., Walega, J., Heikes, B. G., Blake, D. R., Singh, H. B., Anderson, B. E., and Clarke, A. D.: Formaldehyde distribution over North America: Implications for satellite retrievals of

formaldehyde columns and isoprene emission, J. Geophys. Res. - Atmos., 111, doi:10.1029/2005JD006853, URL http://dx.doi.org/10.1029/2005JD006853, 2006.

Millet, D. B., Jacob, D. J., Custer, T. G., de Gouw, J. A., Goldstein, A. H., Karl, T., Singh, H. B., Sive, B. C., Talbot, R. W., Warneke, C., and Williams, J.: New constraints on terrestrial and oceanic sources of atmospheric methanol, Atmos. Chem. Phys., 8, 6887–6905, doi:10.5194/acp-8-6887-2008, URL http://www.atmos-chem-phys.net/8/6887/2008/, 2008.

Mugica, V., Torres, M., Salinas, E., Gutierrez, M., and García, R.: Polycyclic aromatic hydrocarbons in the urban atmosphere of Mexico City, doi:10.5772/10044, URL http://www.intechopen.com/books/air-pollution/polycyclic-aromatic-hydrocarbons-in-the-urban-atmosphere-of-mexico-city, 2010.

Müller, J.-F. and Brasseur, G.: Sources of upper tropospheric HO X : A three-dimensional study, J. Geophys. Res.-Atmos., 104, 1705–1715, doi:10.1029/1998JD100005, URL http://dx.doi.org/10.1029/1998JD100005, 1999.

Müller, M., Mikoviny, T., Jud, W., D'Anna, B., and Wisthaler, A.: A new software tool for the analysis of high resolution PTR-TOF mass spectra, Chemometrics Intell. Lab. Sys., 127, 158 – 165, doi:10.1016/j.chemolab.2013.06.011, URL http://www.sciencedirect.com/science/article/pii/S0169743913001275, 2013.

Nielsen, T., Feilberg, A., and Binderup, M.-L.: The variation of street air levels of PAH and other mutagenic PAC in relation to regulations of traffic emissions and the impact of atmospheric processes, Environ. Sci. and Pollut. Res., 6, 133–137, doi:10.1007/BF02987613, URL http://dx.doi.org/10.1007/BF02987613, 1999.

Niki, H., Maker, P. D., Savage, C. M., and Breitenbach, L. P.: An FTIR study of mechanisms for the HO radical initiated oxidation of C_2H_4 in the presence of NO: detection of glycolaldehyde, Chem. Phys. Lett., 80, doi:10.1016/0009-2614(81)85065-8, URL http://www.sciencedirect.com/science/article/pii/0009261481850658, 1981.

Nisbet, I. C. T. and LaGoy, P. K.: Toxic equivalency factors (TEFs) for polycyclic aromatic hydrocarbons (PAHs), Regulatory Toxicology and Pharmacology, 16, 290 – 300, doi:http://dx.doi.org/10.1016/0273-2300(92)90009-X, URL http://www.sciencedirect.com/science/article/pii/027323009290009X, 1992.

Northway, M. J .and De Gouw, J. A., Fahey, D. W., Gao, R. S., Warneke, C., Roberts, J. M., and Flocke, F.: Evaluation of the role of heterogeneous oxidation of alkenes in the detection of atmospheric acetaldehyde, Atmos. Environ., 38, 6017–6028, doi:10.1016/j.atmosenv.2004.06.039, URL http://www.sciencedirect.com/science/article/pii/S1352231004006429, 2004.

Palmer, P. I. and Shaw, S. L.: Quantifying global marine isoprene fluxes using MODIS chlorophyll observations, Geophysical Research Letters, 32, doi:10.1029/2005GL022592, URL http://dx.doi.org/10.1029/2005GL022592, 2005.

Paulot, F., Wunch, D., Crounse, J. D., Toon, G. C., Millet, D. B., DeCarlo, P. F., Vigouroux, C., Deutscher, N. M., GonzÃ¡lez Abad, G., Notholt, J., Warneke, T., Hannigan, J. W., Warneke, C., de Gouw, J. A., Dunlea, E. J., De MaziÃ¨re, M., Griffith, D. W. T., Bernath, P., Jimenez, J. L., and Wennberg, P. O.: Importance of secondary sources in the atmospheric budgets of formic and acetic acids, Atmos. Chem. Phys., 11, 1989–2013, doi:10.5194/acp-11-1989-2011, URL `www.atmos-chem-phys.net/11/1989/2011/`, 2011.

Paulson, S. E. and Seinfeld, J. H.: Development and Evaluation of a Photooxidation Mechanism for Isoprene, J. Geophys. Res., 97, 20, 703–20,715, doi:10.1029/92JD01914, URL `http://dx.doi.org/10.1029/92JD01914`, 1992.

Phillips, G. J., Pouvesle, N., Thieser, J., Schuster, G., Axinte, R., Fischer, H., Williams, J., Lelieveld, J., and Crowley, J. N.: Peroxyacetyl nitrate (PAN) and peroxyacetic acid (PAA) measurements by iodide chemical ionisation mass spectrometry: first analysis of results in the boreal forest and implications for the measurement of PAN fluxes, Atmospheric Chemistry and Physics, 13, 1129–1139, doi:10.5194/acp-13-1129-2013, URL `http://www.atmos-chem-phys.net/13/1129/2013/`, 2013.

Piccot, S. D., Watson, J. J., and Jones, J. W.: A global inventory of volatile organic compound emissions from anthropogenic sources, J. Geophys. Res. - Atmos., 97, 9897–9912, doi:10.1029/92JD00682, URL `http://dx.doi.org/10.1029/92JD00682`, 1992.

Pozzer, A., Pollmann, J., Taraborrelli, D., Jöckel, P., Helmig, D., Tans, P., Hueber, J., and Lelieveld, J.: Observed and simulated global distribution and budget of atmospheric C_2-C_5 alkanes, Atmos. Chem. Phys., 10, 4403–4422, doi:10.5194/acp-10-4403-2010, URL `http://www.atmos-chem-phys.net/10/4403/2010/`, 2010.

Pozzoli, L., Gilardoni, S., Perrone, M. G., de Gennaro, G., de Rienzo, M., and Vione, D.: Polycyclic Aromatic Hydrocarbons in the Atmosphere: Monitoring, Sources, Sinks and Fate. II: Monitoring and Sources, Ann. Chim., 94, 17–33, doi:10.1002/adic.200490002, URL `http://dx.doi.org/10.1002/adic.200490002`, 2004.

Puxbaum, H., Rosenberg, C., Gregori, M., Lanzerstorfer, C., Ober, E., and Winiwarter, W.: Atmospheric concentrations of formic and acetic acid and related compounds in eastern and northern Austria, Atmos. Environ., 22, 2841–2850, doi:http://dx.doi.org/10.1016/0004-6981(88)90450-7, URL `http://www.sciencedirect.com/science/article/pii/0004698188904507`, 1988.

Ramdahl, T., Alfheim, I., and Björseth, A.: Mobile Source Emissions Including Policyclic Organic Species, chap. PAH Emission from Various Sources and their Evolution Over the Last Decades, pp. 277–297, Springer Netherlands, Dordrecht, doi:10.1007/978-94-009-7197-4_22, URL `http://dx.doi.org/10.1007/978-94-009-7197-4_22`, 1983.

Read, K. A., Carpenter, L. J., Arnold, S. R., Beale, R., Nightingale, P. D., Hopkins, J. R., Lewis, A. C., Lee, J. D., Mendes, L., and Pickering, S. J.: Multiannual Observations

of Acetone, Methanol, and Acetaldehyde in Remote Tropical Atlantic Air: Implications for Atmospheric OVOC Budgets and Oxidative Capacity, Environ. Sci. Technol., 46, 11 028–11 039, doi:10.1021/es302082p, URL http://dx.doi.org/10.1021/es302082p, 2012.

Riemer, D., Pos, W., Milne, P., Farmer, C., Zika, R., Apel, E., Olszyna, K., Kliendienst, T., Lonneman, W., Bertman, S., Shepson, P., and Starn, T.: Observations of nonmethane hydrocarbons and oxygenated volatile organic compounds at a rural site in the southeastern United States, J. Geophys. Res.-Atmos., 103, 28 111–28 128, doi:10.1029/98JD02677, URL http://dx.doi.org/10.1029/98JD02677, 1998.

Rogers, T. M., Grimsrud, E. P., Herndon, S. C., Jayne, J. T., Kolb, C. E., Allwine, E., Westberg, H., Lamb, B. K., Zavala, M., Molina, L. T., Molina, M. J., and Knighton, W. B.: On-road measurements of volatile organic compounds in the Mexico City metropolitan area using proton transfer reaction mass spectrometry, Int. J. Mass Spectrom., 252, 26 – 37, doi:http://dx.doi.org/10.1016/j.ijms.2006.01.027, URL http://www.sciencedirect.com/science/article/pii/S1387380606000583, 2006.

Salisbury, G., Williams, J., Holzinger, R., Gros, V., Mihalopoulos, N., Vrekoussis, M., Sarda-Estève, R., Berresheim, H., von Kuhlmann, R., Lawrence, M., and Lelieveld, J.: Ground-based PTR-MS measurements of reactive organic compounds during the MINOS campaign in Crete,July-August 2001, Atmos. Chem. Phys., 3, 925–940, doi:10.5194/acp-3-925-2003, URL http://www.atmos-chem-phys.net/3/925/2003/, 2003.

Sander, R., Baumgaertner, A., Gromov, S., Harder, H., Jöckel, P., Kerkweg, A., Kubistin, D., Regelin, E., Riede, H., Sandu, A., Taraborrelli, D., Tost, H., and Xie, Z.-Q.: The atmospheric chemistry box model CAABA/MECCA-3.0, Geoscientific Model Development, 4, 373–380, doi:10.5194/gmd-4-373-2011, URL http://www.geosci-model-dev.net/4/373/2011/, 2011.

Sanhueza, E. and Andreae, M. O.: Emission of formic and acetic acids from tropical Savanna soils, Geophys. Res. Lett., 18, 1707–1710, doi:10.1029/91GL01565, URL http://dx.doi.org/10.1029/91GL01565, 1991.

Schade, G. W. and Goldstein, A. H.: Seasonal measurements of acetone and methanol: Abundances and implications for atmospheric budgets, Global Biogeochem. Cy., 20, n/a–n/a, doi:10.1029/2005GB002566, URL http://dx.doi.org/10.1029/2005GB002566, gB1011, 2006.

Schauer, J. J., Kleeman, M. J., Cass, G. R., and Simoneit, B. R. T.: Measurement of Emissions from Air Pollution Sources. 2. C1 through C30 Organic Compounds from Medium Duty Diesel Trucks, Environ. Sci. Technol., 33, 1578–1587, doi:10.1021/es980081n, URL http://dx.doi.org/10.1021/es980081n, 1999.

Shaw, S. L., Mitloehner, F. M., Jackson, W., DePeters, E. J., Fadel, J. G., Robinson, P. H., Holzinger, R., , and Goldstein, A. H.: Volatile Organic Compound Emissions from Dairy Cows and Their Waste as Measured by Proton-Transfer-Reaction Mass Spectrometry,

Environ. Sci. Technol., 41, 1310–1316, doi:10.1021/es061475e, URL http://dx.doi.org/10.1021/es061475e, 2007.

Shen, H., Huang, Y., Wang, R., Zhu, D., Li, W., Shen, G., Wang, B., Zhang, Y., Chen, Y., Lu, Y., Chen, H., Li, T., Sun, K., Li, B., Liu, W., Liu, J., and Tao, S.: Global Atmospheric Emissions of Polycyclic Aromatic Hydrocarbons from 1960 to 2008 and Future Predictions, Environ. Sci. TEchnol., 47, 6415–6424, doi:10.1021/es400857z, URL http://dx.doi.org/10.1021/es400857z, 2013.

Siegl, W. O., Hammerle, R. H., Herrmann, H. M., Wenclawiak, B. W., and Luers-Jongen, B.: Organic emissions profile for a light-duty diesel vehicle, Atmos. environ., 33, 797–805, doi:10.1016/S1352-2310(98)00209-X, URL http://www.sciencedirect.com/science/article/pii/S135223109800209X, 1999.

Sigsby, J. E., Tejada, S., Ray, W., Lang, J. M., and Duncan, J. W.: Volatile organic compound emissions from 46 in-use passenger cars, Environ. Sci. Technol., 21, 466–475, doi:10.1021/es00159a007, URL http://dx.doi.org/10.1021/es00159a007, 1987.

Singh, H., Chen, Y., Tabazadeh, A., Fukui, Y., Bey, I., Yantosca, R., Jacob, D., Arnold, F., Wohlfrom, K., Atlas, E., Flocke, F., Blake, D., Blake, N., Heikes, B., Snow, J., Talbot, R., Gregory, G., Sachse, G., Vay, S., and Kondo, Y.: Distribution and fate of selected oxygenated organic species in the troposphere and lower stratosphere over the Atlantic, J. Geophys. Res.-Atmos., 105, 3795–3805, doi:10.1029/1999JD900779, URL http://dx.doi.org/10.1029/1999JD900779, 2000.

Singh, H., Chen, Y., Staudt, A., Jacob, D., Blake, D., Heikes, B., and Snow, J.: Evidence from the Pacific troposphere for large global sources of oxygenated organic compounds, Nature, 410, 1078–1081, doi:10.1038/35074067, URL http://dx.doi.org/10.1038/35074067, 2001.

Singh, H. B. and Hanst, P. L.: Peroxyacetyl nitrate (PAN) in the unpolluted atmosphere: An important reservoir for nitrogen oxides, Geophys. Res. Lett., 8, 941–944, doi:10.1029/GL008i008p00941, URL http://dx.doi.org/10.1029/GL008i008p00941, 1981.

Singh, H. B., O'Hara, D., Herlth, D., Sachse, W., Blake, D. R., Bradshaw, J. D., Kanakidou, M., and Crutzen, P. J.: Acetone in the atmosphere: Distribution, sources, and sinks, J. Geophys. Res., 99, 1805–1819, doi:10.1029/93JD00764, URL http://dx.doi.org/10.1029/93JD00764, 1994.

Singh, H. B., Kanakidou, M., Crutzen, P. J., and Jacob, D. J.: High concentrations and photochemical fate of oxygenated hydrocarbons in the global troposphere, Nature, 378, 50–54, doi:10.1038/378050a0, URL http://dx.doi.org/10.1038/378050a0, 1995.

Singh, H. B., Salas, L. J., Chatfield, R. B., Czech, E., Fried, A., Walega, J., Evans, M. J., Field, B. D., Jacob, D. J., Blake, D., Heikes, B., Talbot, R., Sachse, G., Crawford, J. H., Avery, M. A., Sandholm, S., and Fuelberg, H.: Analysis of the atmospheric distribution, sources, and sinks of oxygenated volatile organic chemicals based on measurements over

the Pacific during TRACE-P, J. Geophys. Res.-Atmos., 109, doi:10.1029/2003JD003883, URL http://dx.doi.org/10.1029/2003JD003883, 2004.

Sinha, V., Williams, J., Meyerhöfer, M., Riebesell, U., Paulino, A. I., and Larsen, A.: Air-sea fluxes of methanol, acetone, acetaldehyde, isoprene and DMS from a Norwegian fjord following a phytoplankton bloom in a mesocosm experiment, Atmos. Chem. Phys., 7, 739–755, doi:10.5194/acp-7-739-2007, URL http://www.atmos-chem-phys.net/7/739/2007/, 2007.

Smith, D., Diskin, A. M., Ji, Y., and Spanel, P.: Concurrent use of H_3O^+, NO^+, and O_2^+ precursor ions for the detection and quantification of diverse trace gases in the presence of air and breath by selected ion-flow tube mass spectrometry, Int. J. Mass Spectrom., 209, 81–97, doi:10.1016/S1387-3806(01)00478-X, URL http://www.sciencedirect.com/science/article/pii/S138738060100478X, 2001.

Smith, D., Cheng, P., and Spanel, P.: Analysis of petrol and diesel vapour and vehicle engine exhaust gases using selected ion flow tube mass spectrometry, Rapid Commun. Mass Spectrom., 16, 1124–1134, doi:10.1002/rcm.691, URL http://dx.doi.org/10.1002/rcm.691, 2002.

Smith, D., Spanel, P., Dabill, D., Cocker, J., and Rajan, B.: On-line analysis of diesel engine exhaust gases by selected ion flow tube mass spectrometry, Rapid Commun. Mass Spectrom., 18, 2830–2838, doi:10.1002/rcm.1702, URL http://dx.doi.org/10.1002/rcm.1702, 2004.

Spanel, P. and Smith, D.: SIFT studies of the reactions of H_3O^+, NO^+, and O_2^+ with a series of alcohols, Int. J. Mass Spectrom. Ion Processes, 167-168, 375 – 388, doi:10.1016/S0168-1176(97)00085-2, URL http://www.sciencedirect.com/science/article/pii/S0168117697000852, 1997.

Spanel, P. and Smith, D.: SIFT studies of the reactions of H_3O^+, NO^+, and O_2^+ with a series of volatile carboxylic acids and esters, Int. J. Mass Spectrom. Ion Processes, 172, 137–147, doi:10.1016/S0168-1176(97)00246-2, URL http://www.sciencedirect.com/science/article/pii/S0168117697002462, 1998a.

Spanel, P. and Smith, D.: Selected ion flow tube studies of the reactions of H_3O^+, NO^+, and O_2^+ with several aromatic and aliphatic hydrocarbons, Int. J. Mass spectrom., 181, 1–10, doi:10.1016/S1387-3806(98)14114-3, URL http://www.sciencedirect.com/science/article/pii/S1387380698141143, 1998b.

Spanel, P., Jib, Y., and Smith, D.: SIFT studies of the reactions of H_3O^+, NO^+, and O_2^+ with a series of aldehydes and ketones, Int. J. Mass Spectrom. Ion Processes, 165-166, 25–37, doi:10.1016/S0168-1176(97)00166-3, URL http://www.sciencedirect.com/science/article/pii/S0168117697001663, 1997.

Spanel, P., Diskin, A., Wang, T., and Smith, D.: A SIFT study of the reactions of H_3O^+, NO^+, and O_2^+ with hydrogen peroxide and peroxyacetic acid, Int. J. Mass Spectrom.,

228, 269–283, doi:10.1016/S1387-3806(03)00214-8, URL http://www.sciencedirect.com/science/article/pii/S1387380603002148, 2003.

Spivakovsky, C. M., Logan, J. A., Montzka, S. A., Balkanski, Y. J., Foreman-Fowler, M., Jones, D. B. A., Horowitz, L. W., Fusco, A. C., Brenninkmeijer, C. A. M., Prather, M. J., Wofsy, S. C., and McElroy, M. B.: Three-dimensional climatological distribution of tropospheric OH: Update and evaluation, J. Gephys. Res.: Atmos., 105, 8931–8980, doi:10.1029/1999JD901006, URL http://dx.doi.org/10.1029/1999JD901006, 2000.

Staudt, M., Bertin, N., Hansen, U., Seufert, G., Cicciolij, P., Foster, P., Frenzel, B., and Fugit, J.-L.: Seasonal and diurnal patterns of monoterpene emissions from Pinus pinea (L.) under field conditions, Atmos. Environ., 31, 145–156, 1997.

Stohl, A., Eckhardt, S., Forster, C., James, P., Spichtinger, N., and Seibert, P.: A replacement for simple back trajectory calculations in the interpretation of atmospheric trace substance measurements, Atmos. Environ., 36, 4635 – 4648, doi:10.1016/S1352-2310(02)00416-8, URL http://www.sciencedirect.com/science/article/pii/S1352231002004168, 2002.

Stohl, A., Forster, C., Frank, A., Seibert, P., and Wotawa, G.: Technical note: The Lagrangian particle dispersion model FLEXPART version 6.2, Atmos. Chem. Phys., 5, 2461–2474, doi:10.5194/acp-5-2461-2005, URL http://www.atmos-chem-phys.net/5/2461/2005/, 2005.

Stohl, A., Berg, T., Burkhart, J. F., FjÇ$\frac{1}{2}$raa, A. M., Forster, C., Herber, A., Hov, Ø., Lunder, C., McMillan, W. W., Oltmans, S., Shiobara, M., Simpson, D., Solberg, S., Stebel, K., Ström, J., Tørseth, K., Treffeisen, R., Virkkunen, K., and Yttri, K. E.: Arctic smoke - record high air pollution levels in the European Arctic due to agricultural fires in Eastern Europe in spring 2006, Atmos. Chem. Phys., 7, 511–534, doi:10.5194/acp-7-511-2007, URL http://www.atmos-chem-phys.net/7/511/2007/, 2007.

Stull, R. B.: An Introduction to Boundary Layer Meteorology, Kluwer Academic Publishers, 1988.

Su, T. and Bowers, M. T.: Ion-Polar molecule collisions: the effect of ion size on ion-polar molecule rate constants; the parameterization of the average-dipole-orientation theory, Int. J. Mass Spectrom. Ion Phys., 12, 347–356, doi:10.1016/0020-7381(73)80104-4, URL http://www.sciencedirect.com/science/article/pii/0020738173801044, 1973.

Su, T. and Chesnavich, W. J.: Parametrization of the ion-polar molecule collision rate constant by trajectory calculations, J. Chem. Phys., 76, 5183–5185, doi:10.1063/1.442828, URL http://scitation.aip.org/content/aip/journal/jcp/76/10/10.1063/1.442828, 1982.

Taddei, S., Toscano, P., Gioli, B., Matese, A., Miglietta, F., Vaccari, F. P., Zaldei, A., Custer, T., and Williams, J.: Carbon Dioxide and Acetone Air Sea Fluxes over the Southern Atlantic, Environmental Science Technology, 43, 5218–5222, doi:10.1021/es8032617, URL http://dx.doi.org/10.1021/es8032617, 2009.

Takada, H., Onda, T., and Ogura, N.: Determination of polycyclic aromatic hydrocarbons in urban street dusts and their source materials by capillary gas chromatography, Environ. Sci. Technol., 24, 1179–1186, doi:10.1021/es00078a005, URL http://dx.doi.org/10.1021/es00078a005, 1990.

Talbot, R. W., Beecher, K. M., Harriss, R. C., and Cofer, W. R.: Atmospheric geochemistry of formic and acetic acids at a mid-latitude temperate site, J. Geophys. Res. - Atmos., 93, 1638–1652, doi:10.1029/JD093iD02p01638, URL http://dx.doi.org/10.1029/JD093iD02p01638, 1988.

Tie, X., Guenther, A., and Holland, E.: Biogenic methanol and its impacts on tropospheric oxidants, Geophys. Res. Lett., 30, 2003.

Tkacik, D. S., Presto, A. A., Donahue, N. M., and Robinson, A. L.: Secondary Organic Aerosol Formation from Intermediate-Volatility Organic Compounds: Cyclic, Linear, and Branched Alkanes, Environ. Sci. Technol., 46, 8773–8781, doi:10.1021/es301112c, URL http://dx.doi.org/10.1021/es301112c, 2012.

Turulski, J. and Niedzielski, J.: The classical Langevin rate constant for ion/molecule capture: when, if at all, is it constant?, Int. J. Mass. Spectrom. Ion Processes, 139, 155 – 162, doi:http://dx.doi.org/10.1016/0168-1176(94)90030-2, URL http://www.sciencedirect.com/science/article/pii/0168117694900302, 1994.

Tyndall, G. S., Cox, R. A., Granier, C., Lesclaux, R., Moortgat, G. K., Pilling, M. J., Ravishankara, A. R., and Wallington, T. J.: Atmospheric chemistry of small organic peroxy radicals, J. Geophys. Res. - Atmos., 106, 12 157–12 182, 2001.

Tyrlis, E., Tymvios, F. S., Giannakopoulos, C., and Lelieveld, J.: The role of blocking in the summer 2014 collapse of Etesians over the eastern Mediterranean, American Geophysical Union, doi:10.1002/2015JD023543, 2015.

Venkataraman, C. and Friedlander, S. K.: Size Distributions of Polycyclic Aromatic Hydrocarbons and Elemental Carbon. 2. Ambient Measurements and Effects of Atmospheric Processes, Environ. Sci. Technol., 28, 563–572, doi:10.1021/es00053a006, URL http://dx.doi.org/10.1021/es00053a006, 1994.

Vione, D., Barra, S., de Gennaro, G., de Rienzo, M., Gilardoni, S., Perrone, M. G., and Pozzoli, L.: Polycyclic Aromatic Hydrocarbons in the Atmosphere: Monitoring, Sources, Sinks and Fate. II: Sinks and Fate, Ann. Chim., 94, 257–268, doi:10.1002/adic.200490031, URL http://dx.doi.org/10.1002/adic.200490031, 2004.

Warneck, P.: Chemistry of the Natural Atmosphere, Academic Press, 2 edn., 2000.

Warneck, P. and Williams, J.: The Atmospheric Chemist's Companion, Springer, 2012.

Warneke, C., Karl, T., Judmaier, H., Hansel, A., Jordan, A., Lindinger, W., and Crutzen, P. J.: Acetone, methanol, and other partially oxidized volatile organic emissions from dead plant matter by abiological processes: Significance for atmospheric HOx chemistry,

Global Biogeochem. Cy., 13, 9–17, doi:10.1029/98GB02428, URL http://dx.doi.org/10.1029/98GB02428, 1999.

Warneke, C., Van der Veen, C., Luxembourg, S., De Gouw, J. A., and Kok, A.: Measurements of benzene and toluene in ambient air using proton-transfer-reaction mass spectrometry: calibration, humidity dependence, and field intercomparison, Int. J. Mass Spectrom., 207, 167–182, doi:10.1016/S1387-3806(01)00366-9, URL http://www.sciencedirect.com/science/article/pii/S1387380601003669, 2001.

Wei, W., Wang, S., Chatani, S., Klimont, Z., Cofala, J., and Hao, J.: Emission and speciation of non-methane volatile organic compounds from anthropogenic sources in China, Atmos. Environ., 42, 4976 – 4988, doi:10.1016/j.atmosenv.2008.02.044, URL http://www.sciencedirect.com/science/article/pii/S135223100800160X, 2008.

Wennberg, P. O., Hanisco, T. F., Jaeglé, L., Jacob, D. J., Hintsa, E. J., Lanzendorf, E. J., Anderson, J. G., Gao, R.-S., Keim, E. R., Donnelly, S. G., Negro, L. A. D., Fahey, D. W., McKeen, S. A., Salawitch, R. J., Webster, C. R., May, R. D., Herman, R. L., Proffitt, M. H., Margitan, J. J., Atlas, E. L., Schauffler, S. M., Flocke, F., McElroy, C. T., and Bui, T. P.: Hydrogen Radicals, Nitrogen Radicals, and the Production of O3 in the Upper Troposphere, Science, 279, 49–53, doi:10.1126/science.279.5347.49, URL http://science.sciencemag.org/content/279/5347/49, 1998.

Wild, S. R. and Jones, K. C.: Polynuclear aromatic hydrocarbons in the United Kingdom environment: A preliminary source inventory and budget, Environmental Pollution, 88, 91 – 108, doi:http://dx.doi.org/10.1016/0269-7491(95)91052-M, URL http://www.sciencedirect.com/science/article/pii/026974919591052M, 1995.

Williams, J., Holzinger, R., Gros, V., Xu, X., Atlas, E., and Wallace, D. W. R.: Measurements of organic species in air and seawater from the tropical Atlantic, Geophys. Res. Lett., 31, doi:10.1029/2004GL020012, URL http://dx.doi.org/10.1029/2004GL020012, 2004.

Wisthaler, A., Hansel, A., Dickerson, R. R., and Crutzen, P. J.: Organic trace gas measurements by PTR-MS during INDOEX 1999, J. Geophys. Res.-Atmos., 107, INX2 23–1–INX2 23–11, doi:10.1029/2001JD000576, URL http://dx.doi.org/10.1029/2001JD000576, 8024, 2002.

Xu, X., Stee, L. L. P., Williams, J., Beens, J., Adahchour, M., Vreuls, R. J. J., Brinkman, U. A., and Lelieveld, J.: Comprehensive two-dimensional gas chromatography (GC x GC) measurements of volatile organic compounds in the atmosphere, Atmos. Chem. Phys., 3, 665–682, doi:10.5194/acp-3-665-2003, URL http://www.atmos-chem-phys.net/3/665/2003/, 2003.

Yañez-Serrano, A. M., Nölscher, A. C., Williams, J., Wolff, S., Alves, E., Martins, G. A., Bourtsoukidis, E., Brito, J., Jardine, K., Artaxo, P., and Kesselmeier, J.: Diel and seasonal changes of Biogenic Volatile Organic Compounds within and above an Amazonian rainforest site, Atmospheric Chemistry and Physics Discussions, 14, 29 159–29 208,

doi:10.5194/acpd-14-29159-2014, URL http://www.atmos-chem-phys-discuss.net/14/29159/2014/, 2014.

Yang, H.-H., Hsieh, L.-T., Liu, H.-C., and Mi, H.-H.: Polycyclic aromatic hydrocarbon emissions from motorcycles, Atmos. Environ., 39, 17 – 25, doi:10.1016/j.atmosenv.2004.09.054, URL http://www.sciencedirect.com/science/article/pii/S1352231004009446, 2005.

Yang, M., Nightingale, P. D., Beale, R., Liss, P. S., Blomquist, B., and Fairall, C.: Atmospheric deposition of methanol over the Atlantic Ocean, Proceedings of the National Academy of Sciences, 110, 20 034–20 039, doi:10.1073/pnas.1317840110, 2013.

Yang, M., Beale, R., Liss, P., Johnson, M., Blomquist, B., and Nightingale, P.: Air-sea fluxes of oxygenated volatile organic compounds across the Atlantic Ocean, Atmos. Chem. Phys., 14, 7499–7517, doi:10.5194/acp-14-7499-2014, URL http://www.atmos-chem-phys.net/14/7499/2014/, 2014.

Yokelson, R. J., Goode, J. G., Ward, D. E., Susott, R. A., Babbitt, R. E., Wade, D. D., Bertschi, I., Griffith, D. W. T., and Hao, W. M.: Emissions of formaldehyde, acetic acid, methanol, and other trace gases from biomass fires in North Carolina measured by airborne Fourier transform infrared spectroscopy, J. Geophys. Res. - Atmos., 104, 30 109–30 125, doi:10.1029/1999JD900817, URL http://dx.doi.org/10.1029/1999JD900817, 1999.

Yokelson, R. J., Bertschi, I. T., Christian, T. J., Hobbs, P. V., Ward, D. E., and Hao, W. M.: Trace gas measurements in nascent, aged, and cloud-processed smoke from African savanna fires by airborne Fourier transform infrared spectroscopy (AFTIR), J. Geophys. Res. - Atmos., 108, doi:10.1029/2002JD002322, URL http://dx.doi.org/10.1029/2002JD002322, 2003.

Yokelson, R. J., Crounse, J. D., DeCarlo, P. F., Karl, T., Urbanski, S., Atlas, E., Campos, T., Shinozuka, Y., Kapustin, V., Clarke, A. D., Weinheimer, A., Knapp, D. J., Montzka, D. D., Holloway, J., Weibring, P., Flocke, F., Zheng, W., Toohey, D., Wennberg, P. O., Wiedinmyer, C., Mauldin, L., Fried, A., Richter, D., Walega, J., Jimenez, J. L., Adachi, K., Buseck, P. R., Hall, S. R., and Shetter, R.: Emissions from biomass burning in the Yucatan, Atmos. Chem. Phys., 9, 5785–5812, doi:10.5194/acp-9-5785-2009, URL http://www.atmos-chem-phys.net/9/5785/2009/, 2009.

York, D., Evensen, N. M., López Martínez, M., and De Basabe Delgado, J.: Unified equations for the slope, intercept, and standard errors of the best straight line, Am. J. Phys., 72, 367–375, doi:http://dx.doi.org/10.1119/1.1632486, URL http://scitation.aip.org/content/aapt/journal/ajp/72/3/10.1119/1.1632486, 2004.

Yu, S.: Role of organic acids (formic, acetic, pyruvic and oxalic) in the formation of cloud condensation nuclei (CCN): a review, Atmos. Res., 53, 185–217, doi:10.1016/S0169-8095(00)00037-5, URL http://www.sciencedirect.com/science/article/pii/S0169809500000375, 2000.

Yunker, M. B., Backus, S. M., Graf Pannatier, E., Jeffries, D. S., and MacdDonald, R. W.: Sources and Significance of Alkane and {PAH} Hydrocarbons in Canadian Arctic Rivers, Estuar. Coast. Shelf S., 55, 1 – 31, doi:h10.1006/ecss.2001.0880, URL http://www.sciencedirect.com/science/article/pii/S0272771401908807, 2002.

Zervas, E., Montagne, X., and Lahaye, J.: Collection and analysis of organic acids in exhaust gas. Comparison of different methods, Atmos. environ., 33, 495–4962, doi:10.1016/S1352-2310(99)00278-2, URL http://www.sciencedirect.com/science/article/pii/S1352231099002782, 1999.

Zhao, J. and Zhang, R.: Proton transfer reaction rate constants between hydronium ion (H_3O^+) and volatile organic compounds, Atmos. Environ., 38, 2177–2185, doi:10.1016/j.atmosenv.2004.01.019, URL http://www.sciencedirect.com/science/article/pii/S1352231004000895, 2004.

Zhao, Y., Nguyen, N. T., Presto, A. A., Hennigan, C. J., May, A. A., and Robinson, A. L.: Intermediate Volatility Organic Compound Emissions from On-Road Diesel Vehicles: Chemical Composition, Emission Factors, and Estimated Secondary Organic Aerosol Production, Environ. Sci. Technol., 49, 11 516–11 526, doi:10.1021/acs.est.5b02841, URL http://dx.doi.org/10.1021/acs.est.5b02841, 2015.

Zhou, X. and Mopper, K.: Photochemical production of low-molecular-weight carbonyl compounds in seawater and surface microlayer and their air-sea exchange, Mar. Chem., 56, 201–213, doi:10.1016/S0304-4203(96)00076-X, URL http://www.sciencedirect.com/science/article/pii/S030442039600076X, 1997.

List of Figures

List of Tables

A. Initial values in the CAABA/MECCA box model

Compound	Initial value in ppbv
nC_4H_{10}	0.2
NH_3	8
C_2H_6	0.9
C_3H_8	0.5
iC_4H_{10}	0.09
C_2H_2	0.3
Toluene	0.1
CH_3CO_3H	0.04
Benzene	0.05
CH_4	1800
Xylenes	0.09
Ethylbenzene	0.01
Trimethylbenzenes	0.009
$C_{11}H_{14}$ (LHAROM)	0.008
CH_3CO_2H	0.3
CH_3CN	0.01
PAN	0.2
CH_3OOH	0.25
HCN	0.07
MBO	0.002
Methylpropene	0.006
β-Pinene	0.03
Sabinene	0.006
Camphene	0.005

Compound	Initial value in ppbv
α-Pinene	0.025
Carene	0.004
HONO	0.009
cBut-2-ene	0.004
tBut-2-ene	0.003
CH_3OH	3
Styrene	0.003
H_2O_2	1.8
CH_3COCH_3	1
C_5H_8	0.5
HNO_3	0.8
Hydroxyacetone (Acetol)	0.35
Glyoxal	0.06
Methylglyoxal	0.1
CH_3CHO	0.4
$HOCH_2CHO$	0.25
HCOOH	0.25
CO	100
O_3	50
NO_2	2
NO	0.4
HCHO	2
O_2	2.1×10^8
N_2	7.8×10^8
CO_2	4×10^5

B. Molecular classes

Formula	TOF mass
C_6H_{14}	87.1168
C_7H_{16}	101.1325
C_8H_{18}	115.1481
C_9H_{20}	129.1638
$C_{10}H_{22}$	143.1794
$C_{11}H_{24}$	157.1951
$C_{12}H_{26}$	171.2107
$C_{13}H_{28}$	185.2264
$C_{14}H_{30}$	199.2420
$C_{15}H_{32}$	213.2577
$C_{16}H_{34}$	227.2733
$C_{17}H_{36}$	241.2890
$C_{18}H_{38}$	255.3046
$C_{19}H_{40}$	269.3203
$C_{20}H_{42}$	283.3359
$C_{21}H_{44}$	297.3516
$C_{22}H_{46}$	311.3672
$C_{23}H_{48}$	325.3829

(a) Alkanes

Formula	TOF mass
C_6H_{12}	85.1012
C_7H_{14}	99.1168
C_8H_{16}	113.1325
C_9H_{18}	127.1481
$C_{10}H_{20}$	141.1638
$C_{11}H_{22}$	155.1794
$C_{12}H_{24}$	169.1951
$C_{13}H_{26}$	183.2107
$C_{14}H_{28}$	197.2264
$C_{15}H_{30}$	211.2420
$C_{16}H_{32}$	225.2577
$C_{17}H_{34}$	239.2733
$C_{18}H_{36}$	253.2890
$C_{19}H_{38}$	267.3046
$C_{20}H_{40}$	281.3203
$C_{21}H_{42}$	295.3359
$C_{22}H_{44}$	309.3516
$C_{23}H_{46}$	323.3672

(b) Cycloalkanes

Formula	TOF mass
C_6H_{10}	83.0855
C_7H_{12}	97.1012
C_8H_{14}	111.1168
C_9H_{16}	125.1325
$C_{10}H_{18}$	139.1481
$C_{11}H_{20}$	153.1638
$C_{12}H_{22}$	167.1794
$C_{13}H_{24}$	181.1951
$C_{14}H_{26}$	195.2107
$C_{15}H_{28}$	209.2264
$C_{16}H_{30}$	223.2420
$C_{17}H_{32}$	237.2577
$C_{18}H_{34}$	251.2733
$C_{19}H_{36}$	264.2812
$C_{20}H_{38}$	279.3046
$C_{21}H_{40}$	293.3203
$C_{22}H_{42}$	307.3359
$C_{23}H_{44}$	321.3516

(c) Bicycloalkanes

Formula	TOF mass
$C_{10}H_8$	129.0699
$C_{11}H_{10}$	143.0855
$C_{12}H_{12}$	157.1012
$C_{13}H_{14}$	171.1168
$C_{14}H_{16}$	185.1325
$C_{15}H_{18}$	199.1481
$C_{16}H_{20}$	213.1638
$C_{17}H_{22}$	227.1794
$C_{18}H_{24}$	241.1951
$C_{19}H_{26}$	255.2107
$C_{20}H_{28}$	269.2264
$C_{21}H_{30}$	283.2420
$C_{22}H_{32}$	297.2577
$C_{23}H_{34}$	311.2733
$C_{24}H_{36}$	325.2890

(a) Naphthalene derivatives

Formula	TOF mass
$C_{13}H_{10}$	167.0855
$C_{14}H_{12}$	181.1012
$C_{15}H_{14}$	195.1168
$C_{16}H_{16}$	209.1325
$C_{17}H_{18}$	223.1481
$C_{18}H_{20}$	237.1638
$C_{19}H_{22}$	251.1794
$C_{20}H_{24}$	265.1951
$C_{21}H_{26}$	279.2107
$C_{22}H_{28}$	293.2264
$C_{23}H_{30}$	307.2420
$C_{24}H_{32}$	321.2577

(b) Fluorene derivatives

Formula	TOF mass
$C_{14}H_{10}$	179.0855
$C_{15}H_{12}$	193.1012
$C_{16}H_{14}$	207.1168
$C_{17}H_{16}$	221.1325
$C_{18}H_{18}$	235.1481
$C_{19}H_{20}$	249.1638
$C_{20}H_{22}$	263.1794
$C_{21}H_{24}$	277.1951
$C_{22}H_{26}$	291.2107
$C_{23}H_{28}$	305.2264
$C_{24}H_{30}$	319.2420
$C_{25}H_{32}$	333.2577

(c) Anthracene derivatives

Formula	TOF mass
C_3H_6O	59.0491
$C_2H_2O_2$	59.0128
C_4H_6O	71.0491
$C_3H_4O_2$	73.0290
C_4H_8O	73.0648
$C_4H_6O_2$	87.0441
$C_5H_{10}O$	87.0804
$C_5H_4O_2$	97.0284
$C_6H_{12}O$	101.0961
C_7H_6O	107.0491
$C_7H_{14}O$	115.1117
C_8H_6O	119.0491
C_8H_8O	121.0648
$C_8H_{16}O$	129.1274
C_9H_8O	133.0648
$C_9H_{18}O$	143.1430
$C_{10}H_{20}O$	157.1587
$C_{12}H_8O$	169.0648
$C_{11}H_{22}O$	171.1743
$C_{13}H_8O$	181.0648
$C_{12}H_{24}O$	185.1900
$C_{13}H_8O_2$	197.0597
$C_{13}H_{26}O$	199.2056
$C_{14}H_{28}O$	213.2213
$C_{15}H_{30}O$	227.2369
$C_{16}H_{32}O$	241.2526
$C_{17}H_{34}O$	255.2682
$C_{18}H_{36}O$	269.2839
$C_{19}H_{38}O$	283.2995

(a) Aldehydes and ketones

Formula	TOF mass
$C_2H_2O_4$	91.0026
$C_3H_6O_3$	91.0390
C_6H_6O	95.0491
$C_5H_{10}O_2$	103.0754
$C_6H_{12}O_2$	117.0910
$C_7H_6O_2$	123.0441
$C_7H_{14}O_2$	131.1067
$C_4H_6O_5$	135.0288
$C_8H_{16}O_2$	145.1223
$C_9H_{18}O_2$	159.1380
$C_{10}H_{20}O_2$	173.1536
$C_{11}H_{22}O_2$	187.1693
$C_{12}H_{24}O_2$	201.1849
$C_{13}H_{26}O_2$	215.2006
$C_{14}H_{28}O_2$	229.2162
$C_{15}H_{30}O_2$	243.2319
$C_{16}H_{32}O_2$	256.2397
$C_{17}H_{34O2}$	271.2632
$C_{18}H_{36O2}$	285.2788
$C_{19}H_{38O2}$	299.2945
$C_{20}H_{40O2}$	313.3101

(b) Acids

Formula	TOF mass
$C_{10}H_{10}$	131.0855
$C_{14}H_{12}$	181.1012
$C_{18}H_{14}$	231.1168
$C_{20}H_{14}$	255.1168
$C_{22}H_{16}$	281.1325
$C_{26}H_{18}$	331.1481

(c) Dihydronaphthalene derivatives

Formula	TOF mass
$C_{16}H_{10}$	203.0855
$C_{18}H_{12}$	229.1012
$C_{20}H_{12}$	253.1012
$C_{22}H_{14}$	279.1168
$C_{26}H_{16}$	329.1325

(d) Other PAHs

C. Abbreviations

ACEA	European Automobile Manufacturers' Association Chemical Ionization
CIMS	Mass Spectrometer
cps	Counts per second
CYPHEX	Cyprus Photochemistry Experiment
DMS	Dimethylsulfide
EFTA	European Free Trade Association
GC	Gas Chromatography
GC-FID	Gas Chromatograph Flame Ionization Detector
GC-MS	Gas Chromatograph Mass Spectrometer
GHG	Greenhouse Gas
HO_2	Hydroperoxyl radical
H_3O^+	Hydronium ion
IVOC	Intermediate-volatility organic compounds
IUPAC	International Union of Pure and Applied Chemistry
k_{OH}	Reaction rate with OH radicals
MBL	Marine Boundary Layer
ncps	Normalized counts per second
NOx	Sum of nitrogen oxide (NO) and nitrogen dioxide (NO_2)
NO^+	Nitrogen oxide cation
$O_2{}^+$	Oxygen cation
OH	Hydroxyl radical
OVOC	Oxygenated volatile organic compounds
PAN	Peroxyacetyl nitrate
PBL	Planetary Boundary Layer
ppbv	Parts per billion (volume) equals nmol/mol (10^{-9}mol/mol)
pptv	Parts per trillion (volume) equals pmol/mol (10^{-12}mol/mol)
PTR-MS	Proton Transfer Reaction Mass Spectrometer (Quadrupole)
PTR-TOF-MS	Proton Transfer Reaction Time OF Flight Mass Spectrometer
SOA	Secondary Organic Aerosol
SIFT-MS	Selected Ion Flow Tube Mass Spectrometer
VOC	Volatile organic compounds